Determination of the Allowable Parametric Uncertainty in the Closed Loop Via a Skew-μ Based Technique with an Application to the Yaw-Roll Vehicle Model

by

Lowell S. Brown

A dissertation submitted to the Graduate Faculty of
Auburn University
in partial fulfillment of the
requirements for the Degree of
Doctor of Philosophy

Auburn, Alabama
August 5, 2017

Keywords: H-infinity, convex optimization, linear matrix inequality, LMI, parametric uncertainty, roll, relative roll, vehicle dynamics,

Approved by:

David Bevly, Chair, Professor of Mechanical Engineering
John Hung, Professor of Electrical Engineering
George Flowers, Professor of Mechanical Engineering
Dan Marghitu, Professor of Mechanical Engineering

Abstract

In this dissertation, a methodical approach is presented that quantifies how well model parameters need to be known or by how much they can vary in order that the performance of a controller in closed loop is maintained. Unique in the formulation of this parametric approach is the ability to include parameters that are coupled together. This methodical skew μ approach with real parametric uncertainty is applied to the coupled yaw-roll vehicle model. An analysis of the μ-sensitivity of the yaw-roll vehicle model with full parametric uncertainty is also analyzed to ascertain which parameters are the most sensitive and which parameters can be most logically grouped together in the varying subset of the skew μ uncertainty block. A comparison between the vehicle model and high-fidelity simulation model is provided to show the potential limitations of the approach.

Typically, robust control design techniques are used to ensure a system has guaranteed performance within certain margins of operation. However, it is often required to know which parameters and by how much these parameters affect the closed loop performance. In order to achieve guaranteed robustness, robust design techniques tend to broaden the output response often at the cost of a reduction in the performance of closed loop response characteristics. In this dissertation, the method presented seeks to determine how accurate the parameters of system model need to be in order to maintain the performance of an existing controller without broadening the original model response. In effect, a quantification of parameter variance allowed is calculated for a given system model with an existing controller and initial parametric variance assumptions and measurement specifications.

To accomplish this quantification of allowable uncertainty, the infinite norm concept ($\mathcal{H}_\infty$) and the extension to the structured singular value or μ value is utilized. Typically, μ analysis and structured uncertainty are used to account for various types of uncertainty for

the synthesis of a controller. The μ analysis, however, is shown to also be useful in analyzing the allowable uncertainty of a closed loop system for a previously designed controller. Additionally, the linear fractional transformation (LFT) is leveraged to formulate a system model that incorporates uncertainty on the parameters while maintaining the effects of parameter coupling.

With a closed loop around the yaw rate of the coupled yaw-roll vehicle it is shown that the parametric eigenvalue analysis may not reveal accurate sensitivity information about the closed loop system. The μ sensitivity analysis indicates that the center of gravity height and weight split parameters are the most sensitive parameters for the coupled vehicle model. The vehicle system is also understandably sensitive to velocity. Initial uncertainties representative of typical variances and measurement capabilities are applied to the vehicle model for several cases of fixed and varying subsets within the uncertainty block. The skew μ for these cases is then calculated. It is shown that the specific parameters in the fixed subset affect the additional variance allowed on the parameters in the varying subset. Finally, spectral analysis using a CarSim high fidelity vehicle model is performed to confirm the validity of the additional allowable variance on the center of gravity height and weight split parameters that was found via the skew μ based analysis.

In summary, the skew μ analysis is used to calculate the remaining "space" that each parameter can vary given an initial uncertainty for each parameter. If the initial uncertainty is increased for some or all of the parameters then there is less space remaining for further variation of the parameters in the varying subset. Additionally, μ sensitivity and skew μ analysis are shown to be a helpful tool to determine which parameters to focus on for estimation as well as how much the parametric terms of the model can vary for a given controller. With the assumption that a given model is accurate representation of the system a designer determine how much uncertainty is allowable for each parameter in the closed loop under specific initial uncertainty conditions.

Acknowledgments

This dissertation is dedicated to my father, Carey, who has been extremely supportive trough out my life and especially over my years in graduate school. Special thanks to my sister Chelsea for all the end of the day phone calls with discussions on work and life. Thank you to my sister Lindsey and my brother in law Rodolphe Nenert for their support as well. Also, thank you to all the GAVLAB members past and present I have had the pleasure of knowing and researching alongside. Thank you especially to GAVLABers Scott Martin, Grant Apperson, William Woodall, David Hodo, Jonathan Ryan and Ryan Hill. Finally, many thanks to Dave Bevly for giving me the opportunity to pursue both a masters degree and a doctoral degree.

Table of Contents

List of Figures

List of Tables

Chapter 1

Introduction & Motivation

1.1 Introduction

Typically in the controller design process, assumptions are made about the system in the form of a system model. In the classical control approach, model parameter values are assumed constant and a closed loop controller is designed to meet certain performance specifications. In practice these parameters may change or be inaccurately acquired or modeled. Thus, certain classical robust design techniques have been developed and used to allow for small changes in the model and to account for imperfect modeling.

1.2 Robust Design & Model Uncertainty

In the advancements from modern control techniques, uncertainties in the model have been incorporated directly in the robust design process. There is a relationship between the allowable uncertainty and the resulting performance of the system such that as the uncertainty is increased the resulting performance bounds increase. The question posed here is not can a controller be designed such that some measure of robust performance is guaranteed? Rather, the questioned posed is how good does my model need to be? Or framed more specifically, what is the allowable uncertainty for a given system and controller in the closed loop?

1.3 Prior Art

To answer this question of model accuracy, techniques from modern robust design can be leveraged. Specifically the $\mathcal{H}_\infty$ techniques for suboptimal design and controller synthesis is to be utilized.

In brief, the $\mathcal{H}_\infty$ technique makes use of the infinite norm as a design constraint across a range of frequency responses. Additionally, the formulation is well suited for design of multi-input multi-output systems and thus has been used in chemical and industrial process systems such as the distillation column referenced heavily in [1] and analyzed with a parametric uncertainty technique in [2]. The $\mathcal{H}_\infty$ technique has since been picked up by the aerospace industry. Interestingly, the handling of parametric uncertainty has been used to narrow focus on system parameters that most affect the stability of the flight envelope [3]. The parametric $\mathcal{H}_\infty$ approach has also been applied to ground vehicles.

Using a multiplicative perturbation approach, the neglected dynamics of the bicycle model were accounted for in [4], where sidewind was treated as an additive output disturbance. Unique to the $\mathcal{H}_\infty$ approach, the author extended the D-K iteration method of controller synthesis to also optimize the uncertainty models. The author makes the case that this D-K-W iteration scheme allows for the inclusion of information of unstable (saturated) experiments. In [5], parametric uncertainty was incorporated into the bicycle model. Mass and inertia were treated as independent variations though they are physically linked. Additionally, the variations of cornering stiffness were used to "capture" the effect of nonlinear tire dynamics. In [6], the $\mathcal{H}_\infty$ controller synthesis process is used on a non-dimensional form of the bicycle model and the effects of velocity on uncertainty are explored and the operating regions where robust control is not achievable is defined.

Instead of using model uncertainty and performance specifications to design and synthesize a robust control implementation, the $\mathcal{H}_\infty$ techniques in this work are used to uncover the allowable uncertainty. Details of this idea are presented in the latter half of Chapter 2. This approach to uncertainty and sensitivity is similar to that presented by [3] however,

instead of analyzing the state coefficients, an approach that accounts for the uncertain on physical parameters like mass and inertia is implemented.

Parameter sensitivity is a concern that arises out of the parametric approach. Work has been done relatively recently in the area of sensitivity for parametric uncertainty. In [7], the author examines the effect of parameter uncertainty on the output uncertainty across the average output response. Specifically, the analysis is carried out on a tractor and single axle grain cart system and the cornering stiffness parameter is altered via changes to the tire. In [8], the author confirms the differences in stability of an open loop system response and the closed loop control response. A tractor and single axle towed implement system was used experimentally and the need for a high fidelity model at large velocities was additionally confirmed.

To address the sensitivity concerns, an offline approach is presented in [3]. Using the μ analysis of the $\mathcal{H}_\infty$ approach the author develops a skewed-μ tool for sensitivity measurement. This skewed μ analysis is used to determine which uncertain parameter coefficients are the most important for a flight model. The limitations of a traditional open loop sensitivity analysis applied to the closed loop flight system is discussed and the sensitive parameter coefficients identified in open loop analysis are not always the same as the sensitive parameters identified in the closed loop control system.

This skewed-μ method for flight model coefficients from [3] is leveraged and modified in this work to determine the allowable uncertainty for real and repeated parameters using cascaded and parallel connection properties of the linear fractional transformation (LFT) [9].

1.4 Contributions

This dissertation makes the following contributions to the research in the robust control field listed below:

- A methodical approach based on parametric uncertainty for determining how accurate a system model needs to be is presented.
  - Specifically, the approach provides information on how well do model parameters need to be known to maintain the performance of the controller in closed loop.
  - Unique in the formulation of this parametric approach to allowable uncertainty is the ability to include parameters that are coupled together. Prior work [3] in the field does not cover this coupling of parameters when exploring the allowable uncertainty.
- This methodical skew μ approach with real parametric uncertainty is applied to the coupled yaw-roll vehicle model.
- An analysis of the μ-sensitivity of the yaw-roll vehicle model with full parametric uncertainty is also analyzed to ascertain which parameters are the most sensitive and which parameters can be most logically grouped together in the varying subset of the skew μ uncertainty block.
- A comparison between the vehicle model and high fidelity simulation model is provided to show the potential limitations of the approach.

1.5 Outline

The outline of this dissertation is as follows: a review of the classical control concepts is presented in the first part of Chapter 2. Then, a transition to the more modern based robust control concepts rounds out the middle portion with the introduction of the linear fraction transformation (LFT) and the "μ" concept. Finally at the end of the chapter the concept of model uncertainty is covered. Chapter 3 covers the derivation of the coupled yaw-roll vehicle model complete with road bank disturbances. A comparison of the coupled yaw-roll vehicle

model with CarSim high fidelity simulation is presented to show limitations of the model and potential issues with the parametric analysis.

In Chapter 4 two methods by which parametric uncertainty is incorporated into a model is covered with the less complex lateral vehicle model for ease of presentation. A method relying primarily on the classical block diagram signal routing rules and a method that treats parameters as LFT subsystems are compared and the advantages of each are discussed. The chapter ends with the incorporation of uncertainty for all parameters for the coupled yaw-roll model. Next, Chapter 5, gets at the heart of the initial question of how well does a model need to be known. The allowable uncertainty for the coupled yaw-roll model is analyzed with respect to a given controller.

Chapter 6 then covers which parameters of coupled yaw-roll vehicle model most influence the performance via μ-sensitivity analysis of all the uncertainty parameters. The sensitivity information ascertained from the μ-sensitivity analysis is used in Chapter 7 to develop a practical set of uncertainty models. A more meaningful set of initial uncertainties is prescribed based off of operating characteristics, and several cases for the terms that are grouped based on influence and μ sensitivity level are developed. These uncertainty models are then used to better assess what the operating maximum uncertainty is with respect to the fixed subset and the extra variance found from the varying subset of parameters. Finally, Chapter 8 consolidates the conclusions from preceding chapters and highlights areas of future work.

Chapter 2

Stepping from Classical Robust Control concepts to the Modern Formulations

2.1 Introduction

This chapter covers some of the basic principles behind the modern robust control synthesis. Specifically, the $\mathcal{H}_\infty$ method is addressed. Some examples of the technique used on ground vehicles and the dynamic systems are highlighted.

2.2 Robust Control Design

The goal of the robust design approach has been to handle unknown disturbances to the system and to handle minor modeling errors and imperfect parameter identification. For uncertain systems, the robust approach can result in a controller design that accepts a wide range of variations but this accommodation often comes at the cost of the reduction of desired performance specifications. In effect, opening up the "space", measured in terms of open loop frequency response, of the model can result in the need for the loosening of the performance specifications of the closed loop in practice for uncertain systems.

At times it maybe desired to keep tight performance specifications and simply understand by how much a model can vary for the given design; not to expressly design a a closed loop system for some assumed variances. This is the primary motivation for determining the parameter variations allowable of a closed loop system. First, however, a review of the robust control design techniques is useful. An overview of the classical concepts and the formulation of the modern control theories are presented below and are sourced primarily from [1] and [10].

2.2.1 Classical

Classical approaches to robust design are based off the small gain theorem. There are two types of objectives in the classical control formulation. These objectives are embodied by the regulator problem and the servo problem. For a given system with output, y, the plant input, u, can be manipulated to force the system output to behave in a desired fashion. The regulator serves to counteract the effect of a disturbance, d. The servo formulation serves to drive the output to a desired reference response, r. For both cases the controller error, defined as $e = r - y$, is desired to be small or near zero. The algorithm or control law that adjusts the input u is called the controller K. A good controller requires information on the expected disturbances, reference inputs and the models of the plant , G, and the the disturbance, G_d. The linear formulation is thus:

$$y = Gu + G_d d \tag{2.1}$$

At issue is the fact that the plant and disturbance models may not be well known and/or may also change with time. A good approach to handling these unknowns is to leverage the concept of model uncertainty and study the behavior of a class of models. More specifically the single model G can be setup as the perturbation model

$$G_p = G + E \tag{2.2}$$

where E is the uncertain perturbation. This uncertain perturbation E is assumed to be bounded. Typically E is expressed as a set of weighting functions, $w(s)$ and normalized perturbations, Δ. For the normalized perturbations the magnitude is less than or equal to 1.

The following terms defined below are useful classifications of the closed loop feedback behavior:

- Nominal stability (NS): The system is stable with no model uncertainty.

- Nominal Performance (NP): The system satisfies the performance specifications with no model uncertainty.
- Robust stability (RS): The system is stable for all perturbed plants about the nominal model up to the worst-case model uncertainty.
- Robust performance (RP): The system satisfies the performance specifications for all perturbed plants about the nominal model up to the worst-case model uncertainty.

Uncertainty is handled more easily in the frequency domain. Specifically, two systems with similar frequency responses can be described as behaving similarly whereas two systems in a state space representation may exhibit large behavioral differences for a small change in a parameter. Thus it is desirable to work with uncertain systems via transfer functions, $G(s)$, in the frequency domain where $G(j\omega)$ yields the response to a sinusoidal input of frequency ω. For linear, time-invariant systems where the input-output responses are governed by linear ordinary with constant coefficients the transfer function $G(s)$takes the form:

$$G(s) = \frac{y(s)}{u(s)} = \frac{\beta_{n_z} s^{n_z} + \ldots + \beta_1 + \beta_0}{s^n + a_{n-1} s^{n-1} + \ldots + a_1 s + a_0} \tag{2.3}$$

where β and a are independent of time and correlate to the input and output respectively. Also, in Eq. (2.3) n is the order of the denominator (number of pole polynomials) and is known as the order of the system, while n_z is the order of the numerator (the number of zero polynomials). The difference of poles from zeros is referred to as the number of excess poles also known as the relative order. Note, that for multivariable systems, $G(s)$ takes the form of a matrix of transfer functions.

Given a proper system with more poles than zeros, $n > n_z$, $G(s)$ may be expressed by a state space description of the form:

$$\begin{aligned} \dot{x} &= Ax + Bu \\ y &= Cx + Du \end{aligned} \tag{2.4}$$

The transfer function $G(s)$then becomes

$$G(s) = C(sI - A)^{-1} B + D \tag{2.5}$$

Sometimes the transfer function $G(s)$ may be represented in a compact expression of the state space form

$$G(s) \stackrel{s}{=} \left[\begin{array}{c|c} A & B \\ \hline C & D \end{array}\right] \tag{2.6}$$

where the partitions delineate the "sub-blocks" of the A, B, C and D matrices.

Recall that a system is strictly proper if the gain of $G(j\omega)$ approaches zero as the frequency ω approaches infinity. Additionally, a semi-proper system is characterized by the gain $G(j\omega)$approaching a nonzero value, D, as the frequency approaches infinity. Finally a system which is strictly proper or semi-proper is proper.

Note all realistic systems tend to have a zero gain at a sufficiently high frequency and are thus strictly proper. However, a non-zero D-term is often used to model certain high frequency effects. Certain derived functions used for analysis such as the sensitivity function $S = (I + GK)^{-1}$ are also semi-proper.

2.2.2 Classical Feedback

The classical frequency-response techniques have been heavily studied and used in industry for single-input single-output (SISO) feedback control systems. The classical loop shaping methods were formalized in the 1980's. This formalization of the shaping of the closed-loop transfer functions allowed for the extension of the techniques to the multivariable or multi-input multi-output (MIMO) control systems. The formalization of the loop shaping is presented here in this section. The next section will cover some of the multivariable characteristics.

The primary concept used for analysis of feedback systems is the system response to varying sinusoids of frequency inputs. For a stable system of the form $y = G(s)\,u$, a sinusoidal input, $u(t)$, is used with the frequency ω in units of $^{\text{rad}}/_{\text{s}}$ and with a magnitude u_0 where

$$u(t) = u_0 \sin(\omega t + \alpha) \tag{2.7}$$

For this input $u(t)$, the output signal then takes the form

$$y(t) = y_0 \sin(\omega t + \beta) \tag{2.8}$$

where y_0 represents the magnitude of the output. The phase difference in frequencies ϕ, defined as $\phi \triangleq \beta - \alpha$, and ratio of the output to the input, $^{y_0}/_{u_0}$, are used to draw meaning and characterize the system. In the Laplace domain the gain ratio, $^{y_0}/_{u_0}$, and the phase angle shift, ϕ, can be calculated directly from $G(s)$ at each frequency ω by inserting the imaginary number $s = j\omega$. The term $G(j\omega)$ is the frequency response of the system $G(s)$ and describes how the system responds to persistent sinusoidal inputs of frequency ω. The magnitude of the frequency response, $|G(j\omega)|$, is termed the system gain. The frequency response is comprised of a real and imaginary component at each frequency.

$$G(j\omega) = a + jb \tag{2.9}$$

where a represents the real part and b represent the imaginary part.

$$a = \Re\, G(j\omega) \tag{2.10}$$

$$b = \Im\, G(j\omega) \tag{2.11}$$

The magnitude of system gain is then calculated as

$$
\begin{aligned}
{}^{y_0(\omega)}/_{u_0(\omega)} &= |G(j\omega)| \\
&= \sqrt{a^2 + b^2}
\end{aligned} \tag{2.12}
$$

and the phase shift is calculated as

$$
\begin{aligned}
\phi &= \angle G(j\omega)\,[\text{rad}] \\
&= \arctan({}^{b}/_{a})
\end{aligned} \tag{2.13}
$$

Being that both $|G(j\omega)|$ and $\angle G(j\omega)$ depend on the frequency ω these two measures of the system are plotted explicitly in Bode plots (with ω as the independent variable) and also in a Nyquist plot, a type of phase plane plot that is more implicit in its nature. For the Bode plot, a log-scale for frequency and gain and a linear scale for the phase is most often used. The log-scale is usefully for visual identification of poles and zeros and to asymptotically hand sketch the Bode system response. The Bode response is the base from which a lot of the classical loop shaping control concepts are built and from which the modern control concepts expand from.

Feedback control is the primary structure for most practically implemented systems. The structure for a one degree-of-freedom controller is represented by the block diagram shown in Figure 2.1. Observe that the input to the controller $K(s)$ is $r - y_m$, the difference of the measured output y_m from the reference r. The measured output consists of the sum of the actual system output y and any measurement noise n and is thus expressed as $y_m = y + n$. The input to the plant is then formulated as

$$
u = K(s)(r - y - n) \tag{2.14}
$$

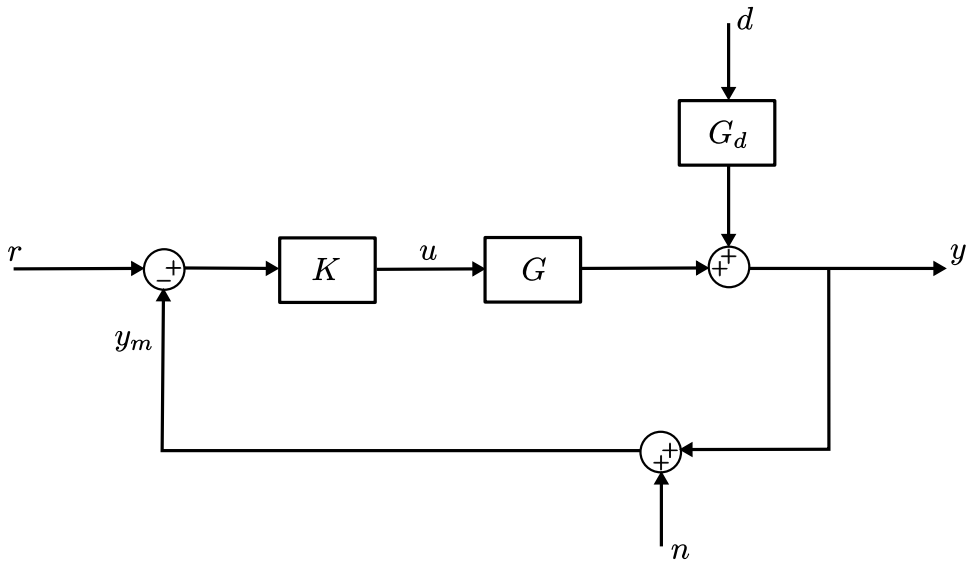

Figure 2.1: Negative Feedback, One Degree-of-Freedom Block Diagram

The objective of control is to design $K(s)$ such that any control error is small with respect to system disturbances d. The control error is then defined as the difference of the output from the reference

$$e = y - r \tag{2.15}$$

Note that the input to the controller K, the difference $r - y_m$, is often referred to as the control error. The true measure of error should be in reference to the actual output y (not the measured output y_m) and the desired reference r.

The plant model is formulated as

$$y = G(s)\,u + G_d(s)\,d \tag{2.16}$$

and for one degree-of-freedom feedback control the input, Eq. (2.3), is substituted into Eq. 2.16 to yield

$$y = GK(r - y - n) + G_d d \tag{2.17}$$

Collecting the output terms the equation becomes

$$(I + GK)\, y = GKr + G_d d - GKn \tag{2.18}$$

and dividing through by $(I + GK)$ produces

$$y = \underbrace{(I + GK)^{-1}\, GK}_{T}\, r + \underbrace{(I + GK)^{-1}}_{S}\, G_d d - \underbrace{(I + GK)^{-1}\, GK}_{T}\, n \tag{2.19}$$

The control error is then

$$\begin{aligned} e &= y - r \\ &= Tr + SG_d d - Tn - Ir \\ &= (T - I)\, r + SG_d d - Tn \\ &= -Sr + SG_d d - Tn \end{aligned} \tag{2.20}$$

Note the fact that $T - I = -S$ or more explicitly:

$$\begin{aligned} T - I &= \left((I + GK)^{-1}\, GK\right) - I \\ &= \tfrac{GK}{I+GK} - \tfrac{I(I+GK)}{I+GK} \\ &= \tfrac{GK - I(I+GK)}{I+GK} \\ &= \tfrac{GK - I^2 - GK}{I+GK} \\ &= \tfrac{-I^2}{I+GK} \\ &= -(I + GK)^{-1} \\ &= -S \end{aligned} \tag{2.21}$$

The corresponding input signal to the plant then becomes

$$u = KSr - KSG_d d - KSn \tag{2.22}$$

Descriptively, the term S is the sensitivity, T is defined as the complimentary sensitivity function and L is the loop transfer function. In summary, the terminology is:

$$\begin{aligned} L &= GK && \text{loop trasnfer function} \\ S &= (I+GK)^{-1} \\ &= (I+L)^{-1} && \text{sensitivity function } \left({}^{y(s)}/_{G_d d(s)}\right) \\ T &= (I+GK)^{-1}GK \\ &= (I+L)^{-1}L && \text{complementary sensititivty function } \left({}^{y(s)}/_{r(s)}\right) \end{aligned}$$

From the above relationships the following observations can be made:

- The sensitivity function, S, is the closed-loop transfer function from the output disturbances to the outputs.
- The complementary sensitivity, T, is the closed-loop transfer function from the reference signals to the outputs.

The complementary sensitivity is termed as such due to the relation

$$S + T = I \tag{2.23}$$

The sensitivity name makes intuitive sense in observation of Eq. 2.19, but the term was originally created by Bode from the differentiation (at each frequency ω) of the closed-loop transfer function T with respect to the plant model G

$$\frac{{}^{dT}/_{T}}{{}^{dG}/_{G}} = S \tag{2.24}$$

Bode termed the result of this differential sensitivity because it gives the relative sensitivity of the closed-loop transfer function T to the relative plant model error. It is also important to note that the equations above are written in matrix form for application to MIMO systems. This matrix representation allows for a more general expression and manipulation that is

presented in a later section. Recall that the generalization for SISO systems with negative feedback is the "forward path" divide by "one plus the loop transmission" or

$$\text{Output} = \frac{\text{"forward path"}}{1 + \text{"loop transmission"}} \cdot \text{Input} \tag{2.25}$$

(The "forward path" term is also referred to as the "direct" transmission.) A more general rule form that relates to the multivariable systems is presented later.

Also recall that the reason for feedback is that a perfect feedforward controller is not feasible in practice due to modeling errors, signal noises, system disturbances and also varying system parameters. Additionally, a plant that is unstable is in practice also only stabilizable via a feedback structure due to the same imperfect knowledge. In summary, feedback is used when any of the following are present in the system:

- Signal uncertainty or unknown disturbances (d)
- Model uncertainty (δ)
- Unstable plant

In this work the ability of feedback to reduce the effect of model uncertainty is the primary focus.

2.2.3 Stability

Recall that for closed loop stability the system is stable "if and only if" all the closed-loop poles reside in the left-half plane (LHP) of the Real-Imaginary graph of the poles. Specifically, the roots of the loop transmission, $1 + G(s)K(s) = 0$, are calculated and plotted and can also be written as $1 + L(s) = 0$. These poles are equal to the eigenvalues of the closed loop state-space A-matrix, $(A - BK)$. The frequency response of $L(j\omega)$ can also be plotted in the complex plane and the number of encirclements of the critical point -1 counted. The number of encirclements is equal to the number of open-loop unstable poles

(RHP-poles). This encirclement method is called the Nyquist stability criterion. Open-loop stable systems are characterized by a phase that falls (with respect to frequency) such that the phase crosses -180 deg only once from above. For a closed-loop system, the the system is stable if and only if the loop gain $|L|$ is less than 1 at the crossover frequency of $-180\,\text{deg}$. Stability is then defined as

$$\text{Stability} \iff |L(j\omega_{180}) < 1| \tag{2.26}$$

where ω_{180} is the phase crossover frequency defined by $\angle L(j\omega_{180} = -180\,\text{deg})$.

While stability is important for a system, the overall performance is ultimate objective of control. That is, to design the closed loop output to behave in a desirable manner. But, under the feedback scheme it is possible to induce instability into the system and it is against this tradeoff that performance improvements are evaluated.

In the time domain, performance is evaluated via the step response with such metrics as rise time, settling time, overshoot, decay ratio and steady-state offset. These measures can be categorized into either speed of the response or quality of the response. For more on the time domain refer to the classical control literature [11, 12, 1]. However, the frequency domain performance metrics are of greater importance to this work.

The advantage of the frequency response is the inclusion of many signals, sinusoids over a range of frequencies. In addition to the frequency response of the loop transfer function, $L(j\omega)$, the responses of the sensitivity, $S(j\omega)$, and complementary sensitivity, $T(j\omega)$, are also analyzed. If $L(s)$ denotes the loop transfer function, then a typical Bode plot represents the phase and magnitude of $L(j\omega)$ and contains the gain margin and phase margin, GM and PM respectively. The gain margin is defined as

$$\text{GM} = {}^{1}/_{|L(j\omega_{180})|} \tag{2.27}$$

where the phase crossover frequency, ω_{180}, is defined as

$$\angle L\left(j\omega_{180}\right) = -180 \tag{2.28}$$

If more than one crossing of the phase angle $\angle L\left(j\omega_{180}\right)$ exists, then the largest value of the gain magnitude at the crossover, $\max\left(\left|L\left(j\omega_{180}\right)\right|\right)$, is taken. The GM is the factor by which the loop gain can be increased before the closed-loop system becomes unstable. By this relation the GM is a safeguard against steady state uncertainty in the plant gain. Typically, a GM greater than 2 is desired.

The phase margin is defined as

$$\mathrm{PM} = \angle L\left(j\omega_c\right) + 180\,\mathrm{deg} \tag{2.29}$$

where the gain crossover frequency, ω_c, is the frequency at which the magnitude of the loop transfer response, $\left|L\left(j\omega_c\right)\right|$, crosses one from above; expressly written that is

$$\left|L\left(j\omega_c\right)\right| = 1 \tag{2.30}$$

The PM discloses how much negative phase, also known as phase lag, can be added to the loop transfer function $L\left(s\right)$ at the crossover frequency ω_c before the phase at this frequency becomes $-180\,\mathrm{deg}$. Recall that the system is stable if and only if $\left|L\left(j\omega_{180}\right)\right| < 1$. Phase lag can be thought of as a system delay. Therefore the PM is a measure of the safeguard against time delay uncertainty. Typically, a PM larger than $30\,\mathrm{deg}$ is desired.

Thus, it is clear how the gain and phase margins provide a metric for evaluating the margin of stability for gain and delay uncertainty. The gain and phase margins are closely related to the peak values of the sensitivity and complimentary sensitivity gain magnitudes, $\left|S\left(j\omega\right)\right|$and $\left|T\left(j\omega\right)\right|$. Relating the disturbance-to-output and the reference-to-output, respectively, these two sensitivity terms are useful measures of performance, and the correlation

to the phase and gain margins yield a metric to evaluate the appropriate tradeoff between performance and stability criteria.

The maximum peaks of the sensitivity and complementary sensitivity functions are defined respectively as

$$M_s = \max_{\omega} |S(j\omega)| \tag{2.31}$$

$$M_T = \max_{\omega} |T(j\omega)| \tag{2.32}$$

This type of maximum is actually the infinite norm, $\mathcal{H}_\infty$, and the peaks can be expressed also as $M_s = \|S(j\omega)\|_\infty$ and $M_T = \|T(j\omega)\|_\infty$. The $\mathcal{H}_\infty$ norm is addressed and discussed more in Section 2.2.5. Because the sum of sensitivities is equal to one, $S + T = 1$, at any frequency the following must be satisfied

$$\begin{aligned} ||S| - |T|| &\leq |S + T| \\ ||S| - |T|| &\leq 1 \end{aligned} \tag{2.33}$$

This implies that the peak sensitivities differ by 1 at the most. Additionally, it means that a large value of M_s occurs if and only if M_T is large. Usually for stable plants $M_s > M_T$ but not always. Note that a large peak value for either sensitivity or complimentary sensitivity indicates poor performance as well as poor robustness. The bound on the complimentary sensitivity is synonymous to the M-encirclements criteria of the Nyquist plot.

Justification for the bounding of the sensitivity peak is found in observations made on the error equations. Referring back to Eq. 2.14-2.20 and removing the control input (set $u = 0$) the control error, $e = y - r$, then becomes

$$e = G_d d - r \tag{2.34}$$

and with feedback accounted for the control error is then

$$e = S(G_d d - r) \tag{2.35}$$

From this relation, it is easy to see that feedback control improves performance by reducing the magnitude of the control error, $|e|$, at all frequencies when the magnitude of the sensitivity is less than one, $|S| < 1$. Because real systems are strictly proper at high frequencies the loop transmission approaches zero, $(L \to 0)$, which conversely means that the sensitivity approaches one, $(S \to 1)$. At low frequencies, the magnitude of the sensitivity is quite small, especially if a system contains an integrator. A peak sensitivity value larger than one, $(M_s > 1)$, is in practice unavoidable at intermediate frequencies where feedback may actually degrade performance. In these respects M_s is a measure of performance.

Additionally, M_s also acts as a robustness measure. By the Nyquist plot criteria, for closed-loop stability to be maintained, the number of encirclements of the critical point by $L(j\omega)$ must not change; therefore, it is desired that L stay away from the critical point. The minimum distance between $L(j\omega)$ and the critical point at -1 on the real axis is in fact the inverse of the peak sensitivity, $1/M_s$. Thus for robustness a smaller M_s is desired to maximize the distance from the critical point. In total, since the peak sensitivity, M_s, is a measure of both stability and performance, it is desired that M_s be close to 1.

Note that maximum peaks of the sensitivity and complimentary sensitivity are closely related to the gain and phase margins. Specifying the maximum peaks of M_s and M_T make it unnecessary to specify the gain and phase margins. Additionally, the maximum peaks can be related to bandwidth and crossover frequency specifications as well as to time domain peaks via the total variation metric. Refer to [1] for further explanation of these relations and also the formulas that relate the maximum peaks to the gain and phase margins discussed above. The important takeaway is that the maximum peaks of sensitivity and complementary sensitivity relate to the more commonly used classical control design techniques. These peaks are crucial to the loop shaping design techniques presented next.

2.2.4 Loop Shaping

There are three broad methods for controller design: Shaping of transfer functions, signal based approaches and numerical optimization. The last, numerical optimization, involves direct optimization of objectives such as rise times and stability margins and includes the on-line techniques such as model predicative control (MPC). The signal based approach includes state-space methods such as the Linear Quadratic Gaussian (LQG) where input signals are assumed to be stochastic. But, by considering sinusoidal signals via a frequency-by-frequency, scheme a signal based, infinite norm, optimal control methodology can be derived. This complex approach to robust performance has produced what is called μ-synthesis and will be discussed in a later section. First, the transfer function shaping method is covered. In the classical approach, the basic loop shaping seeks to shape the open loop transfer function $L(j\omega)$. Typically, the designer's goal is to obtain $|L(j\omega)|$ with some desired bandwidth slope. This shaping of the loop transfer function is difficult for complicated systems. The more modern approach is the shaping of the closed loop transfer functions, S and T, as well as KS, presented above. Optimizations such as the infinite norm approaches are leveraged to solve mixed weight sensitivity conditions.

Specifically, what is meant by the loop shape is the magnitude of the loop transfer function GK (or L) as a function of frequency. The manner in which the selection of K affects the loop gain is important to understand as it provides insight into the modern multivariable techniques. Recall the control error for the closed loop from Eq. 2.20, $e = Sr + SG_d d + Tn$. The desire is to reduce all sources of errors. The perfect control would then be

$$e \approx 0 \cdot r + 0 \cdot d + 0 \cdot n \tag{2.36}$$

It is easy to see the conflict in requirements here. For disturbance rejection and reference tracking the sensitivity must approximately equal 0 which means the complimentary sensitivity is approximately one (or identity): $S \approx 0 \rightarrow T \approx I$ to $\min d \,\&\, \min r$. Indirectly

this means the the loop transfer function must be large in magnitude because $S = {}^{1}/_{(I+L)}$. However, in order to drive the noise transmission to zero, the complementary sensitivity must be approximately 0 which means the sensitivity conversely must be approximately 1 (or identity): $T \approx 0 \rightarrow S \approx I$ to $\min n$. Similarly, the indirect relation is that the loop transmission must be small for the complimentary sensitivity to be small: $L \approx 0$ because $T = {}^{L}/_{(I+L)}$. Thus, T and S are in tension with each other and trade-offs are required in the allowable control, disturbance and noise errors. Additionally, it is often desired that the control input u be small due to energy and actuator hardware concerns. Here, a small u corresponds to small controller gains as evident in the control equation $u = K(r - y_m)$. This small controller gain in turn implies a small loop transfer as $L - GK$.

It would seem that the conflicting design objectives would make anything close to perfect impossible. But sometimes, these objectives occur in different frequency ranges. In practice large loop gains are implemented at low frequencies below crossover and small gains are specified at the higher frequencies above crossover. Typically, a large gain is one such that the loop transfer function is greater than one and a small gain is such the loop transfer function is less than one or $|L| > 1$ and $|L| < 1$, respectively. So, fundamentally loop shaping involves shaping the magnitude of the loop transfer function, $|L(j\omega)|$. However, while shaping the loop works well for simple problems, significant effort is required for more complex systems causing achieving stability becomes increasingly difficult. For specific details on the basics of shaping the loop $|L(j\omega)|$, refer to [1].

A better approach to shaping is found by considering directly the closed-loop transfer functions which determine the final response. The sensitivity and complementary sensitivity, S and T, are well suited closed loop transfer functions for this approach. Approximations of these sensitivities in relation to the loop transfer function are used to design for the small and large gain criteria with respect to the loop transfer function as it's easier to see how

modifying the loop transfer function will affect the controller K. The approximations are

$$|L(j\omega)| \gg 1 \Rightarrow \begin{cases} S \approx L^{-1} \\ T \approx 1 \end{cases}$$
$$|L(j\omega)| \ll 1 \Rightarrow \begin{cases} S \approx 1 \\ T \approx L^{-1} \end{cases} \tag{2.37}$$

But even here the crossover region becomes problematic because $|L(j\omega)|$ is close to 1 and very little can be inferred about S and T from the magnitude of the loop shape $|L(j\omega)|$. Alternatively, direct shaping of the magnitude of the closed loop transfer functions $S(s)$ and $T(s)$ can be carried out. This is possible via the formulation of an $\mathcal{H}_\infty$ optimal control problem. This setup allows the control designer to be concerned only with the selection of reasonable bounds, or weights, on the desired closed loop transfer functions.

2.2.5 Peak Value and the Norm

First an explanation or review of both the $\mathcal{H}_2$ and $\mathcal{H}_\infty$ norm concept is needed. The $\mathcal{H}_\infty$ norm (read as the "H-infinity norm" or simply the "infinite norm") is best understood as the peak value. More specifically, for a stable scalar transfer function $f(s)$ the $\mathcal{H}_\infty$ norm is the peak value of the magnitude of the system as a function of frequency $|f(j\omega)|$. A stable transfer function is specified because the magnitude approaches zero as the frequency approaches infinity. An unstable transfer function may have an unrealizable peak, the magnitude approaches infinity as the frequency approaches infinity. The formal expression for the definition of the infinite norm is then

$$\|f(s)\|_\infty \triangleq \max_\omega |f(j\omega)| \tag{2.38}$$

Note that for engineering purposes the "maximum" is used to define the infinite norm. In the stricter mathematical terms "sup" or supremum is the more technical term to be used instead of the maximum. This is because the supremum is the least upper bound while the maximum is only approached as the frequency approaches infinity. In practice, an infinite frequency is not achievable.

The main purpose of the infinite norm is to characterize the peaks(s) of one or more transfer functions. With a characterization of the peaks, establishing a control method can then be established that seeks to "press down" the peak(s) of the transfer function(s). This method is termed $\mathcal{H}_\infty$ control and will be discussed later.

It may be helpful to understand the infinite norm better by delving deeper into the maximum magnitude which is formally defined as the integral

$$\max_{\omega} |f(j\omega)| = \lim_{p\to\infty} \left(\int_{-\infty}^{\infty} |f(j\omega)|^p \, d\omega \right)^{1/p} \tag{2.39}$$

By raising the transfer function magnitude $|f|$ to an infinite power, the peak value can be easily determined. Also, the limit shown in Eq. 2.39 is effectively what is known as a "Hardy space". The symbol $\mathcal{H}$ represents the "Hardy space". Thus the term $\mathcal{H}_\infty$, in controls terminology, is the set of transfer functions with a bounded ∞-norm. Recall transfer functions bounded in this fashion are simply the set of stable and proper transfer functions.

The "two norm" or $\mathcal{H}_2$ norm can now better understood as it too is a Hardy space of transfer functions but these functions are instead bounded by the "2-norm". These 2-norm bounded functions are a set of stable and strictly proper transfer functions. The $\mathcal{H}_2$ norm is then defined as

$$\|f(s)\|_2 \triangleq \left(\frac{1}{2\pi} \int_{-\infty}^{\infty} |f(j\omega)|^2 \, d\omega \right)^{1/2} \tag{2.40}$$

Note that the $\mathcal{H}_2$ norm of a semi-proper transfer function (a transfer function that has nonzero magnitude as frequency approaches infinity) is infinite but the $\mathcal{H}_\infty$ norm is finite.

The sensitivity function $S = (I + GK)^{-1}$ is one such semi-proper transfer function that has an infinite $\mathcal{H}_2$ norm and a finite $\mathcal{H}_\infty$ norm.

2.3 Modern Control Concepts

The $\mathcal{H}_\infty$ robust approach takes into account both model uncertainties and performance specifications. Used initially in the chemical industry, the matrix based approach is capable of handling multi-input multi-output systems (MIMO). The system of interest can be rearranged into a single compact matrix, denoted M, and a corresponding matrix of uncertainties, denoted Δ. A technique called linear fraction transformation (LFT) handles the rearrangement. Refer to [9] for information on the LFT. Note, the LFT is sometimes also referred to as the linear fractional representation (LFR). A block representation of a system M and uncertainties Δ is shown in Figure 2.2.

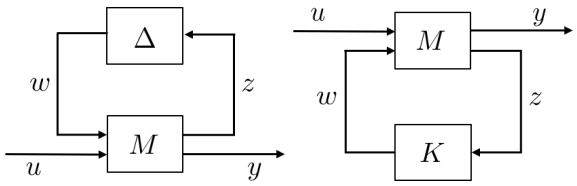

Figure 2.2: Left: M-Δ Upper LFT; Right: M-K Lower LFT

The LFT is a formulation that methodically combines blocks with feedback. It is a reorganized form of the state space system matrices augmented with uncertainty relationships. To represent a system in compact LFT form, the state space equations are rearranged such that input u is mapped to the output y and the input to uncertain block is z and the output from uncertain block is w. This linear feedback mapping from input to output is represented by

$$y = \left[M_{22} + M_{21}\Delta\left(I - M_{11}\Delta\right)^{-1} M_{12}\right] u \tag{2.41}$$

where system M is partitioned into sub-sets correlating to the inputs u and z and the outputs y and w as

$$M = \begin{bmatrix} M_{11} & M_{12} \\ M_{21} & M_{22} \end{bmatrix} \tag{2.42}$$

A system with state vector x and matrices A, B, C, D that includes uncertainty is then described by the set of relations

$$\begin{aligned} \dot{x} &= Ax + B_\Delta w + Bu \\ z &= Fx + Gw + Ju \\ y &= Cx + Hw + Du \end{aligned} \tag{2.43}$$

Writing this set of equations in a compact matrix form yields

$$\begin{bmatrix} \dot{x} \\ z \\ y \end{bmatrix} = \left[\begin{array}{c|cc} A & B_\Delta & B \\ \hline F & G & J \\ C & H & D \end{array}\right] \begin{bmatrix} x \\ w \\ u \end{bmatrix} \tag{2.44}$$

where the partitions correspond to M_{ij} subsets of Eq. 2.42. The uncertain perturbation Δ consists of n uncertain parameters, and its structured form is described by

$$w = \begin{bmatrix} \delta_1 & 0 & 0 \\ 0 & \ddots & 0 \\ 0 & 0 & \delta_n \end{bmatrix} z \tag{2.45}$$

The mapping that the compact matrix form provides is formally defined as the upper LFT

$$F_U(M, \Delta) = M_{22} + M_{21}\Delta\left(I - M_{11}\Delta\right)^{-1} M_{12} \tag{2.46}$$

An upper LFT is characterized by a system block and a second block positioned above and connected via feedback as shown on the left in Figure 2.2. Note that in the nomenclature

$F_U(M, \Delta)$, the subscript U specifies an upper transformation and the first variable, M, inside parenthesis represents the primary matrix in which the input signal u is passed in and the output signal y transmits out of. The second variable, Δ, represents the secondary block that is fed back in either an upper transformation or lower transformation. In other words, the transformation is written as an upper LFT of M in terms of the parameter Δ [1].

A lower LFT is constructed similarly and is given by the equation

$$F_L(M, K) = M_{11} + M_{12}K(I - M_{22}K)^{-1}M_{21} \tag{2.47}$$

Here K is used in place of Δ because the lower LFT is used most commonly to describe closed loop control connections for synthesis of K. The right most block formation in Figure 2.2 represents the signal structure of lower LFT.

Once the system is represented in the general form of the LFT, the modern robust control design and analysis tools can be easily applied. One such concept within the modern robust approach is the structured singular value or μ. The μ term is used to evaluate the robustness of complex uncertainty systems. Expressly written, the term is $\mu_\Delta(M)$ which is the structured singular value of a system M with respect the uncertain matrix Δ and is defined as

$$\mu_\Delta(M) = \frac{1}{\min_\Delta \{\bar{\sigma}(\Delta) : \det(I - \Delta M) = 0\}} \tag{2.48}$$

where $\bar{\sigma}$ is the maximum singular value decomposition of the uncertain matrix Δ. Note that if there is no Δ that satisfies the determinate condition, then $\mu_\Delta(M) = 0$. The system M is within the $n \times n$ complex domain, i.e. $M \in \mathbb{C}^{n\times n}$. In general, it is difficult to calculate μ directly, therefore upper and lower bounds of μ are calculated in practice.

A special case of the structured singular value is the skewed-mu or ν. For the skewed-mu case, a subset of the uncertain parameters are fixed, Δ_f, while the remaining uncertainties are allowed to vary, Δ_v. The whole uncertain matrix is thus $\Delta_s = \text{diag}(\Delta_v, \Delta_f)$. The skewed-mu is then defined as

$$\nu_{\Delta_s}(M) = \frac{1}{\min_{\Delta_s}\{\bar{\sigma}(\Delta_v) : \det(I - \Delta_s M) = 0\}} \tag{2.49}$$

where the magnitude of the fixed uncertainties must be less than one, i.e. $|\Delta_f| < 1$. Similar to the earlier definition, if there is no uncertain matrix Δ_s that satisfies the determinate condition $\det(I - \Delta_s M) = 0$, then the skewed-mu is zero, i.e. $\nu_{\Delta_s}(M) = 0$.

Additionally, the mu-sensitivity can be used to identify the uncertain parameters that are primarily responsible for the amount of robustness of the system. This sensitivity is defined as the change in μ with respect to the incremental change in a specific parameter

$$\text{Sen}_{p_j}^{\mu} = \frac{\partial \mu(M)}{\partial p_j} \approx \frac{|\mu_{\Delta}(M) - \nu_{\Delta_s}(M_\epsilon)|}{\delta p_j} \tag{2.50}$$

where M_ϵ is the perturbed system such that only the jth varying parameter p_j within the uncertain matrix is perturbed. The μ sensitivity can also be defined with respect to the skewed-mu. For more details on the μ sensitivity and the relationship to skewed-mu refer to [3, 13, 14] There are some guidelines for the composition of the fixed and varying uncertain parameters in the general case. It is normally required that the dimension of Δ_f be maximized with respect to Δ_v and that the uncertain parameters with large μ sensitivities should be place in the fixed Δ_f sub-block of uncertainties. For the exploration of parametric uncertainty in this work, the former requirement is generally easily met. Note that the implication of fixing certain parameters means that the bounds on the varying subset of uncertain parameters is relative to the specific fixed subset as well as the level of uncertainty on each within the fixed subset. The later requirement may at times be purposely violated if a single parameter is placed in the varying subset Δ_v.

2.4 Model Uncertainty

It is generally assumed that the uncertainty in a system is structured meaning that the uncertainties are independent of one another. This uncertain block Δ, for structured

uncertainty, is represented by a diagonal matrix where the terms on the diagonal correspond to a respective uncertain channel. There are several types of uncertainties: multiplicative, additive and parametric. The uncertainties can be applied to either the input or the output of a block.

2.4.1 Parametric Uncertainty

Although this work is primarily concerned with parametric uncertainty, multiplicative uncertainty can be used to account broadly for parameter variations. At the basic level, the uncertainty in a parameter can be modeled quite easily with either the upper or lower LFT. Take for example the uncertain longitudinal velocity parameter V_x which is comprised of a nominal value $\bar{V}_x$ and the relative perturbation $p_{V_x}\delta_{V_x}$ such that $V_x = \bar{V}_x\left(1 + p_{V_x}\delta_{V_x}\right)$. The parameter p_{V_x} represents some percentage of uncertainty and the parameter δ_{V_x} is the perturbation step which is bounded from $-1 < \delta_{V_x} < 1$. By Eq. 2.46 the parameter can be expressed as $F_U\left(M_{V_x}, \delta_{V_x}\right) = \bar{V}_x + p_{V_x} \cdot \delta\left(I - 0 \cdot \delta_{V_x}\right)^{-1}\bar{V}_x$ which then takes on compact matrix form

$$V_x = M_{V_x} = \begin{bmatrix} 0 & \bar{V}_x \\ p_{V_x} & \bar{V}_x \end{bmatrix} \tag{2.51}$$

This additive disturbance on velocity is represented in the block diagram in Figure 2.3 and the upper LFT of the additive disturbance is shown in Figure

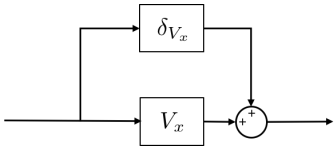

Figure 2.3: Additive Block Diagram of the Uncertain V_x Parameter

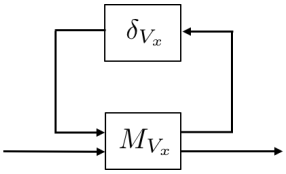

Figure 2.4: Upper LFT of the Uncertain V_x Parameter

Each uncertain parameter modeled in this LFT fashion has the advantage of being able to be combined using the standard interconnection rules specified by the upper and lower LFT definitions in Eq. 2.46 - Eq. 2.47 respectively. This is advantageous because the result of the interconnected LFT is a single but larger size LFT. Refer to [1] for a more practical study on the implementation of the $\mathcal{H}_\infty$ and LFT. The articles by [15] and [16] are recommended tutorials for the structured singular value and mixed sensitivity topics respectively. For more theoretical concerns refer to [17, 18]. For an introduction to nonlinear $\mathcal{H}_\infty$ control refer to [19]. Also, [9] and [20] contain for further details on the interconnection of LFTs. Lastly, note that when dealing with real parametric variations a small amount of complex uncertainty from 1-10% is often added to ensure that a solution to the search for μ can be found [20].

2.5 Conclusion

An overview of the robust classical control theory was presented as review and to easily transition to the sensitivity and complimentary sensitivity concepts that are used in the loop shaping control synthesis techniques. The infinite norm or "H-infinity norm" was also covered as it is the mathematical measure by which the peak value of a system response is characterized. The modern control theory topic was then introduced. First the linear fractional transformation (LFT) was explained. The benefit in this work of the LFT is primarily the formal structure to the system representation that LFT provides. But, the LFT is also extremely useful for multi-input multi-output systems (MIMO). The structured singular value μ term was then discussed. The μ value is the means by which the infinite norm is analyzed at each frequency point of a system. Next, the skew μ concept was presented whereby a subset of varying uncertainties within a block of system uncertainties can be analyzed with respect to a subset of fixed uncertainties. This skew μ concept concept is highly utilized in this dissertation in the proceeding chapters. Finally, the method of modeling real parametric uncertain in the LFT model structure was presented, which is again a concept relied on heavily in this dissertation.

Chapter 3

Vehicle Models

3.1 Introduction

This chapter presents and describes the vehicle models that are used later on as the system of interest. The relationship between the sprung and unsprung mass of the vehicle and the effects of road bank on each mass is discussed. The chapter concludes with a practical discussion on the process by which the uncertainty of parameters are incorporated into the vehicle model.

3.2 Modeling Methodology

Figure 3.1 represents the roll model of the vehicle. In this model the sprung mass rotates about the roll center. The road bank is described by the angle ϕ_r that exist between the road surface and the horizontal plane. The angle ϕ_s describes the suspension roll, or relative roll, that is due to the suspension deflections caused by the dynamics of the vehicle. The sum of the road bank and the relative roll is the total roll indicated by ϕ_v. The center of gravity is denoted by CG and the gravity vector points downward and is denoted by g. The distance from the ground surface to the roll center is h_{rc}, the distance from the roll center to the center of gravity is h_{rg} and the distance between the two wheels is track width, denoted as t_w.

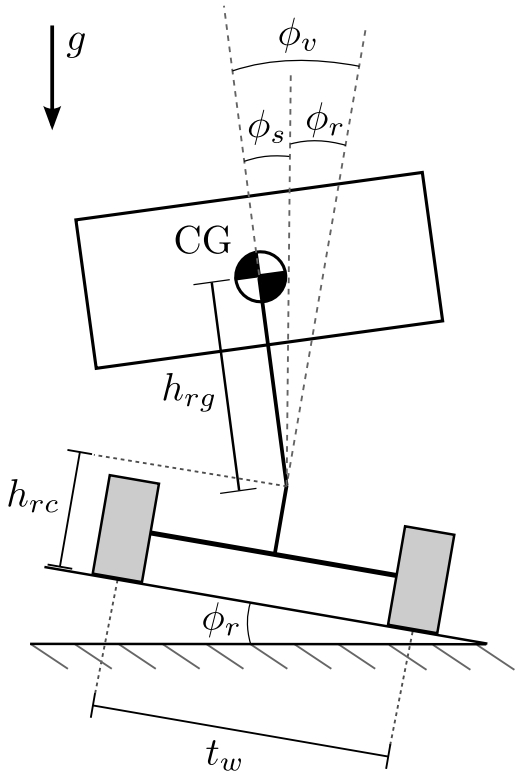

Figure 3.1: Roll Model

Coordinate frames and the transformations between various frames and intermediate frames are used to describe the rotations and rotation rates for the vehicle axle and vehicle body (i.e. the unsprung and sprung masses of the vehicle respectively). The angles and angular rates will then be incorporated into a coupled roll and yaw rate vehicle model. The vehicle model uses steer angle as an input and equations of motion that are functions of velocity. This model is then incorporated into an observer architecture to estimate states not directly measured or generated from the model.

3.2.1 Vehicle Fixed Frames

The vehicle model in this chapter builds off the more detailed roll model in Figure 3.1. The notation a represents the axle frame of the vehicle that originates at the unsprung mass. The notation b still represents the body frame however the body frame is now specified as

originating on the sprung mass of the vehicle. The Euler angle rotation is given by

$$\begin{aligned}\mathbf{C}_n^a &= \begin{bmatrix}1 & 0 & 0\\ 0 & \cos\phi_v & \sin\phi_v\\ 0 & -\sin\phi_v & \cos\phi_v\end{bmatrix}\begin{bmatrix}\cos\theta_v & 0 & -\sin\theta_v\\ 0 & 1 & 0\\ \sin\theta_v & 0 & \cos\theta_v\end{bmatrix}\begin{bmatrix}\cos\psi_v & \sin\psi_v & 0\\ -\sin\psi_v & \cos\psi_v & 0\\ 0 & 0 & 1\end{bmatrix} \\ &= \mathbf{C}_2^a\mathbf{C}_1^2C_n^1\end{aligned} \tag{3.1}$$

Note that this rotation is the inverse of the body to navigation frame rotation matrix used commonly in GNSS filters. Here, the sub and superscript 1 denote the intermediate coordinates given by the rotation about the z axis from the navigation coordinates n. The sub and superscript 2 represent the intermediate coordinates given the rotation about the y axis from the intermediate coordinate 1.

The angular velocity vector of the fixed vehicle axle frame from the navigation frame to the body frame and expressed in the body frame is defined as

$$\boldsymbol{\omega}_{an}^a = \begin{bmatrix}\phi_a\\ \theta_a\\ \psi_a\end{bmatrix} \tag{3.2}$$

By using the angular rate of the Euler angles, the axle frame fixed velocity vector can be written as

$$\begin{aligned}\boldsymbol{\omega}_{an}^a = \begin{bmatrix}\dot\phi_a\\ \dot\theta_a\\ \dot\psi_a\end{bmatrix} &= \mathbf{C}_2^a\begin{bmatrix}\dot\phi_v\\ 0\\ 0\end{bmatrix} + \mathbf{C}_2^a\mathbf{C}_1^2\begin{bmatrix}0\\ \dot\theta_v\\ 0\end{bmatrix} + \mathbf{C}_2^a\mathbf{C}_1^2\mathbf{C}_n^1\begin{bmatrix}0\\ 0\\ \dot\psi_v\end{bmatrix} \\ \begin{bmatrix}\dot\phi_a\\ \dot\theta_a\\ \dot\psi_a\end{bmatrix} &= \mathbf{J}\begin{bmatrix}\dot\phi_v\\ \dot\theta_v\\ \dot\psi_v\end{bmatrix}\end{aligned} \tag{3.3}$$

The Euler rates can then be determined from the axle fixed angular velocity vector by inverting $\mathbf{J}$, the sum of successive rotations in Eq. (3.4).

$$\begin{bmatrix} \dot{\phi}_v \\ \dot{\theta}_v \\ \dot{\psi}_v \end{bmatrix} = \begin{bmatrix} 1 & \sin\phi_v \tan\theta_v & \cos\phi_v \tan\theta_v \\ 0 & \cos\phi_v & -\sin\phi_v \\ 0 & \sin\phi_v/\sin\theta_v & \cos\phi_v/\cos\theta_v \end{bmatrix} \begin{bmatrix} \dot{\phi}_a \\ \dot{\theta}_a \\ \dot{\psi}_a \end{bmatrix} \tag{3.4}$$

$$\begin{bmatrix} \dot{\phi}_v \\ \dot{\theta}_v \\ \dot{\psi}_v \end{bmatrix} = \mathbf{J}^{-1} \begin{bmatrix} \dot{\phi}_a \\ \dot{\theta}_a \\ \dot{\psi}_a \end{bmatrix}$$

Note that because the road bank angle is defined between the vehicle frame and the intermediate coordinates 1, $\dot{\phi}_r$ is not the same as $\dot{\phi}_v$ unless θ_v the Euler pitch is zero. The road bank rate $\dot{\phi}_r$ is the x component of the angular velocity, $\boldsymbol{\omega}_{a1}^1$ which represents the angular velocity of the axle frame with respect to the intermediate coordinates 1. The angular frame rate of the vehicle axle fixed frame is

$$\boldsymbol{\omega}_{a1}^1 = \begin{bmatrix} \dot{\phi}_r \\ \dot{\theta}_r \\ \dot{\psi}_r \end{bmatrix} = \mathbf{C}_2^1 \begin{bmatrix} \dot{\phi}_v \\ 0 \\ 0 \end{bmatrix} + \begin{bmatrix} 0 \\ \dot{\theta}_v \\ 0 \end{bmatrix} \tag{3.5}$$

$$= \left(\mathbf{C}_1^2\right)^{-1} \begin{bmatrix} \dot{\phi}_v \\ 0 \\ 0 \end{bmatrix} + \begin{bmatrix} 0 \\ \dot{\theta}_v \\ 0 \end{bmatrix} \tag{3.6}$$

$$\begin{bmatrix} \dot{\phi}_r \\ \dot{\theta}_r \\ \dot{\psi}_r \end{bmatrix} = \begin{bmatrix} \cos\theta_v \dot{\phi}_v \\ \dot{\theta}_v \\ -\sin\theta_v \dot{\phi}_v \end{bmatrix} \tag{3.7}$$

Thus the road bank rate is defined as

$$\dot{\phi}_r = \cos\theta_v \dot{\phi}_v \tag{3.8}$$

and from Eq.(3.4) the road bank equation can also be written as

$$\dot{\phi}_r = \cos\theta_v \dot{\phi}_a + \sin\phi_v \sin\theta_v \dot{\theta}_a + \cos\phi_v \sin\theta_v \dot{\psi}_a \tag{3.9}$$

Typically the mounting location for an IMU in a vehicle is somewhere on the vehicle body not the vehicle axle. The relationship between the vehicle body fixed frame and the vehicle axle fixed frame is the transformation

$$\mathbf{C}_a^b = \begin{bmatrix} 1 & 0 & 0 \\ 0 & \cos\phi_s & \sin\phi_s \\ 0 & -\sin\phi_s & \cos\phi_s \end{bmatrix} \tag{3.10}$$

Using Eq. (3.10), the IMU measurements in the body fixed frame can be expressed as

$$\boldsymbol{\omega}_{ab}^b = \begin{bmatrix} \dot{\phi}_b \\ \dot{\theta}_b \\ \dot{\psi}_b \end{bmatrix} = \begin{bmatrix} \dot{\phi}_s \\ 0 \\ 0 \end{bmatrix} + \mathbf{C}_a^b \begin{bmatrix} \dot{\phi}_a \\ \dot{\theta}_a \\ \dot{\psi}_a \end{bmatrix} \tag{3.11}$$

This reveals that the roll rate and yaw rate equations for the body fixed frame are

$$\dot{\phi}_b = \dot{\phi}_s + \dot{\phi}_a \tag{3.12}$$

$$\dot{\psi}_b = \cos\phi_v \dot{\psi}_a - \sin\phi_s \dot{\theta}_a \tag{3.13}$$

Note that Eq. (3.12) shows that the roll rate of the body is the sum of the roll rate from the sprung mass (vehicle body) and the roll rate of the axle. Even though the bank of a road is built with "x" amount of bank, the amount "x" is measured perpendicular to the direction

of travel on the road. The bank experienced by a vehicle is only equal to the amount "x" when the orientation of the vehicle is such that the x-axis of the vehicle is parallel to the direction of travel of the road.

To implement the equations into vehicle models, some simplifications need to be made. Eq. (3.9) can be rewritten assuming that the total pitch angle, θ_v, of the vehicle vehicle is small such that $\cos\theta_v \approx 1$ and the variable ϵ_r is created to lump the effects of axle pitch rate, axle yaw rate, total roll and total pitch ,$\dot{\theta}_a$, $\dot{\psi}_a$, ϕ_v and θ_v, together . This yields

$$\dot{\phi}_r \approx \dot{\phi}_a + \epsilon_r \tag{3.14}$$

$$\epsilon_r = \sin\phi_v \sin\theta_v \dot{\theta}_a + \cos\phi_v \sin\theta_v \dot{\psi}_a \tag{3.15}$$

Finally, assuming that the vehicle roll angle ϕ_s and the vehicle axle pitch rate $\dot{\theta}_a$ are small, Eq. (3.13) can be simplified to

$$\dot{\psi}_b \approx \dot{\psi}_a \tag{3.16}$$

3.2.2 Coupled Roll and Yaw Model

The vehicle dynamics are modeled with a bicycle model coupled with a roll model as in [21, 22, 23, 24] . Figure 3.2 displays the two dimensional relationship between the vehicle frame and the navigation frame for reference. The navigation frame, shown in Figure 3.2, is the north-east-down frame thus the lateral velocity for the velocity vector, V, is negative in the vehicle z-up frame. Observe that the vehicles course, the direction of travel and denoted by ν, is not equal to the heading of the vehicle, ψ_b. This results in vehicle side-slip, β, and means that a velocity exists not only in the longitudinal, x direction, of the vehicle but also in the lateral, y direction, of the vehicle. The change in this lateral velocity, $\dot{V}_y$, will be used to formulate the equations of motion.

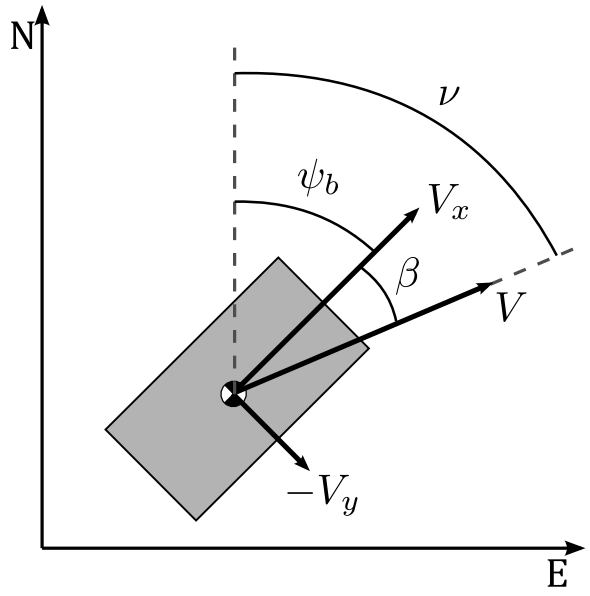

Figure 3.2: Navigation Frame

Figures 3.3 and 3.4 represent the lateral and roll vehicle model. In Figure 3.3, the steer angle is represented by δ, $\dot{\psi}_b$ is the yaw rate of the vehicle body frame, β is the side slip angle at the center of the mass, V_x and V_y are the longitudinal and lateral velocity components of the velocity vector $\mathbf{V}$. The lateral tire forces are denoted as $\mathbf{F}_{yF}$ for the front and $\mathbf{F}_{yR}$ for the rear. Similarly, α_f and α_r are the front and rear axle slip angles.

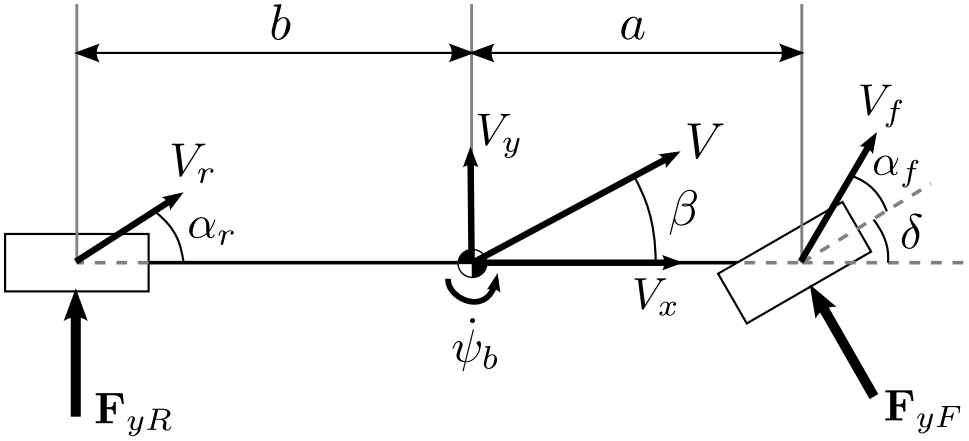

Figure 3.3: Schematic of the Bicycle Model (with all Forces and Angles Shown in Positive Direction)

The tire force is modeled using the cornering stiffness C_α as a linear relationship between the slip angle and tire force such that

$$\mathbf{F}_{yF} = -C_{\alpha f}\alpha_f \tag{3.17}$$

$$\mathbf{F}_{yR} = -C_{\alpha r}\alpha_r \tag{3.18}$$

where $C_{\alpha f}$ and $C_{\alpha r}$ are the cornering stiffness parameters for the front and rear axle respectively. Eq. (3.17) - (3.18) assume small slip angles α_f and α_r such that vehicle operates in the linear region of the tire curve modeled by the cornering stiffness. In the bicycle model the inner and outer slip angles at the wheels are assumed to be equal.

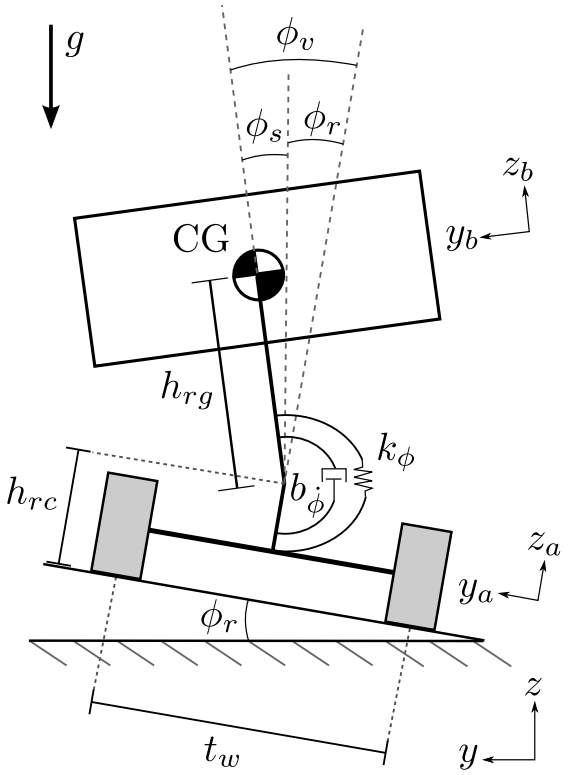

Figure 3.4: Roll Model

Using Newton's relationship to sum sum the forces and moments found in the bicycle model from Figure 3.3 and the roll model in Figure 3.4, the coupled equations of motion for the bicycle and roll model are

$$\dot{V}_y = \frac{I_{eq}C_0}{I_{xx}mV_x}V_y - \left(V_x + \frac{I_{eq}C_1}{I_{xx}mV_x}\right)\dot{\psi}_a - \frac{h_{rg}B_{\dot{\phi}}}{I_{xx}}\dot{\phi}_s + \frac{h\left(mgh_{rg} - K_\phi\right)}{I_{xx}}\phi_s + \frac{I_{eq}C_{\alpha f}}{I_{xx}m}\delta - g\phi_r \quad (3.19)$$

$$\ddot{\psi}_a = -\frac{C_1}{I_{zz}V_x}V_y - \frac{C_2}{I_{zz}V_x}\dot{\psi}_a + \frac{aC_{\alpha f}}{I_{zz}}\delta \quad (3.20)$$

$$\ddot{\phi}_v = -\frac{C_0h_{rg}}{I_{xx}V_x}V_y - \frac{C_1h_{rg}}{I_{xx}V_x}\dot{\psi}_a - \frac{B_{\dot{\phi}}}{I_{xx}}\dot{\phi}_s + \frac{mgh_{rg} - K_\phi}{I_{xx}}\phi_s + \frac{C_{\alpha f}h_{rg}}{I_{xx}}\delta - \ddot{\phi}_a \quad (3.21)$$

where

$$C_0 = C_{\alpha f} + C_{\alpha r} \quad (3.22)$$

$$C_1 = aC_{\alpha f} - bC_{\alpha r} \quad (3.23)$$

$$C_2 = a^2C_{\alpha f} + b^2C_{\alpha r} \quad (3.24)$$

$$I_{eq} = I_{xx} + mh_{rg}^2 \quad (3.25)$$

In these equations, I_{zz} is the moment of inertial about the z, or yaw, axis. The total mass of the vehicle is represented by m. The terms a and b denote the front and rear weight splits relative to the center of gravity. The effect of the unsprung mass is assumed to be minimal. Therefore, this yaw dynamic model assumes a mass-less axle. The moment of inertia about the x axis, the roll axis, is represented by I_{xx}. K_ϕ is the roll stiffness and $B_{\dot{\phi}}$ is the roll damping. The term h_{rg} is the distance from the roll axis to the center of gravity on the sprung mass. The angular acceleration of the axle, $\ddot{\phi}_a$, is related through Eq. (3.14) because the axle frame is assumed to remain in contact with the ground surface by means of the tires.

The coupled roll and bicycle model is represented in state space with the state transition matrix $\mathbf{A}$, input vector $\mathbf{B}$, and two disturbance vectors B_{w1} and B_{w2} such that

$$\dot{\mathbf{x}} = \mathbf{A}\mathbf{x} + \mathbf{B}\delta + \mathbf{B}_{w1}\phi_r + \mathbf{B}_{w2}\ddot{\phi}_a \quad (3.26)$$

where

$$\mathbf{A} = \begin{bmatrix} \frac{I_{eq}C_0}{I_{xx}mV_x} & -\left(V_x + \frac{I_{eq}C_1}{I_{xx}mV_x}\right) & -\frac{h_{rg}B_{\dot{\phi}}}{I_{xx}} & \frac{h\left(mgh_{rg}-K_\phi\right)}{I_{xx}} \\ -\frac{C_1}{I_{zz}V_x} & -\frac{C_2}{I_{zz}V_x} & 0 & 0 \\ -\frac{C_0h_{rg}}{I_{xx}V_x} & -\frac{C_1h_{rg}}{I_{xx}V_x} & -\frac{B_{\dot{\phi}}}{I_{xx}} & \frac{mgh_{rg}-K_\phi}{I_{xx}} \\ 0 & 0 & 1 & 0 \end{bmatrix} \tag{3.27}$$

$$\mathbf{B} = \begin{bmatrix} \frac{I_{eq}C_{\alpha f}}{I_{xx}m} \\ \frac{aC_{\alpha f}}{I_{zz}} \\ \frac{C_{\alpha f}h_{rg}}{I_{xx}} \\ 0 \end{bmatrix} \tag{3.28}$$

$$\mathbf{B}_{w1} = \begin{bmatrix} -g \\ 0 \\ 0 \\ 0 \end{bmatrix} \tag{3.29}$$

$$\mathbf{B}_{w2} = \begin{bmatrix} 0 \\ 0 \\ -1 \\ 0 \end{bmatrix} \tag{3.30}$$

The state vector $\mathbf{x}$ is

$$\mathbf{x} = \begin{bmatrix} V_y \\ \dot{\psi}_a \\ \dot{\phi}_s \\ \phi_s \end{bmatrix} \tag{3.31}$$

3.2.3 Yaw model

Note, in Section 4.3 a vehicle model that includes only the lateral dynamics is used to demonstrate some of the basics of the process for including parametric uncertainty in a model. This reduced state model decouples the roll states from coupled yaw-roll model. The equations of motion for the yaw model reduce to

$$\dot{V}_y = \frac{C_0}{mV_x}V_y - \left(V_x + \frac{C_1}{mV_x}\right)\dot{\psi}_a + \frac{C_{\alpha f}}{m}\delta \tag{3.32}$$

$$\ddot{\psi}_a = -\frac{C_1}{I_{zz}V_x}V_y - \frac{C_2}{I_{zz}V_x}\dot{\psi}_a + \frac{aC_{\alpha f}}{I_{zz}}\delta \tag{3.33}$$

3.3 Model Accuracy and Fidelity

Simulations are performed using CarSim 9, a commercial software package used heavily in the automotive industry, for system development. The software, developed by Mechanical Simulation Corporation, provides a high fidelity simulation environment, and allows the user to view a number of vehicle outputs. The software has been accepted by industry as accurately representing vehicle dynamics. CarSim data is often used as a truth measurement in simulation. The coupled roll and bicycle model is validated against the CarSim high fidelity model for a small SUV. Steer angle and velocity output from CarSim simulations were used as inputs to the coupled vehicle model simulations performed in Matlab. The output states from the coupled vehicle model were then compared to the corresponding vehicle states from the same CarSim simulations.

3.3.1 CarSim and the Double Lane Change

The vehicle used in the simulations was the Class SUV in CarSim which has vehicle parameters typically associated with the SUV or crossover class of vehicle. The parameters for the SUV are provided in Table A.1 of Appendix A. A maneuver called the double lane change (DLC) is the industry standard for testing dynamic roll properties for various vehicles.

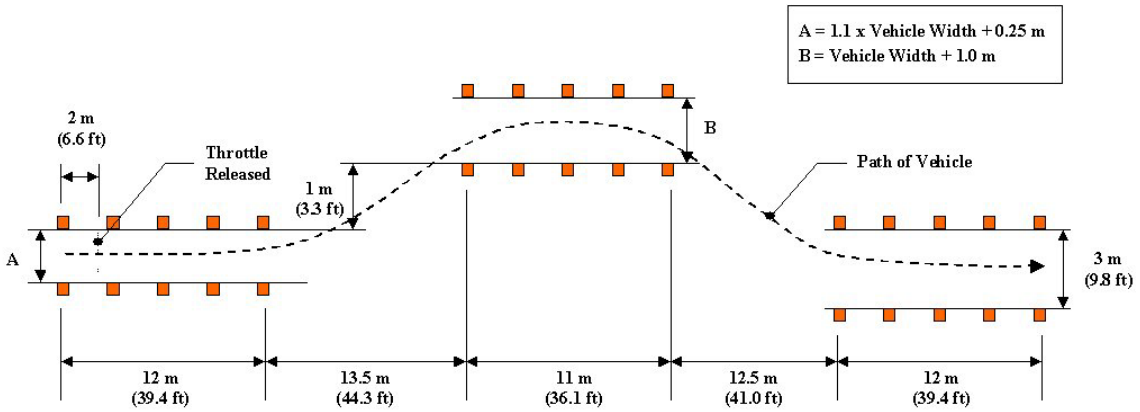

Figure 3.5: ISO 3888-2 Double Lane Change Specification

Figure 3.5 represents the ISO 3888-2 standard for a DLC [25]. Observe that the width of the starting lane and intermediate lane are function of the vehicle width. For verification of the model, the steer input (and other relevant inputs such as road bank where required) from the CarSim data was feed into the vehicle model in MATLAB and the output channels from the vehicle model and the CarSim model data were compared.

3.3.2 Model Validation

The steering input for the double lane change (DLC) is represented in Figure 3.6. This steering input is the angle δ at the tire as modeled by the yaw model from Figure 3.3. Figures 3.7 and 3.8 show the output comparison of a DLC maneuver at 20 km/hr. At this speed the coupled vehicle model and the CarSim model compare quite well.

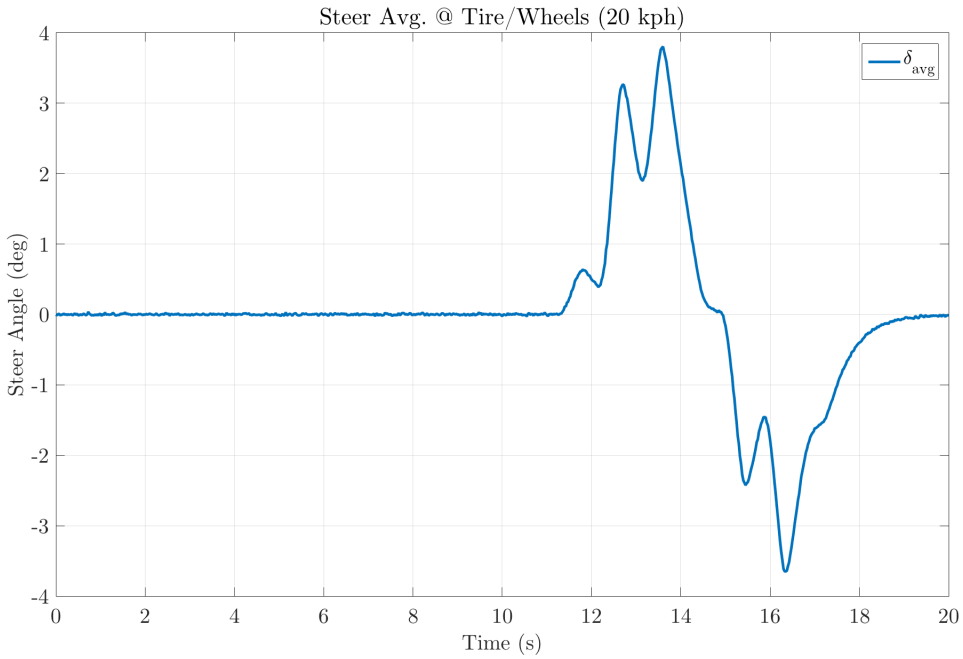

Figure 3.6: Input of Steer Angle to the Model for a DLC at 20 km/hr

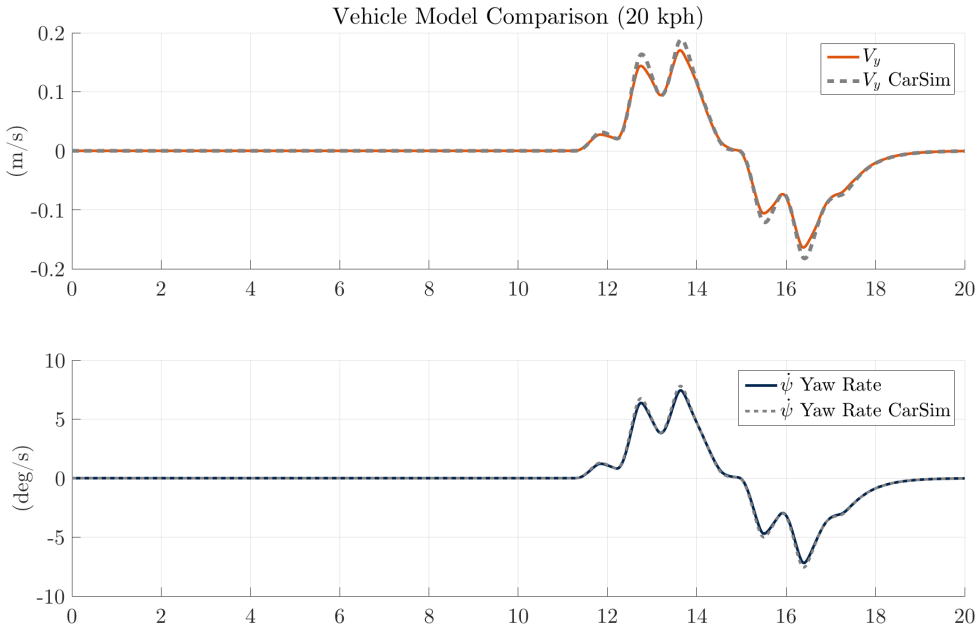

Figure 3.7: Model Comparison of Lateral Velocity and Yaw Rate for a DLC at 20 km/hr

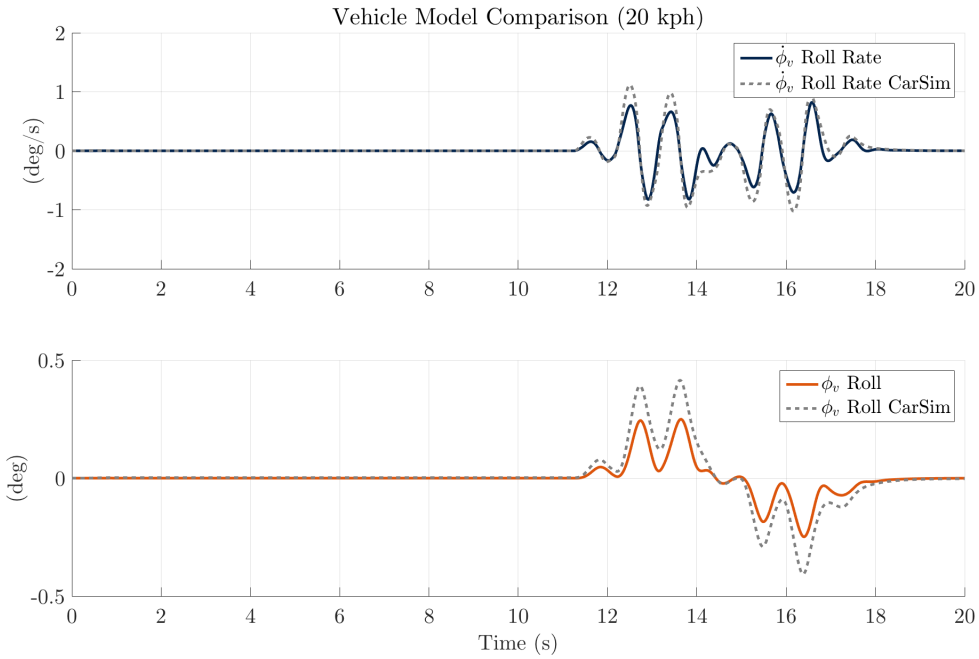

Figure 3.8: Model Comparison of Roll Rate and Roll for a DLC at 20 Km/hr

At higher speeds the coupled vehicle model and the CarSim models diverge more significantly. Figures 3.9 - 3.11 represent the same double lane change maneuver performed at 90 km/hr. Note that for this faster target speed the steering is much more aggressive in both magnitude and that the minor correction present in the Figure 3.6 at 20 km/hr target now become full counter steer correction in Figure 3.11 at the 90 km/hr target speed. A double lane change at this highway speed is indeed a very aggressive maneuver.

Noticeably in Figure 3.9 and 3.10, all four states of the coupled yaw-roll model are marked by deviations from the higher fidelity CarSim simulation data. This separation is due potentially to the non-linear saturation from the tire forces that are unmodeled in the linear tire model used in the coupled vehicle model. The presence of nonlinear springs and dampers in the suspension of the CarSim model are another example where differences in outputs may be attributed. The tire model used in coupled yaw-roll model does not account for changes in tire loading which can greatly affect the available force in the lateral and longitudinal directions generated at the tire contact patch. From this, it can be concluded

that at low speeds and low dynamics the coupled vehicle model is an appropriate model, but at high speeds and high dynamics the coupled vehicle model is not as reliable.

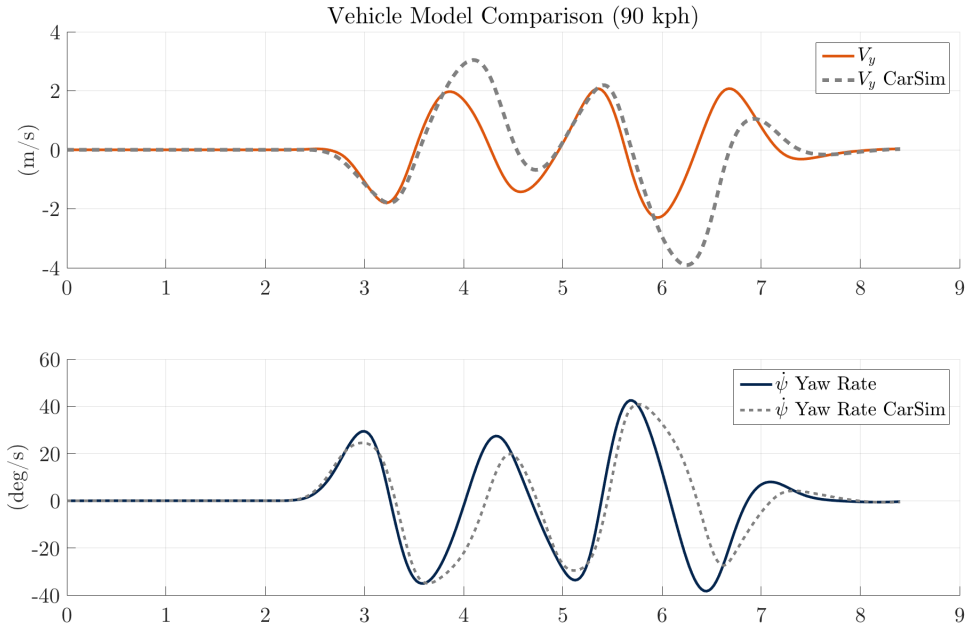

Figure 3.9: Model Comparison of Lateral Velocity and Yaw Rate for a DLC at 90 km/hr

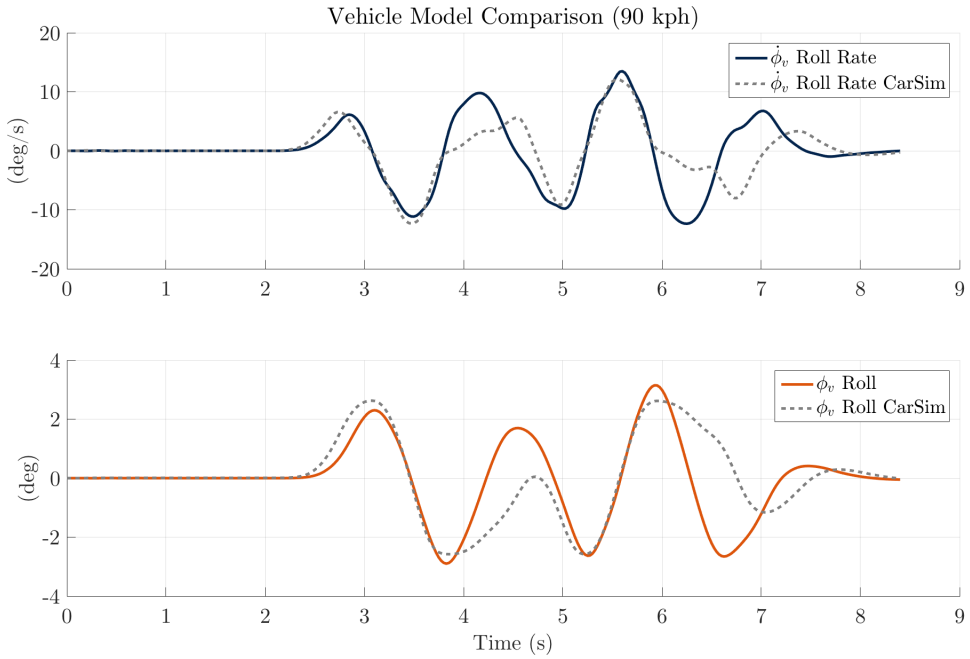

Figure 3.10: Model Comparison of Roll Rate and Roll for a DLC at 90 km/hr

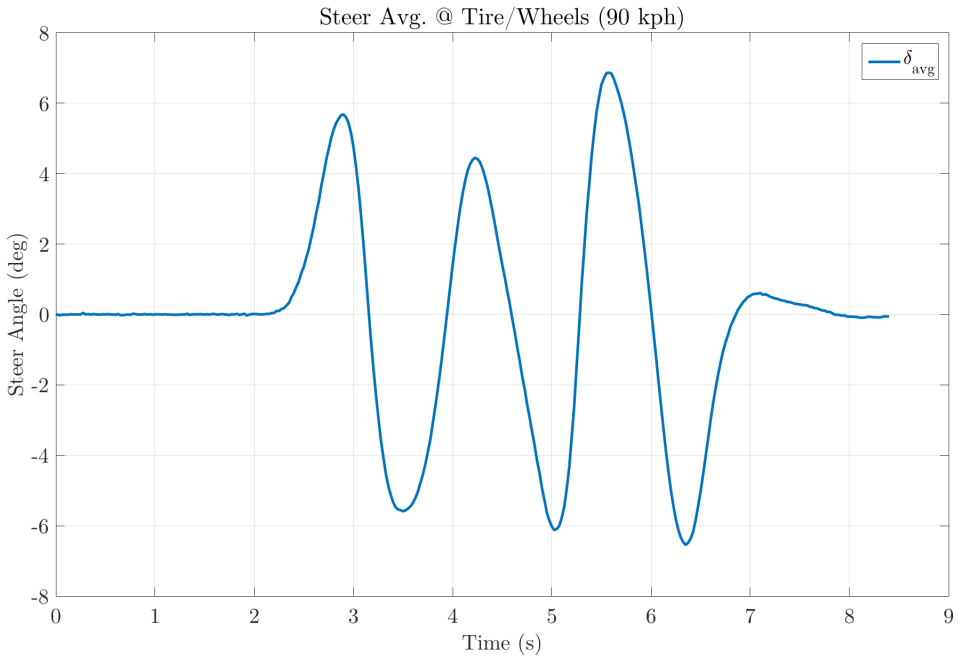

Figure 3.11: Steer Input for Model Comparison of a DLC at 90 km/hr

The errors of each state are shown in Figures 3.12 and 3.13 to give a better visualizations of the scale in time of the differences between the coupled model and the CarSim high fidelity simulation. It is clear that the peak error is much greater at the higher target speed of 90 km/hr. But, aggregating these errors into a single root mean squared metric for the entire run at the given target speed quantifies the trend of the suitability of the coupled yaw-roll model.

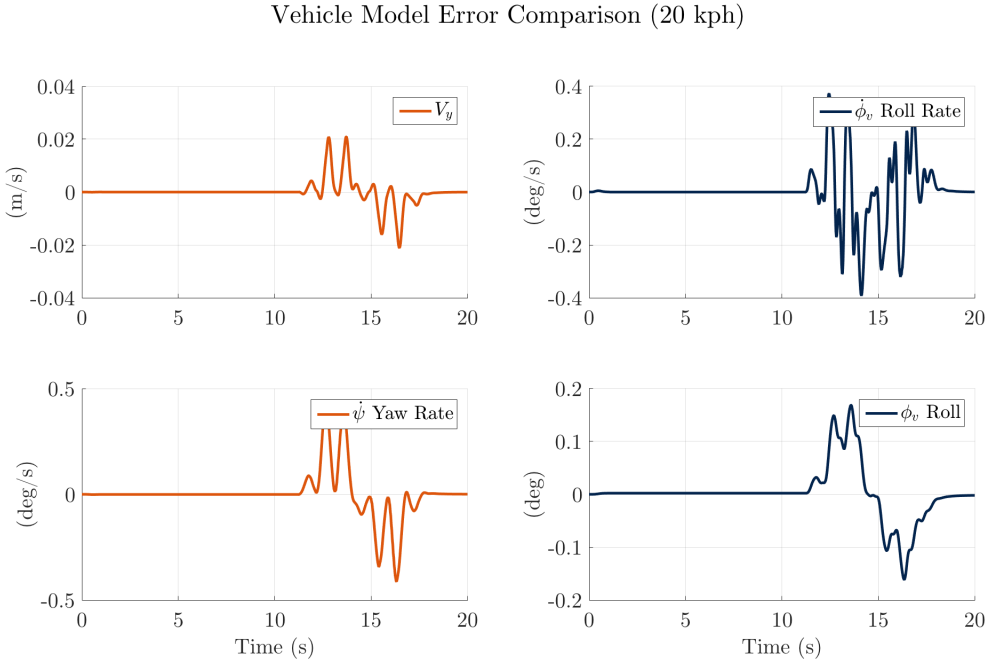

Figure 3.12: Model Comparison Errors for a DLC at 20 km/hr

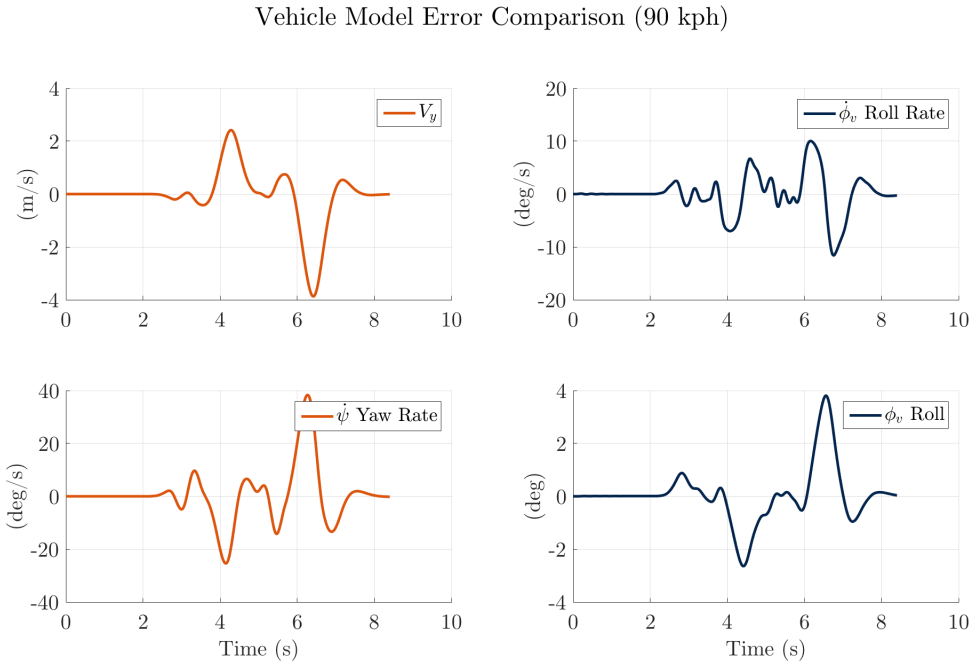

Figure 3.13: Model Comparison Errors for a DLC at 90 km/hr

3.3.3 Root Mean Squared ErrorAnalysis

Assessing the model in terms of the root mean squared (RMS) error is beneficial to broadly capture the reliability of the model across a range of target speeds. Figure 3.14 represents the lateral velocity and yaw rate RMS errors for the coupled yaw-roll model at various set speeds. While Figure 3.15 portrays the RMS error for the roll and roll rate states. The model deviations, viewed holistically as RMS errors across several target speeds, demonstrate a nonlinear and increasing trend in errors that correlates with the target speed of the maneuver. This further validates that the model is less reliable at the higher dynamics due to the higher speeds.

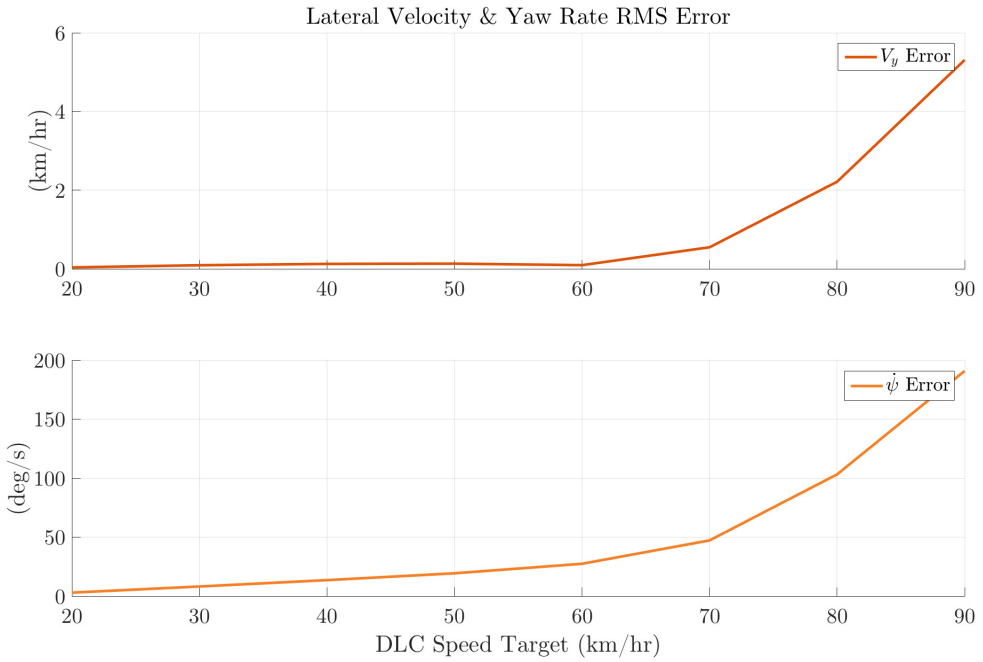

Figure 3.14: RMS Error of Lateral Velocity and Yaw Rate for the DLC across the Range of Target Speeds

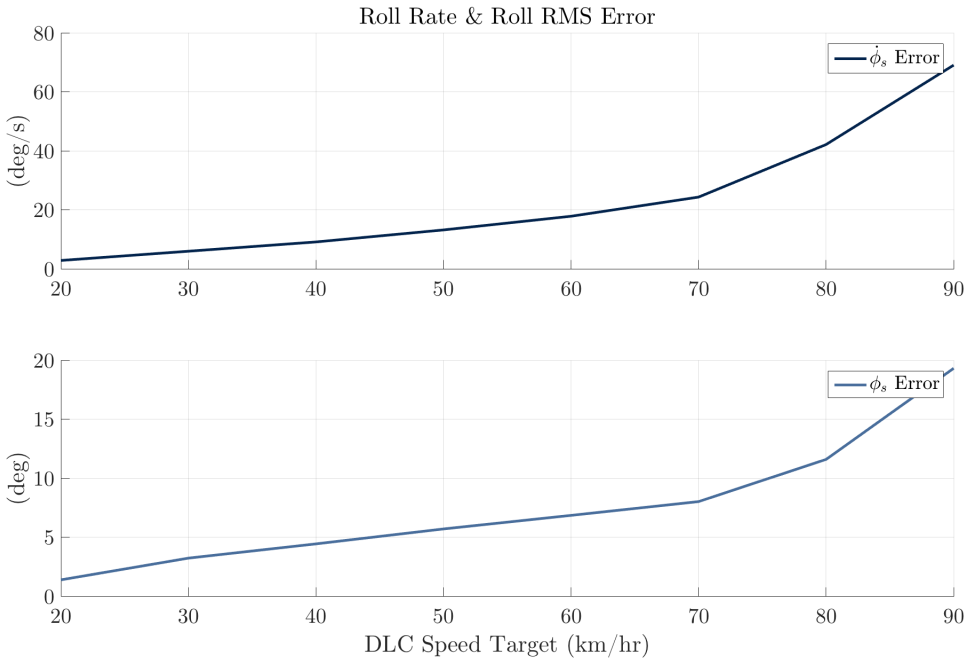

Figure 3.15: RMS Error of Roll Rate and Roll for the DLC across the Range of Target Speeds

3.4 Conclusion

The couple yaw-roll model was derived and validated against the higher fidelity CarSim vehicle system for the Class D SUV. The parameters for the coupled yaw-roll model were pulled from the information available on the CarSim Class D SUV and approximated where appropriate. For example, the slope of the tire force curve vs slip angle was used for the cornering stiffness values. Both the yaw-roll model and the CarSim system were subjected to an industry standard double lane change (DLC) maneuver across several target speeds to excite the dynamics. Analysis showed that the yaw-roll model represents the system sufficiently around moderate speeds of 60 kph and below. Above these moderate speeds for the high dynamic maneuvers the yaw-roll model becomes less reliable. This reliability was quantified with a root mean squared analysis of the errors for the lateral velocity, yaw rate, roll rate and roll vehicle states. A quadratic trend in the errors of these states was observed with the errors being less at the lower velocities.

Chapter 4

Accounting for Parametric Uncertainty Vehicle Models

4.1 Introduction

This chapter presents methods for incorporating the uncertainty of the parameters in the vehicle models. The issue of coupled and repeated parameters is tackled with a tedious but systematic approach using the LFT. The chapter concludes with system responses of the vehicle model plants under various combinations of uncertainty perturbations.

4.2 Model Limitations and Parametric Uncertainty

The amount of deviation seen in the vehicle states at higher dynamic conditions in the previous chapter serves as a rough indicator of the overall confidence in any calculations of allowable parametric uncertainties. However, this should not be a deterrence to exploring the parametric uncertainty bounds of the model. The designer must keep in mind the limitations of any model of interest that doesn't capture the dynamics of the system. A parametric model with greater system response matching can be expected to have more reliable uncertainty bounds. It is important therefore to understand the limits of the model as whole before considering the limits of the parameters within the model.

4.3 Incorporating Uncertainty

To incorporate uncertainty for simple systems with decoupled and non-repeated parameters the process is fairly straightforward and can be achieved in several ways. The first method is via the system equations and involves isolating the parameters and manipulation of the state space matrices. This method is ideal for simple systems or systems with only a

few parameters of interest that have no coupling. The equation method can also be used on systems where the parameters are grouped as a single term that affects the state. However, it is not recommended to group parameters for the uncertainty perturbations with the hope of decoupling the parameters post skew μ calculations as the decoupling is nontrivial and may not be feasible. However, some methods in the literature rely on polynomial functions and finite impulse response models to handle correlated parameter variations [2]. Other research of parametric uncertainty either examine systems without coupling and repeated parameter instances [26] or the parametric terms are treated as state coefficients [3].

An alternate and preferred method draws heavily from the LFT concepts. Though this LFT building block method is more tedious, it is much more elemental in process and the technique can handle both repeated parameters and parameters that are coupled via multiplication. Both a standard system equation method and an LFT base-block method are presented for demonstration purposes with a relatively simple version of the vehicle model that consists of the just the lateral dynamics. The yaw model equations of motion from Eq. 3.32 and 3.33 are reprinted here for convenience of reference in the next section.

$$\dot{V}_y = \frac{C_0}{mV_x}V_y - \left(V_x + \frac{C_1}{mV_x}\right)\dot{\psi}_a + \frac{C_{\alpha f}}{m}\delta$$

$$\ddot{\psi}_a = -\frac{C_1}{I_{zz}V_x}V_y - \frac{C_2}{I_{zz}V_x}\dot{\psi}_a + \frac{aC_{\alpha f}}{I_{zz}}\delta$$

4.3.1 System Equation Uncertainty Incorporation Technique

Once the system equation is derived and the parameters of interest are selected, this technique requires the generation of a block diagram directly from the system equations. For this initial example, the front and rear cornering stiffnesses are selected as the parameters of which the variation and affects thereof are of interest. Once the basic block diagram is created, the blocks containing parameter variations are augmented with a variation signal specific to the instance in the diagram where the parameter appears. Figure 4.1 is representation of the block diagram of the lateral vehicle dynamics with the variations of front

and rear cornering stiffnesses included. Then the states, state derivatives and inputs to the system are appropriately labeled. Additionally, the signal entering the variation block δ_p is label z_n and the signal exiting the variation block is labeled d_n, where p is the parameter symbol and n is the variation signal number. For parameters that are repeated, there will be multiple entrance and exit signals matching the number of times the parameter appear in the block diagram.

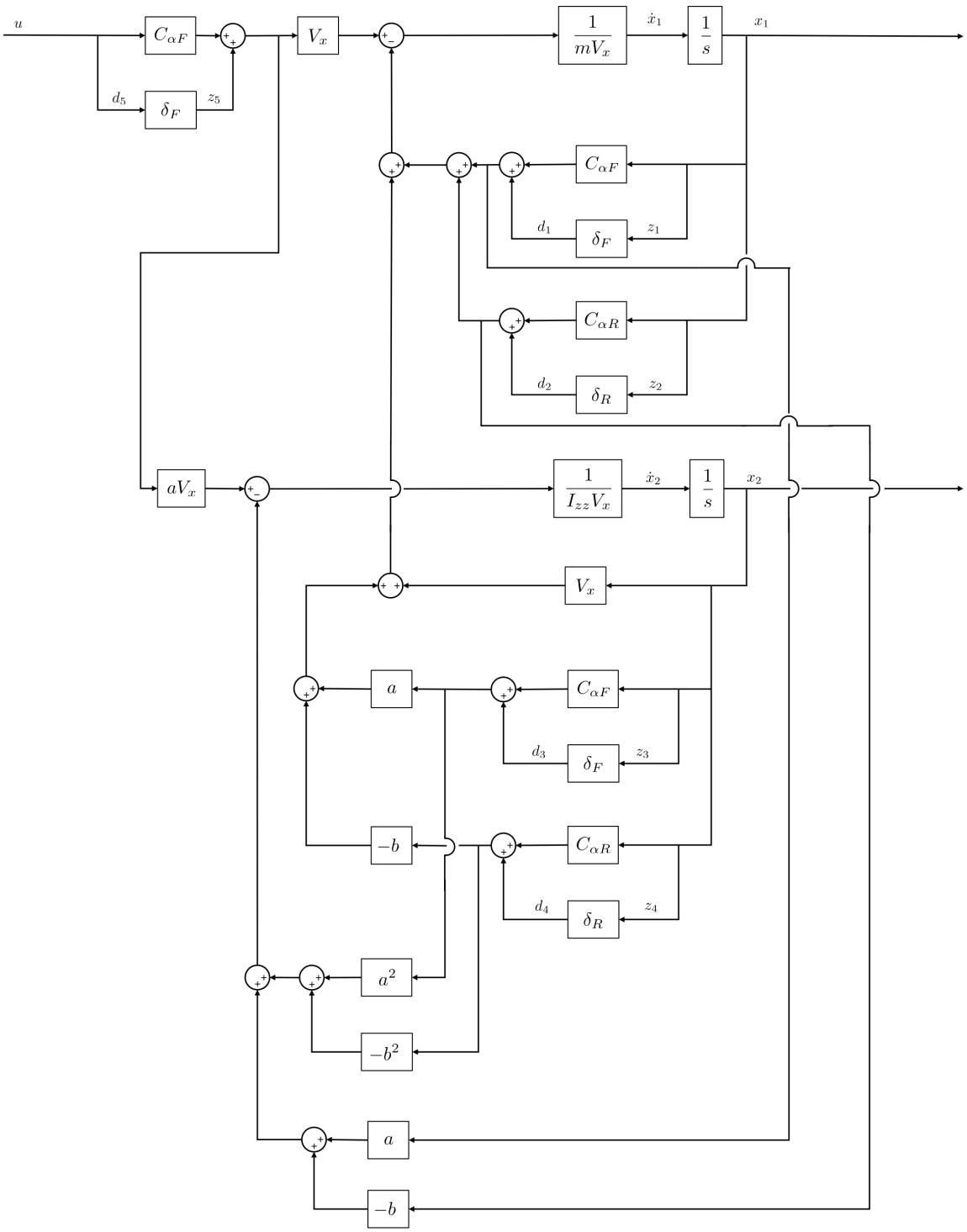

Figure 4.1: Block Diagram of the Lateral Vehicle Dynamics with Uncertainty on $C_{\alpha F}$ and $C_{\alpha R}$

The new system of equations with the variations included becomes

$$\dot{x}_1 = -\frac{(C_{\alpha F}+C_{\alpha R})}{mV_x}x_1 + \left(-V_x - \frac{(aC_{\alpha F}-bC_{\alpha R})}{mV_x}\right)x_2 - \frac{1}{mV_x}d_1 - \frac{1}{mV_x}d_2 - \frac{a}{mV_x}d_3 + \ldots$$
$$\frac{b}{mV_x}d_4 + \frac{V_x}{mV_x}d_5 + \frac{V_x C_{\alpha F}}{mV_x}u \tag{4.1}$$

$$\dot{x}_2 = -\frac{(aC_{\alpha F}-bC_{\alpha R})}{I_{zz}V_x}x_1 - \frac{\left(a^2C_{\alpha F}+b^2C_{\alpha R}\right)}{I_{zz}V_x}x_2 - \frac{a}{I_{zz}V_x}d_1 + \frac{b}{I_{zz}V_x}d_2 - \frac{a^2}{I_{zz}V_x}d_3 + \ldots$$
$$\frac{b^2}{I_{zz}V_x}d_4 + \frac{aV_x}{I_{zz}V_x}d_5 + \frac{aV_x C_{\alpha F}}{I_{zz}V_x}u \tag{4.2}$$

where x_1 is the lateral velocity V_y and x_2 is the yaw rate $\dot{\psi}$. The mappings from uncertainty to system states are

$$\begin{aligned} z_1 &= x_1 \\ z_2 &= x_1 \\ z_3 &= x_2 \\ z_4 &= x_2 \\ z_5 &= u \end{aligned}$$

These mappings to the system states are used to construct a matrix representation of the vehicle system with uncertainties. The state space representation then becomes

$$\begin{bmatrix} \dot{x}_1 \\ \dot{x}_2 \end{bmatrix} = \underbrace{\begin{bmatrix} -\frac{(C_{\alpha F}+C_{\alpha R})}{mV_x} & -V_x - \frac{(aC_{\alpha F}-bC_{\alpha R})}{mV_x} \\ -\frac{(aC_{\alpha F}-bC_{\alpha R})}{I_{zz}V_x} & -\frac{\left(a^2C_{\alpha F}+b^2C_{\alpha R}\right)}{I_{zz}V_x} \end{bmatrix}}_{A} \begin{bmatrix} x_1 \\ x_2 \end{bmatrix} + \dots$$

$$\underbrace{\begin{bmatrix} -\frac{1}{mV_x} & -\frac{1}{mV_x} & -\frac{a}{mV_x} & -\frac{b}{mV_x} & \frac{1}{m} \\ -\frac{a}{I_{zz}V_x} & \frac{b}{I_{zz}V_x} & -\frac{a^2}{I_{zz}V_x} & -\frac{b^2}{I_{zz}V_x} & \frac{a}{I_{zz}} \end{bmatrix}}_{B_{\Delta,\,\mathrm{Pre}}} \begin{bmatrix} d_1 \\ d_2 \\ d_3 \\ d_4 \\ d_5 \end{bmatrix} + \underbrace{\begin{bmatrix} \frac{C_{\alpha F}}{m} \\ \frac{aC_{\alpha F}}{I_{zz}} \end{bmatrix}}_{B} u \tag{4.3}$$

$$\begin{bmatrix} z_1 \\ z_2 \\ z_3 \\ z_4 \\ z_5 \end{bmatrix} = \underbrace{\begin{bmatrix} 1 & 0 \\ 1 & 0 \\ 0 & 1 \\ 0 & 1 \\ 0 & 0 \end{bmatrix}}_{F} \begin{bmatrix} x_1 \\ x_2 \end{bmatrix} + \underbrace{\begin{bmatrix} 0 & \cdots & 0 \\ & \ddots & \\ \vdots & 0 & \vdots \\ & & \ddots \\ 0 & \cdots & 0 \end{bmatrix}}_{G} \begin{bmatrix} d_1 \\ d_2 \\ d_3 \\ d_4 \\ d_5 \end{bmatrix} + \underbrace{\begin{bmatrix} 0 \\ 0 \\ 0 \\ 0 \\ 1 \end{bmatrix}}_{J} u \tag{4.4}$$

$$y = \underbrace{\begin{bmatrix} 0 & 1 \end{bmatrix}}_{C} \begin{bmatrix} x_1 \\ x_2 \end{bmatrix} + \underbrace{\begin{bmatrix} 0 & 0 & 0 & 0 & 0 \end{bmatrix}}_{H} \begin{bmatrix} d_1 \\ d_2 \\ d_3 \\ d_4 \\ d_5 \end{bmatrix} + \underbrace{[0]}_{D} u \tag{4.5}$$

Note that the matrix $B_{\Delta,\,\mathrm{Pre}}$ is what is derived via block diagram rules from the system diagram. To capture the effect of variation in parameters, this pre-matrix is multiplied by a

diagonal matrix of the relative variations and is described by,

$$B_{\Delta} = B_{\Delta,\,\mathrm{Pre}} S_{5\times 5} \tag{4.6}$$

where

$$B_{\Delta,\,\mathrm{Pre}} = \begin{bmatrix} -\frac{1}{mV_x} & -\frac{1}{mV_x} & -\frac{a}{mV_x} & -\frac{b}{mV_x} & \frac{1}{m} \\ -\frac{a}{I_{zz}V_x} & \frac{b}{I_{zz}V_x} & -\frac{a^2}{I_{zz}V_x} & -\frac{b^2}{I_{zz}V_x} & \frac{a}{I_{zz}} \end{bmatrix} \tag{4.7}$$

and

$$S_{5\times 5} = \begin{bmatrix} p_{C_{\alpha F}}\bar{C}_{\alpha F} & 0 & 0 & 0 & 0 \\ 0 & p_{C_{\alpha R}}\bar{C}_{\alpha R} & 0 & 0 & 0 \\ 0 & 0 & p_{C_{\alpha F}}\bar{C}_{\alpha F} & 0 & 0 \\ 0 & 0 & 0 & p_{C_{\alpha R}}\bar{C}_{\alpha R} & 0 \\ 0 & 0 & 0 & 0 & p_{C_{\alpha F}}\bar{C}_{\alpha F} \end{bmatrix} \tag{4.8}$$

Denoting the relative variation with an S_x where x is the uncertain parameter the matrix that injects uncertainty into the nominal system is then

$$B_{\Delta} = \begin{bmatrix} -\frac{S_{\alpha F}}{mV_x} & -\frac{S_{\alpha R}}{mV_x} & -\frac{aS_{\alpha F}}{mV_x} & -\frac{bS_{\alpha R}}{mV_x} & \frac{S_{\alpha F}}{m} \\ -\frac{aS_{\alpha F}}{I_{zz}V_x} & \frac{bS_{\alpha R}}{I_{zz}V_x} & -\frac{a^2S_{\alpha F}}{I_{zz}V_x} & -\frac{b^2S_{\alpha R}}{I_{zz}V_x} & \frac{aS_{\alpha F}}{I_{zz}} \end{bmatrix} \tag{4.9}$$

This matrix representation with uncertain channels included is now in a form that can be compacted. The upper LFT is then populated with matrices as marked by the under braces.

Applying the mapping from Eq. 2.44 is then

$$\left[\begin{array}{c} \dot{V}_y \\ \ddot{\psi} \\ \hline z_1 \\ z_2 \\ z_3 \\ z_4 \\ z_5 \\ y \end{array}\right] = M_{8\times 8} \left[\begin{array}{c} V_y \\ \dot{\psi} \\ \hline d_1 \\ d_2 \\ d_3 \\ d_4 \\ d_5 \\ u \end{array}\right] \tag{4.10}$$

$$M_{8\times 8} = \left[\begin{array}{cc|cccccc} -\frac{C_0}{mV_x} & -V_x - \frac{C_1}{mV_x} & -\frac{S_{\alpha F}}{mV_x} & -\frac{S_{\alpha R}}{mV_x} & -\frac{aS_{\alpha F}}{mV_x} & -\frac{bS_{\alpha R}}{mV_x} & -\frac{S_{\alpha F}}{m} & \frac{C_{\alpha F}}{m} \\ -\frac{C_1}{I_{zz}V_x} & -\frac{C_2}{I_{zz}V_x} & -\frac{aS_{\alpha F}}{I_{zz}V_x} & \frac{bS_{\alpha R}}{I_{zz}V_x} & -\frac{a^2S_{\alpha F}}{I_{zz}V_x} & -\frac{b^2S_{\alpha R}}{I_{zz}V_x} & \frac{aS_{\alpha F}}{I_{zz}} & \frac{aC_{\alpha F}}{I_{zz}} \\ \hline 1 & 0 & 0 & & \cdots & & 0 & 0 \\ 1 & 0 & & \ddots & & & & 0 \\ 0 & 1 & \vdots & & 0 & & \vdots & 0 \\ 0 & 1 & & & & \ddots & & 0 \\ 0 & 0 & 0 & & \cdots & & 0 & 1 \\ 0 & 1 & 0 & 0 & 0 & 0 & 0 & 0 \end{array}\right] \tag{4.11}$$

The structured uncertainty diagonal matrix for the uncertain signal map is then

$$\left[\begin{array}{c} d_1 \\ d_2 \\ d_3 \\ d_4 \\ d_5 \end{array}\right] = \left[\begin{array}{ccccc} \delta_{C_{\alpha F}} & 0 & 0 & 0 & 0 \\ 0 & \delta_{C_{\alpha R}} & 0 & 0 & 0 \\ 0 & 0 & \delta_{C_{\alpha F}} & 0 & 0 \\ 0 & 0 & 0 & \delta_{C_{\alpha R}} & 0 \\ 0 & 0 & 0 & 0 & \delta_{C_{\alpha F}} \end{array}\right] \left[\begin{array}{c} z_1 \\ z_2 \\ z_3 \\ z_4 \\ z_5 \end{array}\right] \tag{4.12}$$

where $\delta_{C\alpha F}$ and $\delta_{C\alpha R}$ take on a value between one and negative one when implemented. The lateral vehicle dynamic model is now defined in terms of the LFT and is ready for manipulation with the $\mathcal{H}_\infty$ robust control techniques. A controller can be designed using the $\mathcal{H}_\infty$ techniques. Or, as is the focus for this dissertation, the parametric uncertainty can be assessed systematically in this compact LFT form.

4.3.2 LFT Block Uncertainty Incorporation Technique

The base block LFT technique starts with the generation of LFT blocks for the parameter in isolation. As described in Section 2.4 via Eq. 2.51, each parameter can be modeled with a single uncertainty signal in the upper LFT format. Recall from Figure 2.3 that the additive block for the uncertainty single parameter model is easily converted to an upper LFT. A lower LFT can also be used for the basic LFT blocks for single parameters. The designer just needs to keep consistent track of the input and output channels during the combining of LFT blocks. This can be quite challenging in practice for systems with a lot of uncertain parameters and/or with systems that have a lot of combinations of LFTs.

It is common practice to represent uncertainty with the upper LFT where the uncertainty block is above the system block. Refer back to Figure 2.2 for block diagram of the general LFT structure. Similarly, it also common for closed loop control to be represented with the lower LFT where the controller block is below the system block. However, both the upper and lower LFT formulations can be used to accurately represent either a control block or an uncertainty block.

The scalar variations for $C_{\alpha F}$ and $C_{\alpha R}$ are expressed as

$$\begin{aligned} C_{\alpha F} &= \bar{C}_{\alpha F}\left(1 + p_{C_{\alpha F}}\delta_{C_{\alpha F}}\right) \\ C_{\alpha R} &= \bar{C}_{\alpha R}\left(1 + p_{C_{\alpha R}}\delta_{C_{\alpha R}}\right) \end{aligned} \tag{4.13}$$

Recall for a general parameter x, an over bar denotes the nominal value, $\bar{x}$, and p_x is the percentage variation from nominal parameter. A parameter x with uncertainty is then more

generically defined as

$$x = \bar{x}\left(1 + p_x \delta_x\right) \tag{4.14}$$

where δ_x is the perturbation step which is bounded from $-1 < \delta_x < 1$. This perturbation step is what forms the structured (diagonal matrix) uncertainty block. Additionally, the relative variation in terms of parameter units is then formally defined as

$$s_x = p_x \bar{x} \tag{4.15}$$

From the lower LFT definition $F_L\left(M, K\right) = M_{11} + M_{12}K\left(I - M_{22}K\right)^{-1} M_{21}$, first presented in Eq. 2.47, the cornering stiffnesses can be written in terms of a nominal value and perturbation as

$$\begin{aligned} F_L\left(M_{C_{\alpha F}}, \delta_{C_{\alpha F}}\right) &= \bar{C}_{\alpha F} + p_{C_{\alpha F}} \cdot \delta \left(I - 0 \cdot \delta_{C_{\alpha F}}\right)^{-1} \bar{C}_{\alpha F} \\ F_L\left(M_{C_{\alpha R}}, \delta_{C_{\alpha R}}\right) &= \bar{C}_{\alpha R} + p_{C_{\alpha R}} \cdot \delta \left(I - 0 \cdot \delta_{C_{\alpha R}}\right)^{-1} \bar{C}_{\alpha R} \end{aligned} \tag{4.16}$$

Finally, the two uncertain cornering stiffness terms can be written in the compact form of the lower LFT subsystem blocks as shown earlier in Eq. 4.17.

$$C_{\alpha F} = M_{C_{\alpha F}} = \begin{bmatrix} \bar{C}_{\alpha F} & p_{C_{\alpha F}} \\ \bar{C}_{\alpha F} & 0 \end{bmatrix} \quad C_{\alpha R} = M_{C_{\alpha R}} = \begin{bmatrix} \bar{C}_{\alpha R} & p_{C_{\alpha R}} \\ \bar{C}_{\alpha R} & 0 \end{bmatrix} \tag{4.17}$$

Any parameters that are constant and without uncertainty, like the wheel base L, are modeled as a simple gain block.

The next step is to combine the base parameter block systems and gain parameter blocks into the larger subsystems. These subsystems will then be combined together to yield the upper LFT system for the full yaw vehicle model with structured uncertainty. This block construction and combining is most easily carried out in MATLAB with the μ toolbox.

The μ toolbox has many built in features for manipulating matrices and performing frequency domain control analysis. It is possible to create and manipulate LFTs without the toolbox, but the designer will have to reproduce many of the capabilities of the μ tools.

This would be akin to using the bode plot function versus coding up the frequency phase and magnitude response oneself. Although, it may be beneficial at first to understand the interworking concepts and create user developed tools, it is more practical to use the built in functionality once basics are mastered.

Note, for this dissertation the base parameter uncertainty block systems were created early on in the lower LFT form. The larger subsystems, however, were developed in the form of the upper LFT because the upper form is more commonly understood to represent uncertainty. Conversion of the uncertain base parameter systems from the lower LFT to upper LFT would have also required extensive alterations to the larger subsystem block comprised of the base block lower LFTs. Therefore the base block LFTs for uncertain parameters were kept in the lower LFT form.

Figure 4.2 shows the construction of base blocks and gain blocks for the yaw model with uncertainty on the cornering stiffnesses. The note at the beginning of the code delineated by the percent symbol is a breakdown of the signal map from input to output of a generic lower LFT matrix denoted `mXx`.

```
% Lower LFTs
% [  y ]  =          [ u  ]
% [z_Xx]    [mXx] * [w_Xx]
% where:
% [mXx] == lower LFT
% y == output of LFT mXx
% zXx == applied perturbation state of mXx
% u == input state to mXx
% w_Xx == input perturbation multiplier [-1 1] into to mXx

mCaf = [C_af P_Caf;...
        C_af     0];
mCar = [C_ar P_Car;...
        C_ar     0];

gainVx = nd2sys(Vx,1);
gaina = nd2sys(a,1);
gainb = nd2sys(L-a,1);
gainL = nd2sys(L,1);
gainMass = nd2sys(m,1);
gainInvMass = nd2sys(1,m);
gainInvInertia = nd2sys(1,Izz);
gainInvVx = nd2sys(1,Vx);
intgrtr = nd2sys(1,[1 0]);
```

Figure 4.2: MATLAB Based Construction of Base Parameter System for the Yaw Model

The construction of the subsystem blocks is a bit more involved due to tracking of signals, especially since the base parameter blocks were created as lower LFTs. The subsystem blocks are created using the `sysic` function from the μ toolbox. This function requires the base system names to be declared by `systemnames`, a name for the combined system/subsystem is set with sysoutname, input signals to the combined system/subsystem are set with `inputvar` and the output of the combined system/subsystem is established with outputvar. The output will always be an output of one or more of the base systems or subsystems. The input call `input_to_X` is the primary signal building device. Here, `X` is a base system or subsystem named in systemnames. Figure 4.3 includes the construction of a few subsystems for the yaw vehicle model with uncertain cornering stiffness. A comment on the order of input

and output signals for an upper LFT is also included for clarity on the signal order that is specified in the parenthesis proceeding a few of the base systems in the `input_to_X` call. If a system is scalar (i.e. SISO), it is not necessary to specify the input and output channel numbers. Each subsystem in the model is simply a section of blocks and/or series of blocks from Figure 4.1.

Once all subsystems have been constructed they can be combined into a single LFT that represents the entire system and all the uncertain signals and feedback. Figure 4.4 contains the MATLAB code that pulls together all the subsystems for the vehicle yaw model of Figure 4.1.

```
% Upper LFTs
% [z_Xx]  =          [w_Xx]
% [  y ]    [mXx] *  [ u  ]
% [mXx_invrt] == upper LFT
% y == output of LFT mXx_invrt
% zXx == applied perturbation state of mXx_invrt
% u == input state to mXx
% w_Xx == input perturbation multiplier [-1 1] into to
   mXx_invrt

% mUsys1
systemnames = 'mCaf gainVx'; % Lower LFTs
sysoutname = 'mUsys1';
inputvar = '[w_Caf; control]';
input_to_mCaf = '[control; w_Caf]';
input_to_gainVx = '[mCaf(1)]';
outputvar = '[mCaf(2); gainVx(1)]'; %[z_Caf; Caf*Vx]; %UpperLFT
    out
cleanupsysic = 'yes';
sysic;
minfo(mUsys1)

% mFwdPathVxM
systemnames = 'gainInvVx gainInvMass intgrtr'; %UpperLFT,
   scalarGain, 1out-1inSystem
sysoutname = 'mFwdPathVxM';
inputvar = '[error1]';
input_to_gainInvMass = '[error1]';
input_to_gainInvVx = '[gainInvMass(1)]';
input_to_intgrtr = '[gainInvVx(1)]';
outputvar = '[intgrtr(1)]'; %[1/(m*Vx)*1/s]; [x_1]; %UpperLFT
cleanupsysic = 'yes';
sysic;
minfo(mFwdPathVxM)
```

Figure 4.3: MATLAB Based Construction of a Few Subsystems for the Yaw Model

```
%IMPORTANT: inputvar, outputvar and delta block (order of
   perturbations)
%are all correlated must have order correct

% G_vehYaw_CaFR_LFTblocks
systemnames = 'mUsys1 mUsys2 mFwdPathVxM mFwdPathVxIzz mCo mC1
   mVxC1 mC2';
sysoutname = 'G_vehYaw_CaFR_LFTblocks';
inputvar = ['[w_Caf3; w_Car1; w_Caf4; w_Car2; w_Caf5; w_Car3;'
   ...
                    'w_Caf6; w_Car4; w_Caf1; w_Caf2;'...
                    'u_steer]'];
input_to_mUsys1 = '[w_Caf1; u_steer]';
input_to_mUsys2 = '[w_Caf2; u_steer]';
input_to_mFwdPathVxM = '[mUsys1(2)-mCo(3)-mVxC1(3)]';
input_to_mFwdPathVxIzz = '[mUsys2(2)-mC1(3)-mC2(3)]';
input_to_mCo = '[w_Caf3; w_Car1; mFwdPathVxM(1)]';
input_to_mC1 = '[w_Caf4; w_Car2; mFwdPathVxM(1)]';
input_to_mVxC1 = '[w_Caf5; w_Car3; mFwdPathVxIzz(1)]';
input_to_mC2 = '[w_Caf6; w_Car4; mFwdPathVxIzz(1)]';

outputvar = ['[mCo(1); mCo(2);  mC1(1); mC1(2); ' ...
                 'mVxC1(1); mVxC1(2); mC2(1); mC2(2); mUsys1(1)
                    ; mUsys2(1); ' ...
                 'mFwdPathVxIzz(1)]']; %[x2]
cleanupsysic = 'yes';
sysic;
minfo(G_vehYaw_CaFR_LFTblocks)
seesys(G_vehYaw_CaFR_LFTblocks)
```

Figure 4.4: MATLAB Based Construction from LFT Subsystems of the Yaw Model with Uncertain Cornering Stiffness

Notice that feedback is handled with the `input_to_X` calls by the subtraction of the subsystems. Specifically, this is done for the subsystems mFwdPathVxM and mFwdPathVxIzz with the outputs of the smaller subsystems matching feedback junctions observed in the block diagram of Figure 4.1. For a full definition of all the subsystems, refer to Appendix A.2.1 where the full script that constructs all the subsystems blocks of the yaw model with uncertain cornering stiffness can be found.

4.3.3 Comparison of the Equation Based Approach and the LFT Base Block Method

The two approaches, the system equation method and the base block LFT technique, for constructing the system LFT with uncertainty for the vehicle yaw model should have identical response outputs. It is straightforward and necessary to check the nominal system, subset matrices A, B, C and D. The subset matrices, B_Δ, F, G, H and J, that map the uncertainties to parameters in the nominal system are not guaranteed to match if the number of instances of the repeated parameters is not identical. This is easy to see by the fact that the equation based technique has a structured uncertainty block, Δ, of size 5×5 and the LFT base block technique has a Δ of size of 10×10.

The reason for this difference in uncertainty block size is that LFT base block method is more reliably constructed if each instance of an uncertain parameter is accounted for during the subsystem designation and construction. It is possible to intelligently "reuse" uncertainty parameter channels without creating another named instance. Note, a named instance is for example `w_Caf1`, `w_Caf2` ... etc. This "reuse" of instances though becomes confusing very quickly. Therefore, for better tracking of the block interconnections and better repeatability in application of the base block method to other systems it is recommended to uniquely name most if not every repeated instance of an uncertain parameter at the expense of a larger sized structured uncertainty, Δ. Conversely, when using the equation based technique, the designer often intuitively "reuses" uncertain parameter instances at the signal split junctions in the block diagram, shown in Figure 4.1.

The block diagram for the LFT base block method with size 10×10 uncertainty Δ block has the same general form as Figure 4.1, but is less compact due to the additional blocks and more explicit uncertainty signal channels. Additionally, the equation based technique can be applied for this 10×10 case and the system nominal response and response with varying levels of uncertainty injected on the parameters should be identical to both the 5×5 equation based technique response and the 10×10 LFT base block method response.

It is important to check these responses on a simple model with limited uncertain parameters because the base block method often yields LFT system matrices that account for parameter uncertainty in different order than the hand calculated equation based method. For example, the B_Δ matrices of the equation based method and the LFT base block method are similar but in a different order. Backing out the symbolic representation for the LFT base block method, the matrix is

$$B_\Delta = \begin{bmatrix} -\frac{S_{\alpha F}}{mV_x} & -\frac{S_{\alpha R}}{mV_x} & 0 & 0 & -\frac{aS_{\alpha F}}{mV_x} & -\frac{bS_{\alpha R}}{mV_x} & 0 & 0 & \frac{S_{\alpha F}}{m} & 0 \\ 0 & 0 & -\frac{aS_{\alpha F}}{I_{zz}V_x} & \frac{bS_{\alpha R}}{I_{zz}V_x} & 0 & 0 & -\frac{a^2S_{\alpha F}}{I_{zz}V_x} & -\frac{b^2S_{\alpha R}}{I_{zz}V_x} & 0 & \frac{aS_{\alpha F}}{I_{zz}} \end{bmatrix} \tag{4.18}$$

and the B_Δ for the equation based technique is

$$B_\Delta = \begin{bmatrix} -\frac{S_{\alpha F}}{mV_x} & -\frac{S_{\alpha R}}{mV_x} & -\frac{aS_{\alpha F}}{mV_x} & -\frac{bS_{\alpha R}}{mV_x} & 0 & 0 & 0 & 0 & \frac{S_{\alpha F}}{m} & 0 \\ 0 & 0 & 0 & 0 & -\frac{a^2S_{\alpha F}}{I_{zz}V_x} & -\frac{b^2S_{\alpha R}}{I_{zz}V_x} & -\frac{aS_{\alpha F}}{I_{zz}V_x} & \frac{bS_{\alpha R}}{I_{zz}V_x} & 0 & \frac{aS_{\alpha F}}{I_{zz}} \end{bmatrix} \tag{4.19}$$

Here it's easy to see that the uncertain channels are equal in effect but are ordered differently. The other matrices within the LFT that inject uncertainty into the nominal system will be similarly ordered. Note that determining a match based on a comparison of the system LFT matrices from the two methods can be a bit challenging to decipher when looking at the numeric non-symbolic representations. Therefore, a comparison of the outputs of the both nominal system and the uncertain perturbations of the parameters is useful.

First the Δ perturbation block needs to be created such that the diagonal values between -1 and 1 can be applied to the system M once connected. This connection is made via the upper LFT of the system M and the Δ perturbation block, $M_\Delta = F_U(M, \Delta)$. In MATLAB, `ndgrid()` is useful for creating a gridded variable to insert along the diagonals with respect to each uncertain variable. The Δ block can be easily looped through different perturbation scenarios when diagonals are constructed in this fashion. The `starp()` function is used to implement both the upper and lower types of LFT connections, where the

connection type depends on the order of the inputs to the function call. Specifically, the call `starp(delta, M)` with an uncertainty matrix Δ as the first input and the system M as the second input yields an upper LFT; while ordering the inputs with the system M first and a matrix such as a controller K second yields a lower LFT, or `starp(M, K)`.

A comparison of the frequency response output of open loop system derived via the system equation method and the base block LFT technique is presented in Figure 4.5. This comparison of the nominal system outputs and the outputs with various parameter perturbations shows the respective outputs to match. A lot of effort has been spent to show the equivalency between the two methods for deriving a system model that includes the parametric uncertainty. The reason for this effort is that the hand derivation via the system equation method becomes more tedious as the number of uncertain parameters increases and also not very practical in the presence of uncertain parameters that are coupled.

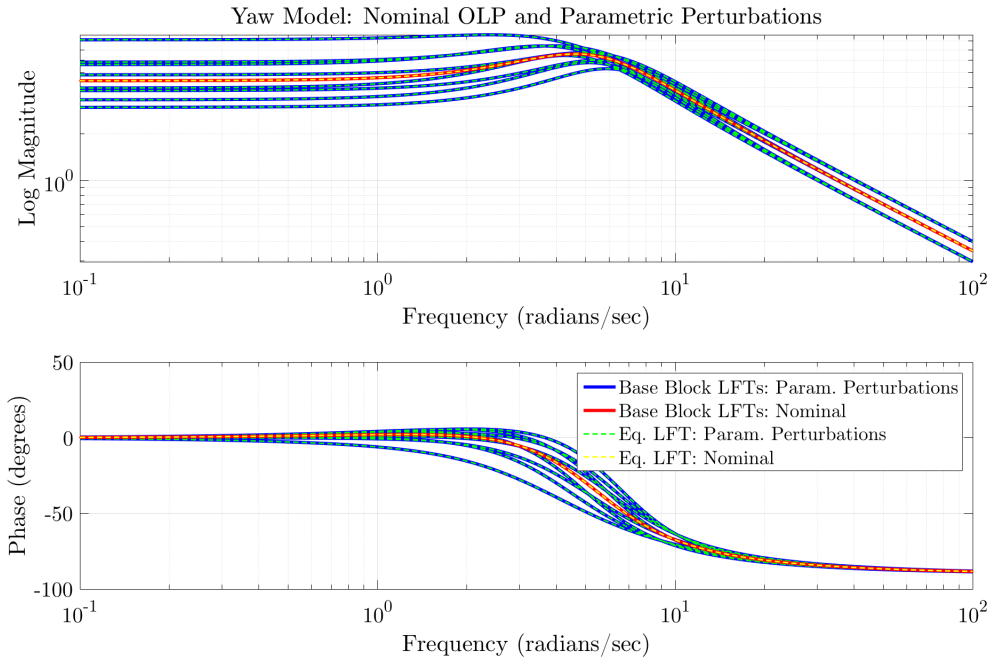

Figure 4.5: Open Loop Frequency Response with 15% Uncertainty on the Cornering Stiffnesses for the Class D SUV at 120 kph

4.3.4 Coupled Yaw-Roll Model with Full Parametric Uncertainty

In this section, focus returns to the coupled yaw-roll model which is better representation of the vehicle system dynamics than just the two state yaw model. As mentioned above each uncertain parameter is again combined via the interconnections of the larger block diagram. Instead of using the additive block (shown in Figure 2.3), it is helpful in practice to represent each uncertain parameter as an LFT matrix M_p where the subscript p is the uncertain parameter of interest.

Note, for this model there is quite a number of instances of repeated parameters. However, this is easily handled by collecting and reorganizing the like repeated parameters into groups along the diagonal of the structured uncertain matrix Δ. This reorganization is carried out after the interconnections of all M_p blocks and feedback of the system has been setup and the system LFT calculated. The yaw-roll vehicle model with uncertainty on the following 10 parameters m, I_{zz}, V_x, $C_{\alpha f}$, $C_{\alpha r}$, a, I_{xx}, h_{rg}, K_ϕ, and $B_{\dot{\phi}}$ is described by Figure 4.6. For this model, only the front weight split term, a, is used to capture changes in loading conditions. It would not make sense practically for both the terms a and b to vary for a normal vehicle with a wheel base, L, that is structurally fixed length. Therefore, the corollary rear weight split term b is represented in terms of the fixed length L and varying front weight split a, i.e. $b = L - a$.

Due to the number of instances of uncertain parameters for the yaw-roll model only the base LFT method was used to construct the LFT of the system. The procedure is the same as described for the yaw model, but with more base block LFTs in place of the gain blocks for the parameters that are now modeled with uncertainty. The final construction step from the LFT subsystems to the open loop system is shown in Appendix A.2.3.

The coupled yaw-roll vehicle model with uncertainty is transformed into the $M-\Delta$ upper LFT by combining the base LFT formulations of the uncertain parameters. This produces a system M with uncertain Δ matrix composed of ten perturbation variables. However, as mentioned previously, the parameters are repeated and the size of the uncertain matrix is

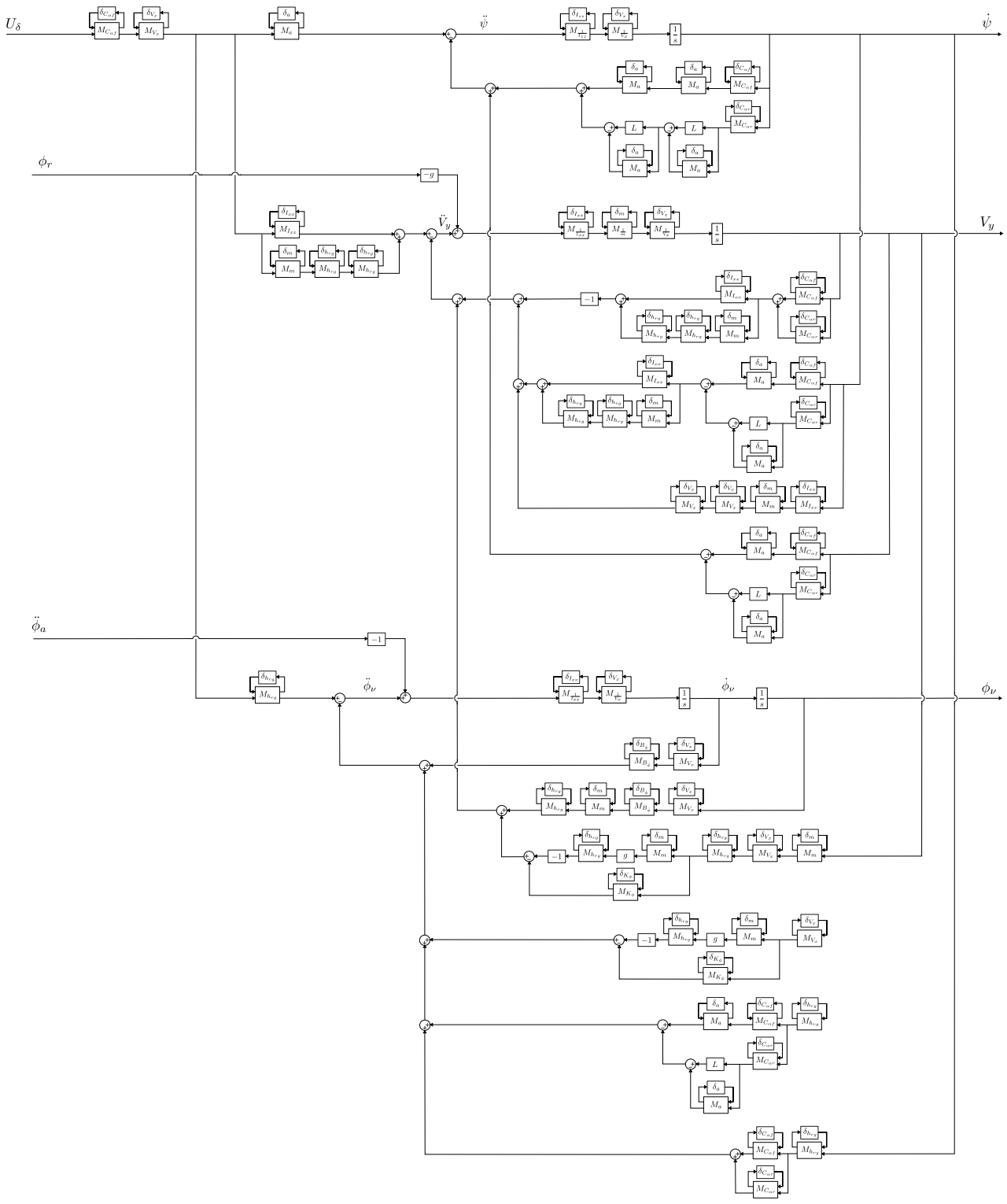

Figure 4.6: Vehicle Coupled Yaw-Roll Model with Parametric Uncertainty for All Parameters

much larger at 71×71 in size. Grouping the like parameters together the uncertainty matrix takes the form

$$\Delta = \text{diag}\left(\begin{bmatrix} \Delta_{a,11\times11} & \Delta_{m,9\times9} & \Delta_{Izz,1\times1}\cdots \\ \Delta_{V_x,12\times12} & \Delta_{C_{\alpha f},9\times9} & \Delta_{C_{\alpha r},6\times6}\cdots \\ \Delta_{I_{xx},6\times6} & \Delta_{h_{rg},13\times13}\cdots & \\ \Delta_{K_\phi,2\times2} & \Delta_{B_{\dot{\phi}},2\times2} \end{bmatrix} \right) \tag{4.20}$$

where the subset $\Delta_{p,n\times n}$ are the n number of collected diagonal perturbations. Rearranging the uncertainty matrix is accomplished via rearrangement of the input and output channels of the system LFT matrix M. This is accomplished easily with the μ toolbox in MATLAB using the sel() function to specify the input and output channels. An example of this rearrangement is shown in Figure 4.7 where the variable `GK_clp_vary` is the frequency response matrix, (a matrix that can vary in size based on the vector of frequency points desired), of the closed loop system. Note that `GK_clp_vary` contains both a controller K and the uncertain block Δ.

```
% Isolate repeated params
i_SetParm = 1:71;
i_a = [20:21,38:41,44:45,55:56,68];
i_m = [2,11,15,23,29,32,34,50,63];
i_Izz = [4];
i_Vx = [3,5,7,16:17,28,31,47,48,61,67,70];
i_Caf = [8,18,36,42,53,58,60,66,69];
i_Car = [9,19,37,43,54,59];
i_Ixx = [1,6,10,14,22,62];
i_hrg = [12:13,24:25,27,30,35,51,52,57,64:65,71];
i_Kphi = [33,49];
i_Bphid = [26,46];

% Calc Mu Basline but account for repeated variables for baseline
   Mu calculation GK_clp_Uncert_varyCollectRepeats = sel(
   GK_clp_vary, ...
[i_a i_m i_Izz i_Vx i_Caf i_Car i_Ixx i_hrg i_Kphi i_Bphid], ...
[i_a i_m i_Izz i_Vx i_Caf i_Car i_Ixx i_hrg i_Kphi i_Bphid]);
```

Figure 4.7: Method for Reorganizing the Yaw-Roll LFT System with Full Parametric Uncertainty

The closed loop process is discussed in detail in, Chapter 5. Here, a look at the open loop response confirms that the nominal system still matches the output response of the original system without the uncertainty as expected. A mathematical check on the nominal system can also be carried out by extracting the nominal state matrix A and input matrix B from the open loop LFT matrix. Also, differencing the original system matrices from the corresponding LFT extracted matrices should yield null matrices for each if the LFT was properly constructed. Ensuring the uncertainty is incorporated correctly is a bit more tedious and involves tracing signals through the base block and subsystems to ensure it matches the LFT block diagram routing, shown in Figure 4.6.

Note that it is also recommended to first work with a simple system such as a traditional mass-spring -damper system to build confidence in the understanding of the uncertain block connections. Once the process is mastered some coupled uncertainties can be added by, for example, squaring the spring stiffness parameter to ensure LFT connections are being handled correctly. Any errors on this common system are much easier to isolate and this experience will reduce errors in the connections in a more complicated system.

The perturbed frequency response of the open loop yaw-roll system for the Class D SUV is shown in Figure 4.8. The velocity for this analysis was 120 $^{km}/_{\text{hr}}$ and each parameter was given a 15% uncertainty value. Hence the variance on the output response for the yaw is quite large when 10 parameters can vary even at such a low percentage. To demonstrate that the uncertainty is functioning, the uncertainty for each parameter was lowered in 5 percent increments in Figures 4.9 and 4.10. Additionally, Figures 4.11-4.13 represent the frequency response with 15 percent uncertainty on each parameter at speeds 20, 50 and 90 kph respectively to show the effect of speed on the output response when the uncertainty is held constant. As the speed decreases there are less extreme variances in the output response of the yaw state. By inspection the uncertain perturbations for the open loop cases shown in Figures 4.8 - 4.13 are found to be within the reasonable realm of vehicle dynamic responses.

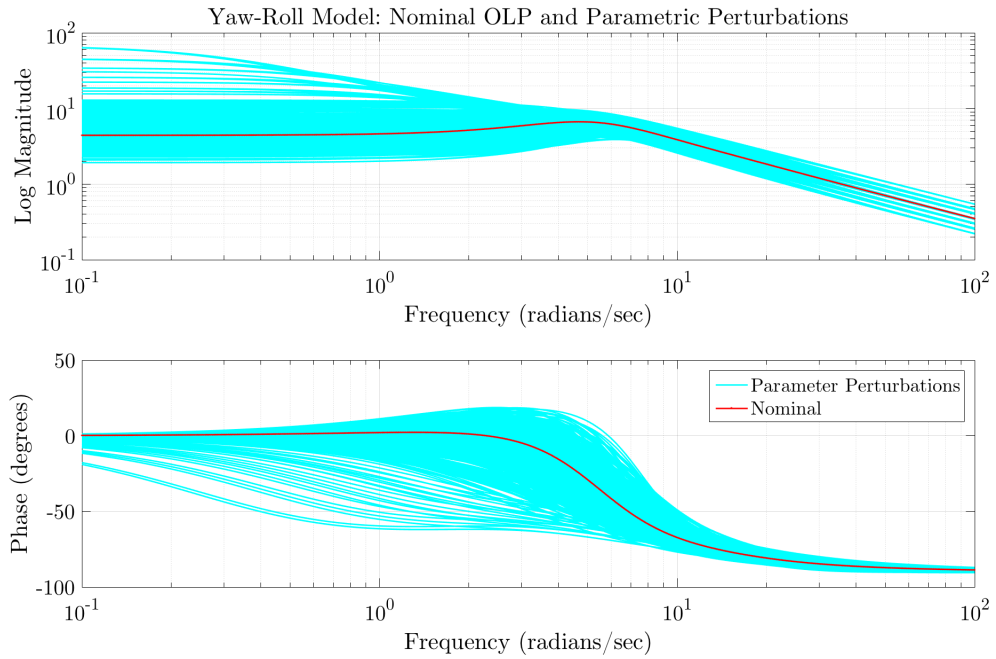

Figure 4.8: Vehicle Yaw Rate Perturbed OLP Frequency Response at 120 $^{km}/_{\text{hr}}$ and 15% Initial Uncertainty in Each Parameter

In the next chapter, the loop is closed with feedback of the yaw rate and a suitable controller applied to the system.

4.4 Conclusion

Parametric uncertainty for the vehicle system was first incorporated into the less complicated yaw model with the development of a block diagram that accounts for variations via an additive block. Two approaches for producing the governing system matrices were presented. The first was a direct method in which the classic block diagram rules are used to manually derive the equations. The second approach leverages the definition of the LFT by condensing each parameter and respective additive variation block into single LFT matrix blocks that capture the parameter and variation affects. The LFT blocks are then combined into a single larger LFT block that represents the system and an upper LFT diagonal block that represents the uncertainty or variation of the parameters. The output responses of the two approaches were compared to show that both produce an accurate representation of both

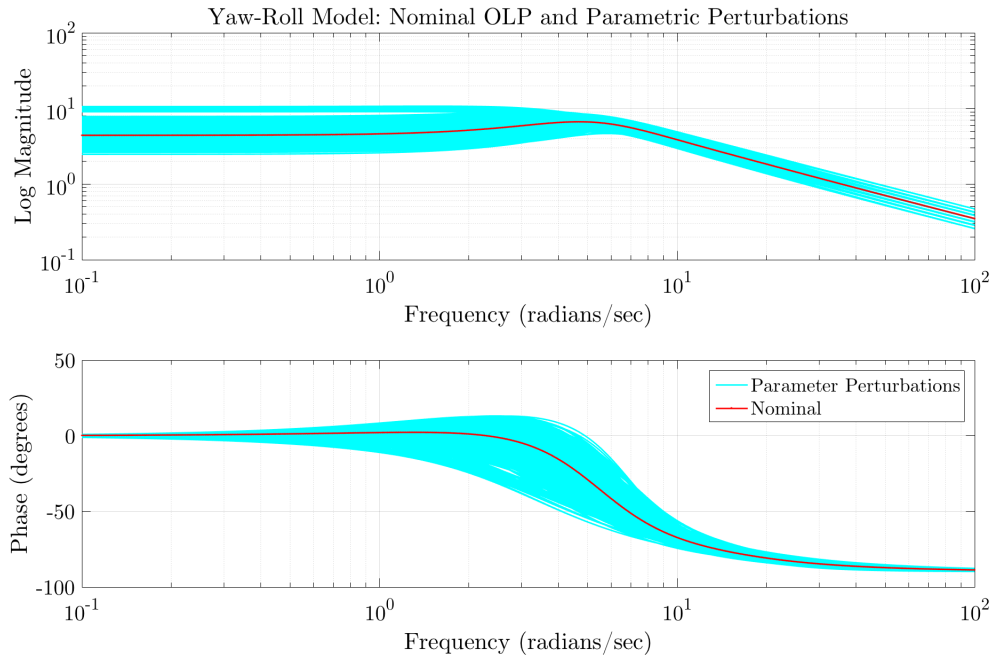

Figure 4.9: Vehicle Yaw Rate Perturbed OLP Frequency Response at 120 $^{km}/_{\text{hr}}$ and 10% Initial Uncertainty in Each Parameter

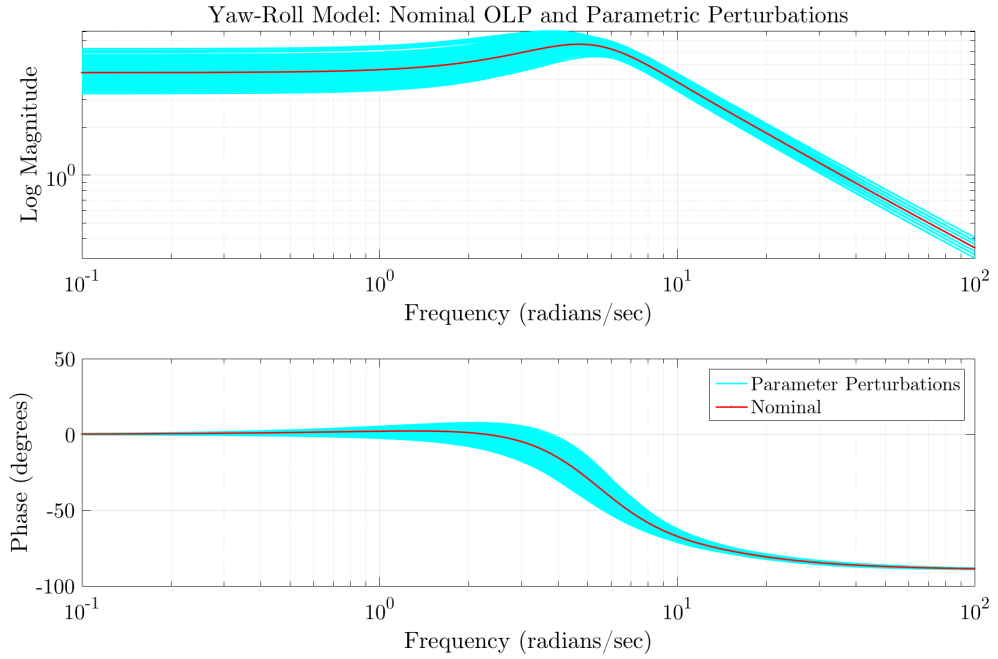

Figure 4.10: Vehicle Yaw Rate Perturbed OLP Frequency Response at 120 $^{km}/_{\text{hr}}$ and 5% Initial Uncertainty in Each Parameter

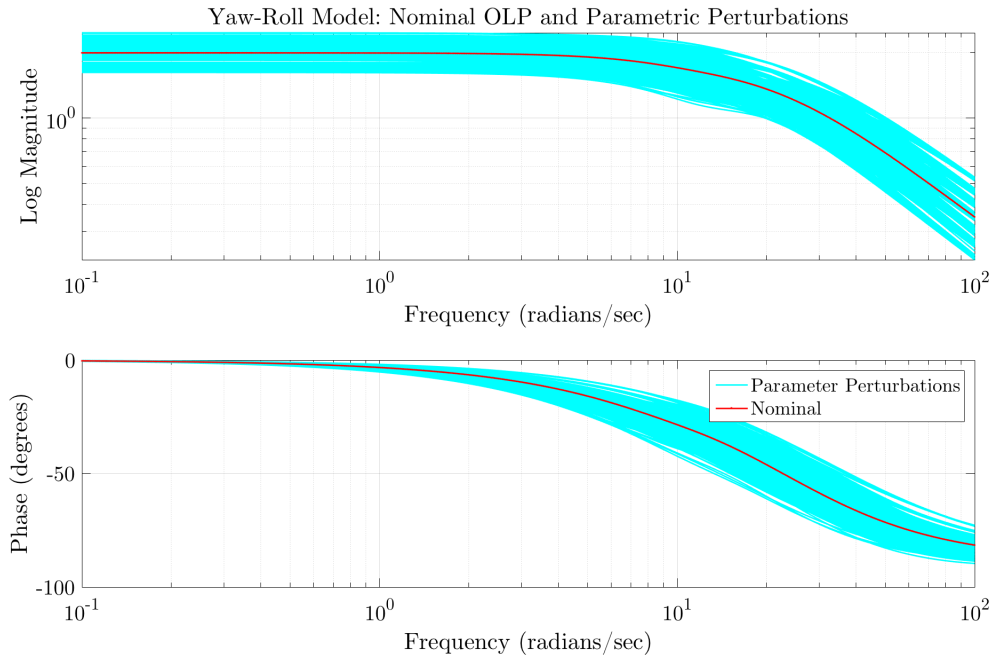

Figure 4.11: Vehicle Yaw Rate Perturbed OLP Frequency Response at 20 $^{km}/_{\text{hr}}$ and 15% Initial Uncertainty in Each Parameter

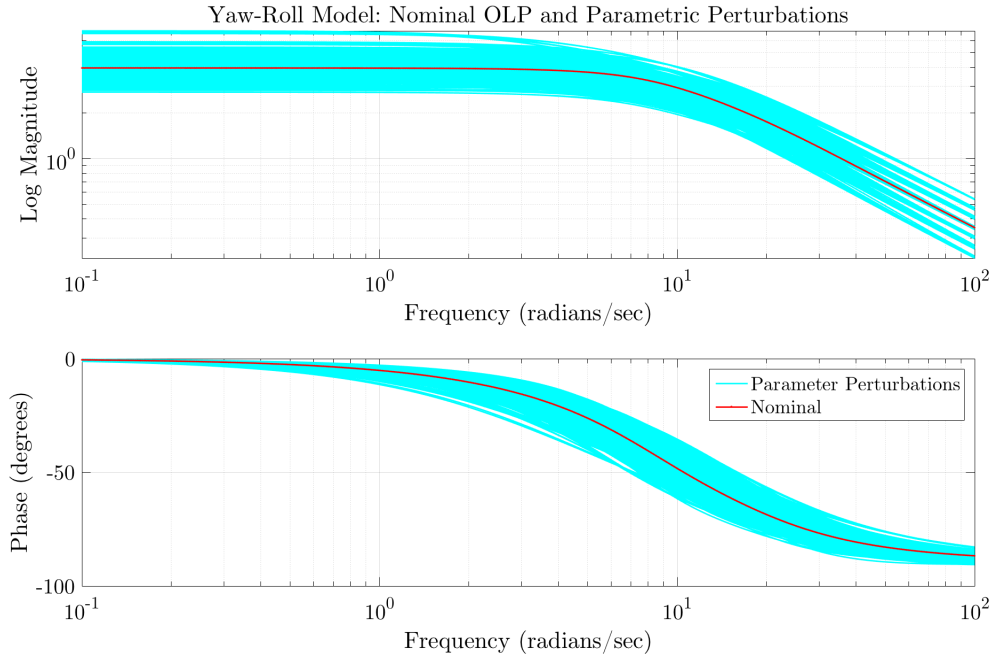

Figure 4.12: Vehicle Yaw Rate Perturbed OLP Frequency Response at 50 $^{km}/_{\text{hr}}$ and 15% Initial Uncertainty in Each Parameter

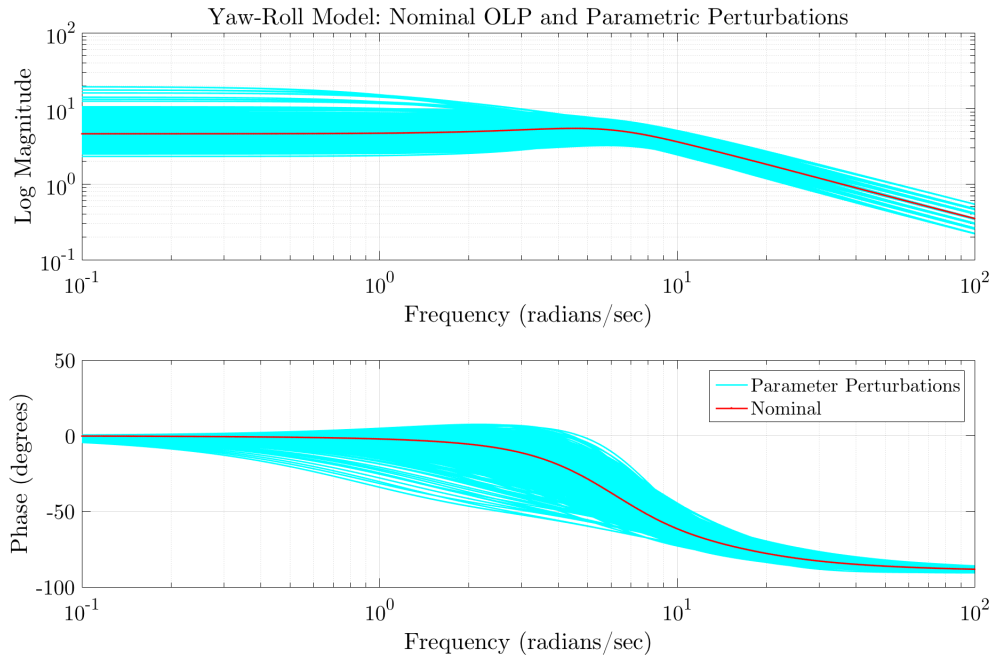

Figure 4.13: Vehicle Yaw Rate Perturbed OLP Frequency Response at 90 $^{km}/_{\text{hr}}$ and 15% Initial Uncertainty in Each Parameter

the nominal system response and the response with uncertainty injected via the structured uncertainty block. The LFT base block method was then used to produce the uncertainty model of the more complicated coupled yaw-roll vehicle system. For the yaw-roll model with full parametric uncertainty the LFT block method is better suited method due to the number of uncertain channels, amount of repeated parameters and the coupling of several of the parameters. Note that while the base block LFT method can handle some cases of parameter coupling, it is not capable of representing other nonlinearities such as sine and cosine operations. The open loop response for yaw-roll system was then analyzed at several operating velocities with an initial uncertainty of 15 % on all the parameters showing how the parameter variations affected the frequency response of the system.

Chapter 5

Skew μ Analysis of Closed Loop Coupled Vehicle Model with Full Parametric Uncertainty

5.1 Introduction

In this chapter, the coupled yaw-roll vehicle model representing a Class D SUV is closed around the yaw rate with a controller K. Analysis of the remaining "space" of uncertainty for a given parametric dimension for the closed loop system is performed. Specifically, uncertainty model cases are created where only a single parameter is placed in the varying subset Δ_v with the remaining fixed parameters residing in the subset Δ_f. This chapter analyzes how each parameter isolated in the varying subset is affected by the operating velocity of the model and the initial uncertainties specified for the entire uncertainty set Δ.

5.2 Controller Design and Closed Loop Response

The closed loop for yaw rate control was examined with a fixed proportional-integral controller (PI) where $K_p = 2$ and $K_i = 0.125$. In the LFT block form the controller is then

$$K = \begin{bmatrix} 0 & 2 \\ 1 & 0.125 \end{bmatrix}$$

This PI controller was selected because the system did not need derivative control as the system was stable in the open loop and demonstrated a damped response without a controller. A lower LFT is used then to combine the system $M_K = F_L\left(M_\Delta, K\right)$. The repeated parameters were then grouped together and the closed loop system M_K rearranged accordingly.

One additional step is required, which is to formally define the input and outputs of the M_Δ LFT for the closed loop system before performing the lower LFT operation that yields

the resultant M_K. This input-output setup step is again performed with the μ toolbox `sysic` function. Figure 5.1 shows the steps needed to close the loop around the yaw rate. The signal connections and signal names for the M_Δ system `G_vYawRoll_FullLFT` are specified with the variables `inputvar`, `outputvar` and `input_to_G_vYawRoll_FullLFT`. Also, notice that a disturbance is also incorporated on the on the yaw rate output of M_Δ with the `outputvar`. The star product function, `starp()`, is then used to generate M_K, or clp_SysIcKCtrl as it's labeled in the script excerpt.

```
systemnames = 'G_vYawRoll_FullLFT';
inputvar = '[pert{71};dist;control]';
outputvar = '[G_vYawRoll_FullLFT(1:71);-G_vYawRoll_FullLFT(72)-dist]';
input_to_G_vYawRoll_FullLFT = '[pert;control]';
sysoutname = 'sys_ic_vYawRoll_FullLFT';
cleanupsysic = 'yes';
sysic;

clp_SysIcKCtrl = starp(sys_ic_vYawRoll_FullLFT,Kctrl_modal);
```

Figure 5.1: Script showing the setup of the Inputs and Outputs for Feedback to Properly Carry Out the Lower LFT of the Yaw-Roll Model with the Controller K

The yaw response of the simulated closed loop system is represented by Figure 5.2. Here, the step inputs are in red and the yaw rate output is in cyan. The closed loop frequency responses are shown in Figure 5.3. Here the frequency response of a disturbance is also included to show the effect that control has on the output disturbance rejection.

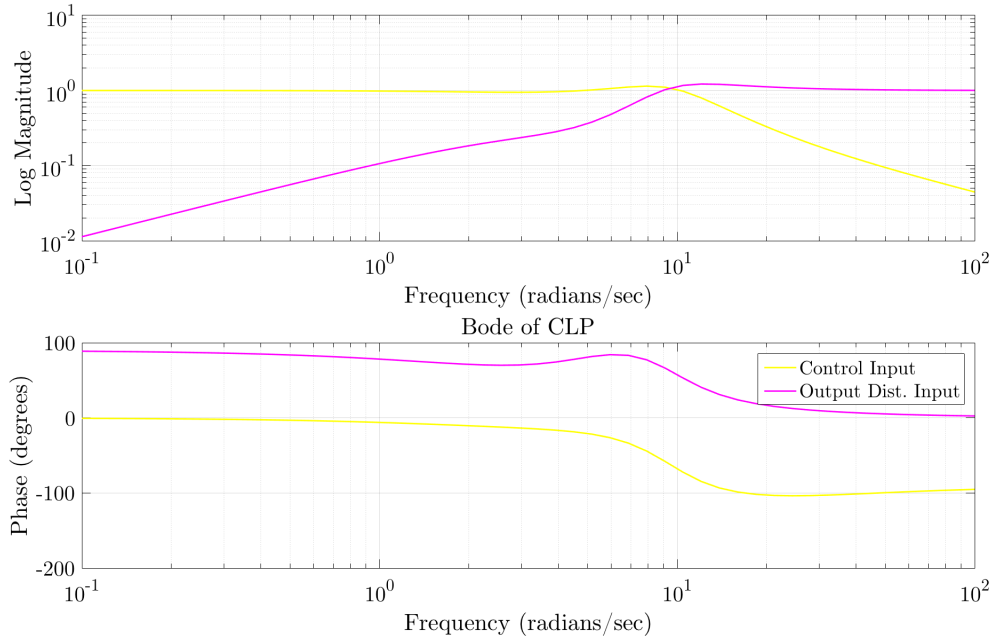

Figure 5.3: Closed Loop Frequency Response of the Yaw-Roll Model with Controller K at 120 $^{km}/_{\text{hr}}$

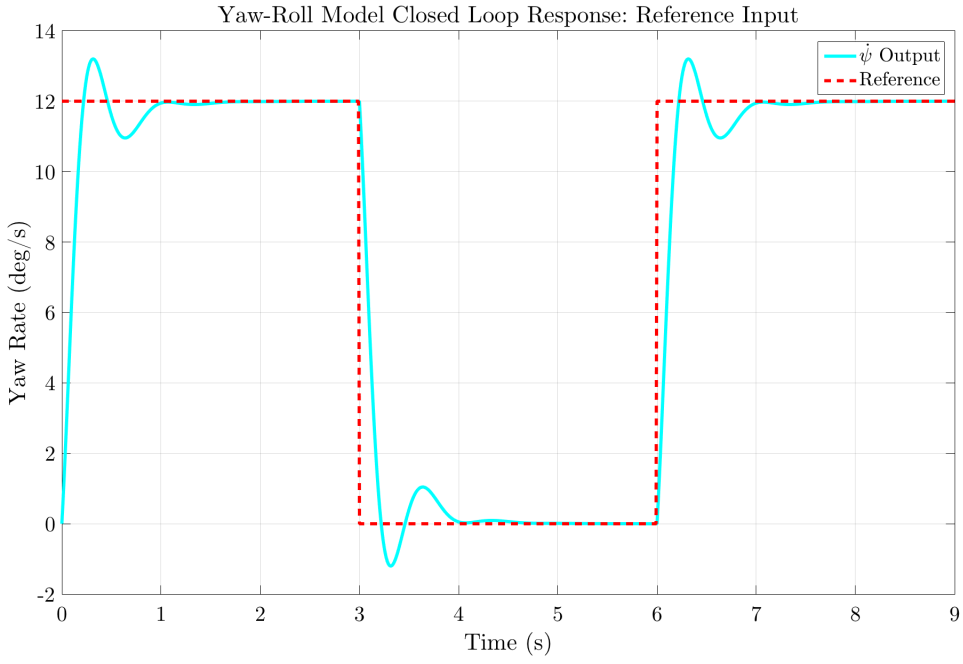

Figure 5.2: Closed Loop Transient Response of the Yaw-Roll Model with Controller K at 120 $^{km}/_{\text{hr}}$

More important though to the topic at hand is a look at some initial μ analysis of the closed loop system. Remember that a μ value less the one ensures the system is stable, but a μ above one does not necessarily mean the system is unstable. If the μ value is above one it means only that all specified conditions and performance of the controller and system are not met.

5.3 μ and Skew μ Analysis

It is useful to first examine the μ value of the the entire system with some initial uncertainty value assigned to each parameter in the set Δ. Note the entire set of uncertainties in the Δ block are fixed for the mu analysis. Only, the skew μ analysis has fixed and varying subsets, Δ_f and Δ_v respectively, within the entire set Δ_s of uncertain parameters. These initial uncertain values are based on assumptions made about the system. A set of assumptions can be thought of as a scenario or model that has a different purpose in highlighting characteristics of the perturbations of the system. For example the "extra space" of uncertainty for parameters is different if a scenario/model has initial uncertainty of 1% for each parameter versus a case where initial uncertainty is say 15%. The former assumes either the uncertain parameters will not vary much or that the parameters are well known and/or easily measurable. Conversely the latter case is a model/scenario where it is assumed that the parameters are not well know and/or the parameters may vary under operational conditions quite a bit [27].

These scenarios are determined by the interest of the designer and the physical characteristics of the system. For example, the cornering stiffness is not always well known and there is some debate among vehicle dynamics community whether it is a uniform value for all tire-surface interactions. Other parameters may be measured with confidence but may vary under operating conditions. An example of this operational variance is the weight split, which may be well known but is subject to change slightly with various loadings of the vehicle.

5.3.1 μ for the Coupled Yaw-Roll Model with Full Parametric Uncertainty

The μ analysis for the coupled yaw-roll model with full parametric uncertainty for the 10 parameters, m, I_{zz}, V_x, $C_{\alpha f}$, $C_{\alpha r}$, a, I_{xx}, h_{rg}, K_ϕ, and $B_{\dot{\phi}}$, but with the repeated instances treated as independent occurrences is shown Figure 5.4. Recall from Eq. 4.20 and the development of the yaw-roll vehicle model that there 71 total entries in the Δ block, but only 10 uncertain parameters. The μ analysis for the case where the instances of repeated parameters are collected is shown in Figure 5.5. For the case where repeated instances are collected the scaling that occurs the μ algorithm is applied to the collection of instances for each term. For example, all 11 instances of the weight split parameter a are treated as a single uncertain parameter when occurrences collected. Therefore, specifying repeated terms means the μ is calculated for the correct amount of uncertain terms which is 10 parameters not 71. Thus, these two figures are presented to highlight the importance of collection of repeated parameters. It is important to have the proper scaling applied at every instance of a repeated parameter in system model, because the fully independent case is not an accurate representation of the how the system is affected by changes in each parameter. The two plots are for a system with 15% initial uncertainty on all 10 parameters. Notice that when all 71 uncertain channels can vary independently as in Figure 5.4 the upper bound of the μ value shown in yellow is around 2.4, which is greater one. Thus, the system can't be guaranteed to meet performance specification and may not be stable. However, for the analysis where the repeated instances of uncertain parameters are collected, Figure 5.5, the system μ values are below one for all frequencies and the peak of the upper bound is just under 0.7 which indicates there is "space" remaining among the parameters for more uncertainty along any of the parameter dimensions or combination thereof.

If the the μ analysis of the system reveals the overall max μ value to be one or greater there is no need to perform any further skew μ analysis as the system cannot handle any additional uncertainty. In the event where the system μ is equal one or near a value of one it is recommended to reconsider the assumptions made regarding the initial uncertainties. It

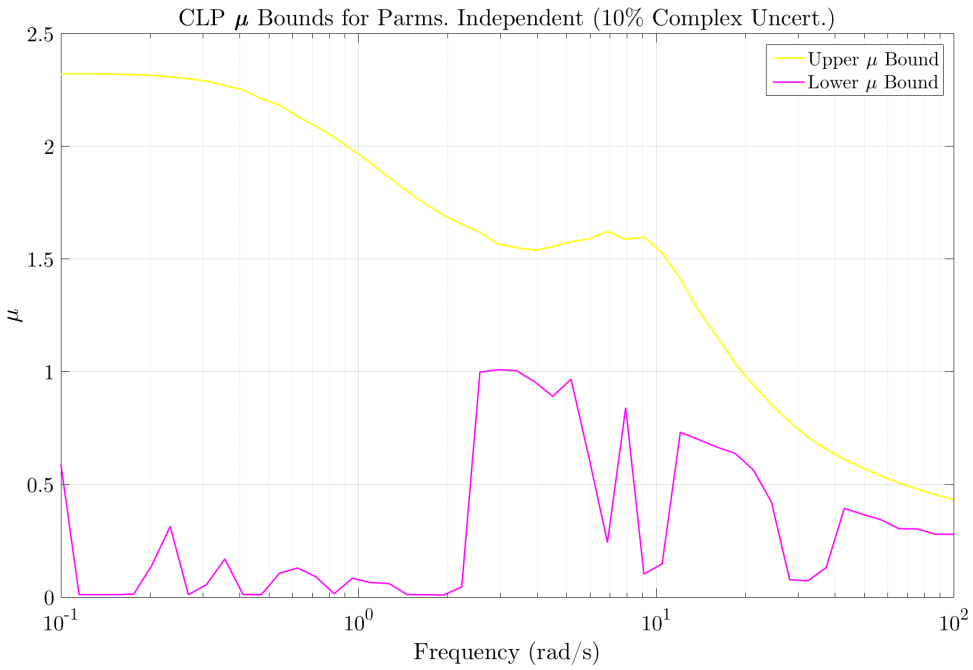

Figure 5.4: Fully Independent μ Analysis for Yaw-Roll at 120 kph with 15% Uncertainty on Each Parameter

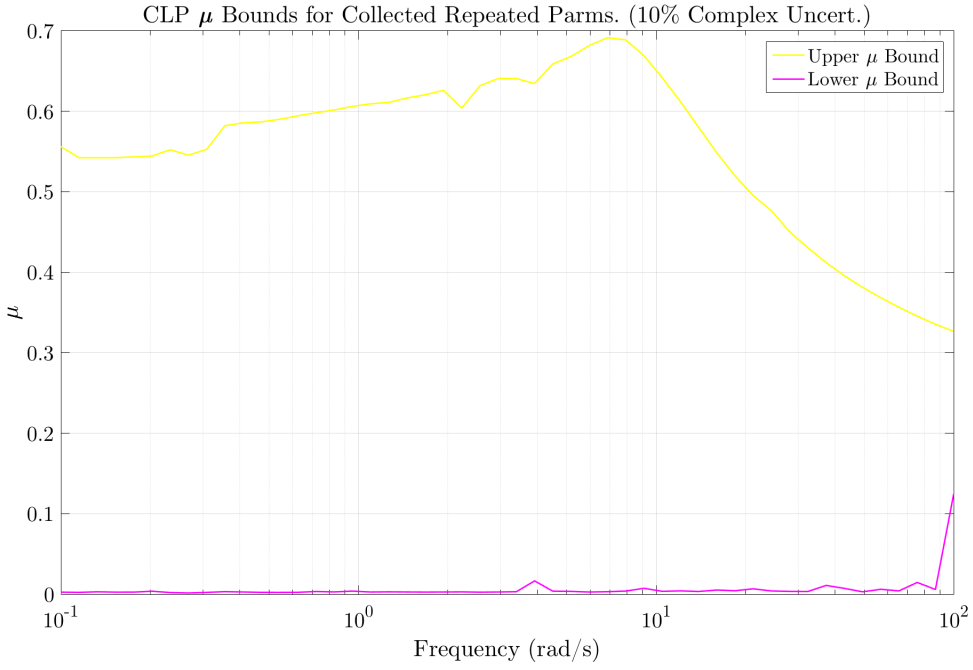

Figure 5.5: Collected Parameter μ Analysis for Yaw-Roll at 120 kph with 15% Uncertainty on Each Parameter

would also be possible to redesign the controller. But, assuming the controller is kept as is, it may mean that certain parameters need to be measured more precisely or that to achieve a greater variance on desired parameter(s) the variance of some or all of the other parameters must be narrowed to operate within a tighter range. Such narrowing specification may not be physically possible due to the system operating conditions. Also, the manner in which parameters are measured or estimated may prevent such narrowing of the initial uncertainty of some parameters.

Also of importance for the topic of parametric uncertainty and the μ calculation is that these parametric uncertainties are real terms, not complex terms, which often makes the convergence of the μ solution much more difficult. For this reason real parametric uncertainty is often avoided in place of complex uncertainty added to the system holistically when the goal is to synthesize a controller. In the controller synthesis case, the complex uncertainty is generally applied to either the input or output of a system. As mentioned earlier this uncertainty can be either additive or multiplicative complex uncertainty depending on what type of system uncertainty is being modeled. When designing a controller, the added effort of accounting for the parametric uncertainty often is not worth pursuing when the other methods can so easily account for the effects of parameter uncertainty. In the brief section on parametric uncertainty in [1] the input/output methods show mathematically why time spent on parameter uncertainty methods is not well spent for controller synthesis. The work presented in the dissertation, however, seeks to address directly the effect of parametric variations on the the closed loop system, so the extra effort is required.

The computational issue of the real parametric variance is a problem that must be dealt with. When an uncertainty block consists of all real perturbations then the μ calculation function is not necessarily continuous, which is pointed out in [28]. These discontinuities for the purely real perturbation case can cause problems in the calculations of the lower bound such that the lower bound converges to a value much lower than the upper bound or the solution may not converge at all. In [20] a technique for mixing real parametric variations

with some desired percentage of complex uncertainty is presented for the purpose of increasing the likelihood of convergence of the μ calculation. The uncertain block Δ is converted from a purely real termed to a block with the real subsets of parameters added to similarly sized weighted complex subset blocks along the diagonal. Effectively what was once a range of real perturbation values is now a "disc" in the real-imaginary plane. Mathematically Δ becomes Δ_{RC}, "Delta real-complex"

$$\Delta = \Delta_R \rightarrow \Delta_R + \alpha^2 \Delta_C \tag{5.1}$$

$$\Delta_{RC} = \Delta_R + \alpha^2 \Delta_C \tag{5.2}$$

This weighted complex additive factor is incorporated to the "varying" system, typically a frequency response, by essentially multiplying the real uncertainty of the uncertain Δ_R block by a complex variance, Δ_C, that is weighted by a value α. Because right and left sided matrix multiplication is used, the total weight applied is α^2. Typically α is kept small, but even a larger α of 0.4 is only adding 16% complexity to the uncertainty model. Another effect of this left and right side multiplication is that the size of the Δ block is doubled when a percentage of complexity is added. This real-complex uncertainty block is denoted as Δ_{RC}. The equations below outline the extra steps required for building the weighted Δ_{RC}, which involves altering the system M, M_{vary}, to account for the increase in size of the uncertainty block. The subscript "vary" refers to frequency points set by the designer, which cause the size of the system M to change with respect to the number of frequency points.

$$W_L = \begin{bmatrix} I_{n\times n} \\ \alpha I_{n\times n} \end{bmatrix} \tag{5.3}$$

$$W_R = W_L' = \begin{bmatrix} I_{n\times n} & \alpha I_{n\times n} \end{bmatrix} \tag{5.4}$$

$$M_{mix} = W_L M_{\text{vary}} W_R \tag{5.5}$$

$$\Delta_{RC} = \begin{bmatrix} \Delta_R \\ \Delta_C \end{bmatrix} \tag{5.6}$$

$$\text{bounds}_{RC} = \mu\left(M_{mix}, \Delta_{RC}\right) \tag{5.7}$$

Note that the effect of adding a small amount of complexity to each uncertain parameter results in a slightly more conservative solution in the μ bound results. This conservativeness means that the upper bound solution of μ is slightly larger than would be the case for the purely real condition based solution. A comparison of the effects of the upper and lower bound solutions versus the complex value weighting α can be found in [20]. Additionally, mixed real and complex parametric uncertainties are discussed in [29] and the real parametric perturbation case is well presented for a helicopter model in [30].

5.3.2 Skew μ for the Each Uncertain Parameter of the Coupled Yaw-Roll Model

Once the μ for the system is found to not be above one and the assumptions on the model or models for initial uncertainty are satisfactory the skew μ analysis can be performed. The maximum skew μ is the primary interest, but examining the skew μ across the frequency spectrum helps to understand the important frequencies with respect to the parameter variations.

Unique to this dissertation, the real parametric uncertainty with weighted complex uncertainty technique was extended to the skew μ case. This conservativeness for the skew μ case means that the solution of allowable parametric variances, which comes from the upper bound, might be less than the system could handle in reality. There is still concern with the lower bound as it is used as a measure for the tolerance of solution convergence. Thus, it is important to perform the skew μ search over a continuous set of conditions.

The process for the skew μ calculation is slightly different than the single μ calculation for the system. The skew μ calculation is an iterative process where only the designated subset of parameters of the system is scaled by k, the inverse of the current μ upper bound.

After scaling the subset, the whole system is tested with a calculation of a new μ value, called the skewed-mu. This process is repeated until the tolerance set on the difference between current and previous lower bound of the μ solution is met or the maximum number of iterations is exceeded. This specified tolerance is why the lower bound is still important even though the upper bound is used to implement the parameter scaling.

For the vehicle model, it has been shown in [6] that velocity greatly affects the lateral dynamics of a vehicle system even though it is often used as a "static" parameter for the vehicle model to operate about. For this reason the skew μ is analyzed at several velocity points. Also, the initial uncertainty was made uniform across the parameters for simplicity. However, it is also advantageous to consider how well a parameter may be measured and how much it is expected to vary. For example, the cornering stiffness, C_α, is known to vary by up to 30 % depending on the range of driving conditions due to changes in tire loading and other factors.

No specific assumptions about the uncertainty or practical expected variation of parameters were made for the initial study of the vehicle system presented in the next subsections. This type of equal weighted uncertainty modeling of the initial uncertainty is useful to gauge how each parameter can independently vary before the μ condition is violated. The skew μ analysis for the vehicle model with equal initial uncertainties is presented below for several operating speeds.

5.3.2.1 Skew μ for 15% initial uncertainty at 50, 90 and 120 kph

In Section 5.3.1, an initial uncertainty model of 15% uncertainty for all parameters was examined. A value of 15% keeps the parameters very close to their nominal values. But, with a total of 10 parameters, all with initial uncertainty, the resulting system has quite a bit of uncertainty incorporated into the vehicle model. In this section, the skew μ analysis is carried out such that the varying subset is comprised of only one parameter. However, the varying Δ_v subset is not scalar but is a diagonal matrix containing all the repeated instances

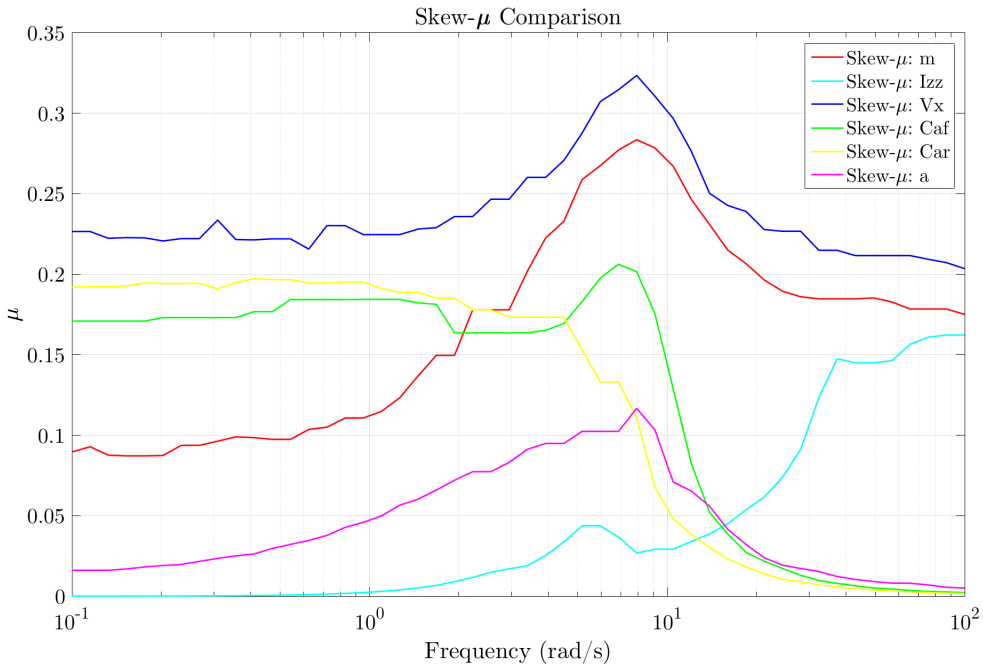

Figure 5.6: Skew μ with 15% Uncertainty Each Parameter for Speed of 120 kph

of the variable of interest. The fixed subset Δ_f likewise contains the collected uncertainty instances of the other 9 parameters.

Recall from Figure 5.5 that the maximum value of the upper μ bound was roughly 0.7 for a vehicle traveling at 120 kph a velocity that it is within the range of typical vehicle speeds on the highway. Therefore, there is space remaining for additional uncertainty in the system. Figures 5.6 and 5.7 show the skew μ results of the vehicle system at 120 kph with initial 15% uncertainty for each parameter both in the fixed subset and for the single parameter in varying subset.

For this case, while the initial uncertainties are somewhat small and the velocity is relative high, there is still a relatively large "space" remaining on almost every parameter that is isolated in the Δ_v varying subset when all others are fixed and a skew μ is calculated. Note, while the isolated cases are presented together in the same plots only one parameter, as specified in the legend, was allowed to vary while the other nine were held to the initial uncertainty bounds.

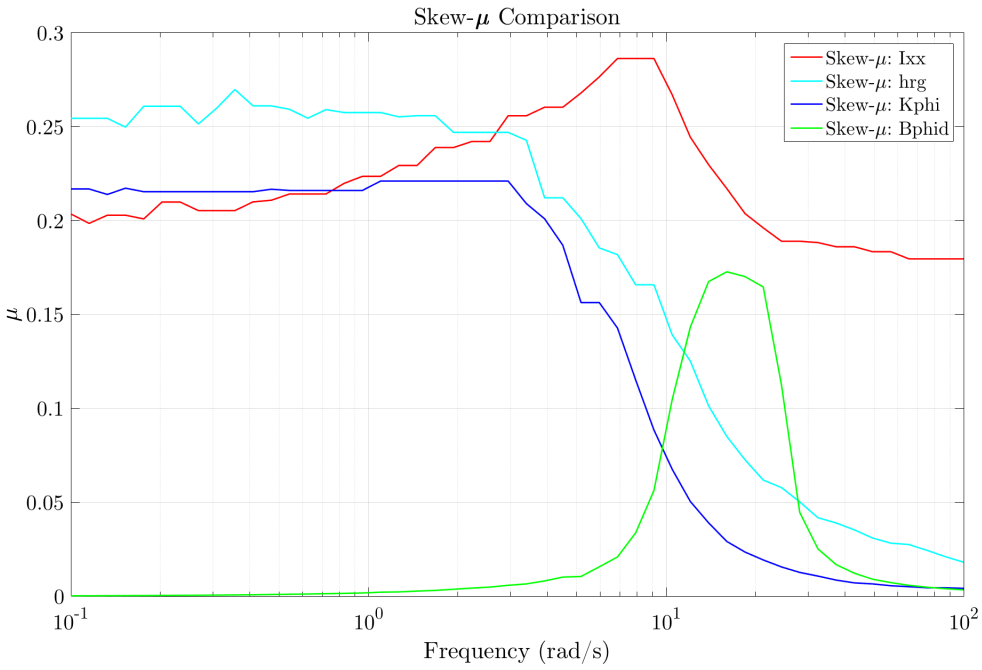

Figure 5.7: Skew μ with 15% Uncertainty Each Parameter for Speed of 120 kph

Table 5.1 represents the uncertainty for the yaw-roll model with an initial uncertainty of 15% for all parameters and a V_x of 120 kph. Recall, that the skew μ is the inverse of the allowable scaling that is applied to the Δ_v varying subset and represented in column two of the table. The table also includes the value change for each parameter that the respective scaling would apply to the appropriate nominal parameter. Columns four and five contain the maximum and minimum of each parameter when the delta value is added and subtracted respectively. Finally, the last column contains the percent difference of the nominal parameter to the maximum (and minimum) scaled parameter. This percent difference is the most useful measure for quickly understanding how much the parameter is affected in physical terms. Note that any negative values in the minimum may not be a realistic value. For example the negative inertia would not be achievable in reality.

The skew μ results for the identical initial uncertainty cases are presented in Figures 5.8- 5.11. Figures 5.8 and 5.9 are for the 90 kph case ($\approx$56 mph) and Figures 5.10 and 5.11 are for a vehicle speed of 50 kph ($\approx$ 35 mph).

Table 5.1: Available Uncertainty for Yaw-Roll Model at 120 $^{km}/_{\text{hr}}$ and Initial Uncertainty 15%

Param.	Scale ($^1/_\mu$)	Nominal Param.	Delta Param.	Max. Param.	Min. Param.	%-Diff.
m	4.05	1430	869.69	2299.69	560.31	60.82 %
I_{zz}	8.48	2059.2	2619.92	4679.12	-560.72	127.23 %
V_x	3.46	33.33	20.27	53.61	13.06	51.84 %
$C_{\alpha f}$	5.50	68439.81	41624.12	110064.92	26816.68	82.56 %
$C_{\alpha r}$	5.11	68439.81	41624.12	110064.92	26816.68	76.62 %
a	12.62	1.050	0.639	1.689	0.41	189.23 %
I_{xx}	3.94	700.7	426.15	1126.85	274.55	59.15 %
h_{rg}	4.31	0.650	0.383	1.013	0.25	64.71 %
K_ϕ	4.94	216148.33	131456.03	347603.69	84691.64	74.16 %
$B_{\dot{\phi}}$	6.25	16825.90	10233.15	27059.09	6592.79	93.68 %

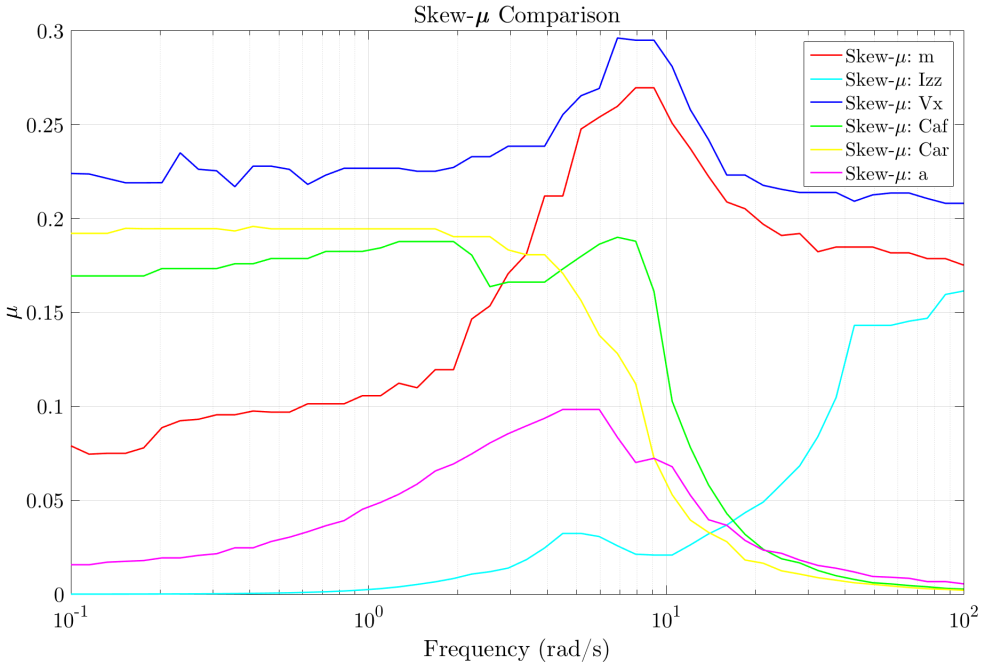

Figure 5.8: Skew μ with 15% Uncertainty Each Parameter for Speed of 90 kph

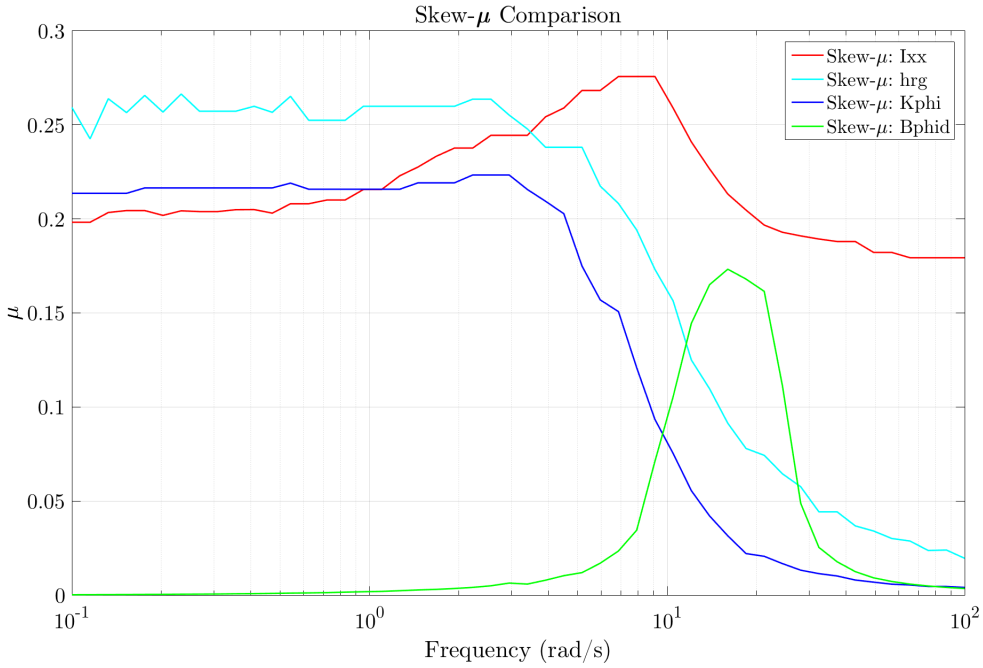

Figure 5.9: Skew μ with 15% Uncertainty Each Parameter for Speed of 90 kph

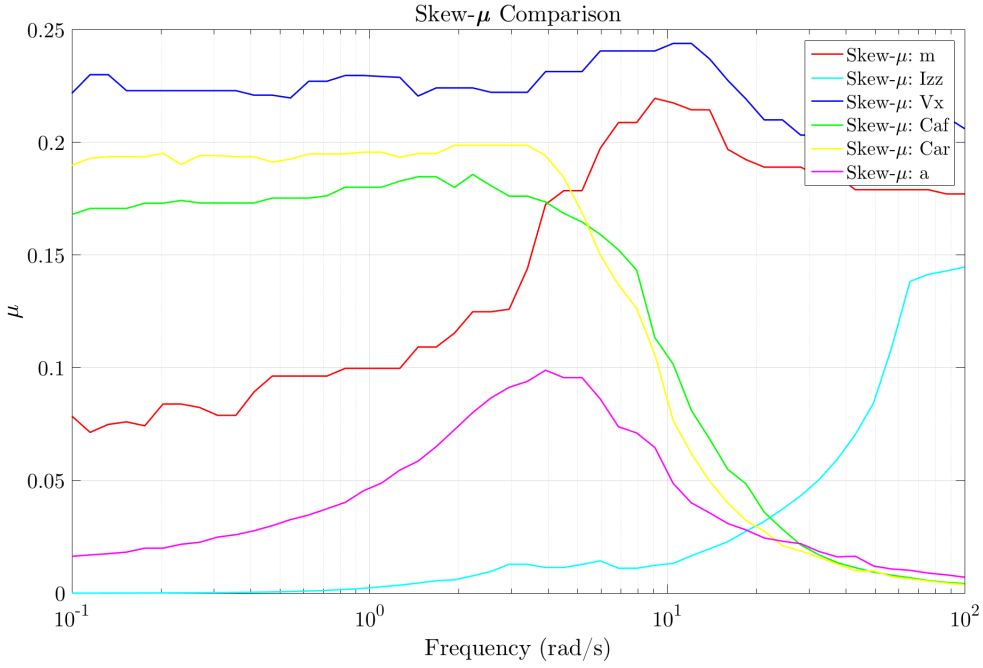

Figure 5.10: Skew μ with 15% Uncertainty Each Parameter for Speed of 50 kph

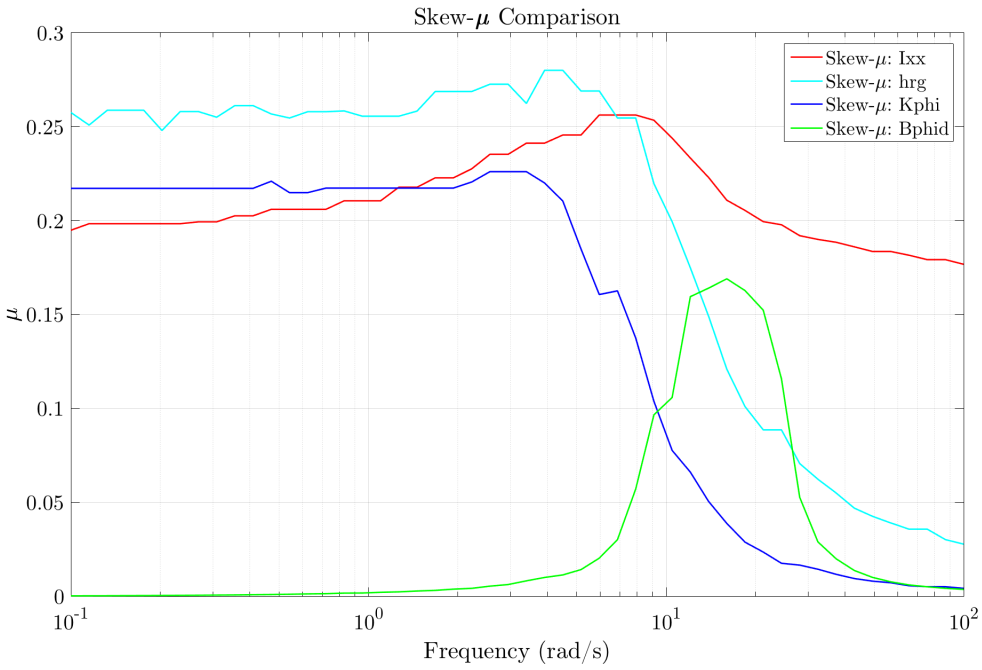

Figure 5.11: Skew μ with 15% Uncertainty Each Parameter for Speed of 50 kph

It is difficult to discern trends in the peak skew μ or the span values across the range of frequencies as the speed is lowered except for the longitudinal velocity V_x parameter. The decreasing trend for the peak μ value of V_x is μ values of roughly 0.31, 0.29 and 0.24. Note, that this decrease in μ for the V_x parameter is akin to an increase in the scaling value k for the V_x parameter. Therefore, it makes since that as the velocity is reduced in the nominal system more "space" for variation is available.

Another observation made of the skew μ is that frequencies of 5 to 8 rad/s are roughly the peak in parameter scaling for most of the parameters. The exceptions at which the peak occurs at a greater frequency are the suspension dampening, $B_{\dot{\phi}}$, that peaks around 16 rad/s and the yaw inertia, I_{zz}, which peaks at the end of the tested frequency window, 100 rad/s. Since the primary concern is with the overall maximum, it is interesting to see where these peaks occur. Most seem to occur near the typical steering input cutoff range of 1-2 Hz (or 6.3 rad/s to 12.6 rad/s). The skew μ for yaw inertia, I_{zz}, even has a small sub-peak at roughly 8 rad/s for speeds of 120 kph and 90 kph.

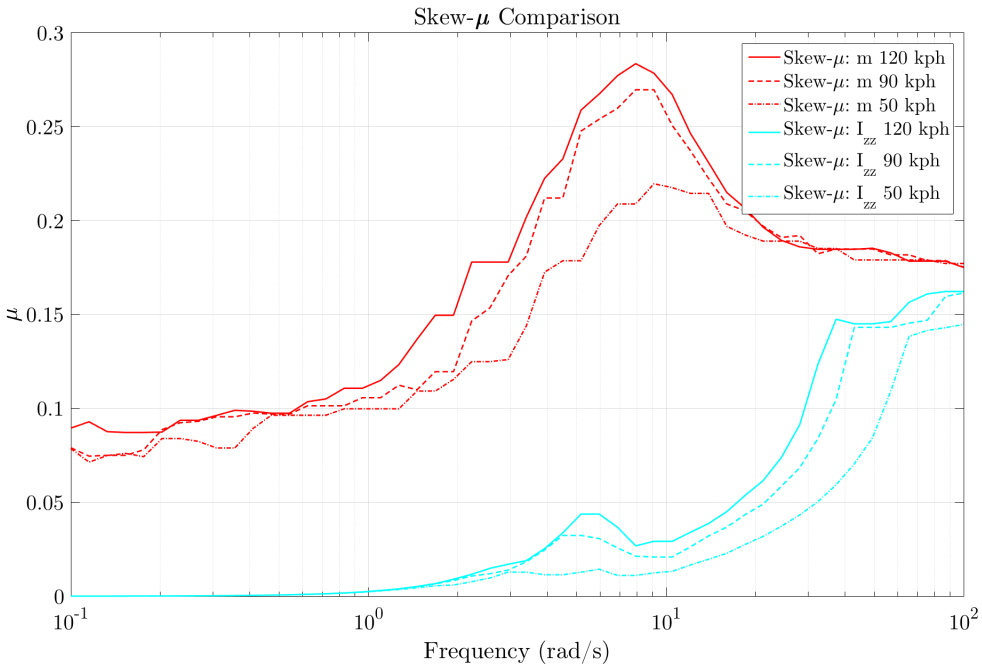

Figure 5.12: Skew μ of Mass and Yaw Inertia with 15% Initial Uncertainty on Each Parameter for Speeds of 50, 90 and 120 kph

It would be intuitively expected that many of the parameters would be influenced by a change in speed because the lateral and roll dynamic outputs for the vehicle model are observed to be less intense in magnitude at the lower speeds across the frequency spectrum. However, this is less obvious in the Figures 5.8- 5.11. Therefore examining several skew μ results overlaid with respect to speed is more useful.

5.3.2.2 Skew μ with initial uncertainty of 5%, 10% and 15% at 120 kph

The idea in this section is to see how the skew μ for the single-isolated varying parameter in the set Δ_v is affected when the initial uncertainty, for the cases in which initial uncertainty is set uniform across all the parameters in the total set Δ_s, is altered. Because the overall μ value decreases with a decrease in the uncertainty of parameters, it is expected that the skew μ for all the cases would decrease, i.e. that the scaling k applied for each parameter in the varying set would increase. With a lower initial uncertainty there is more "space" for variation among the parameters in the varying set. Keep in mind that for the skew μ cases

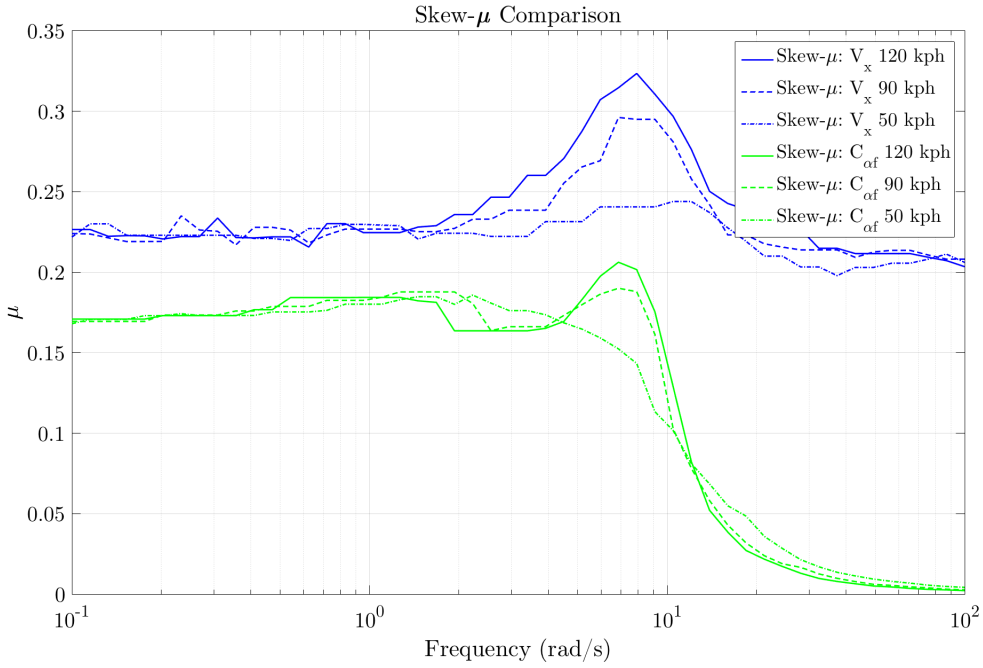

Figure 5.13: Skew μ of Velocity and Front Cornering Stiffness with 15% Initial Uncertainty on Each Parameter for Speeds of 50, 90 and 120 kph

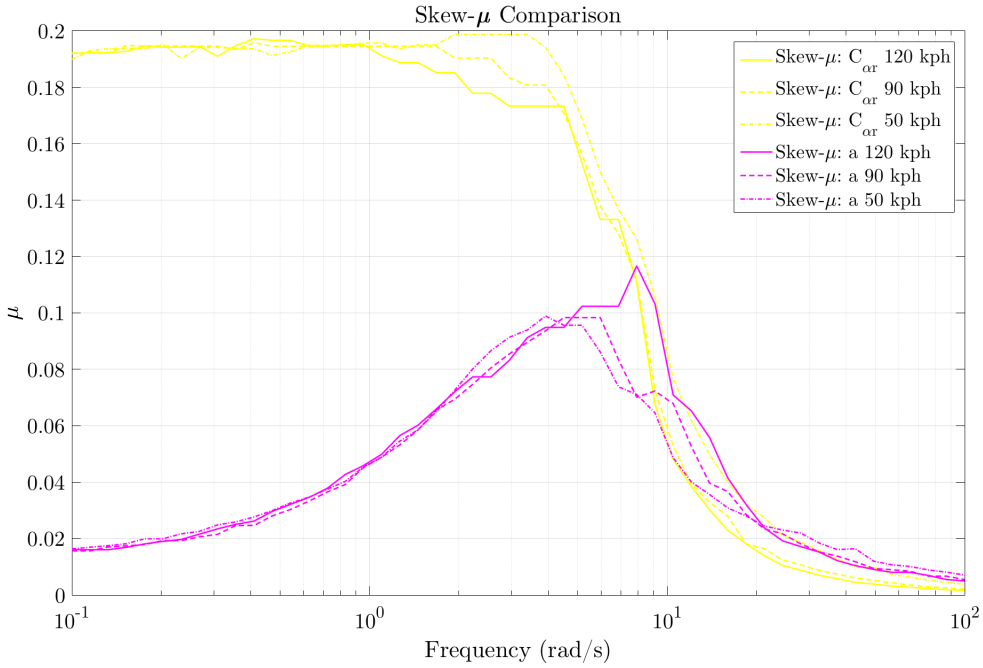

Figure 5.14: Skew μ of Rear Cornering Stiffness and Weight Split 'a' with 15% Initial Uncertainty on Each Parameter for Speeds of 50, 90 and 120 kph

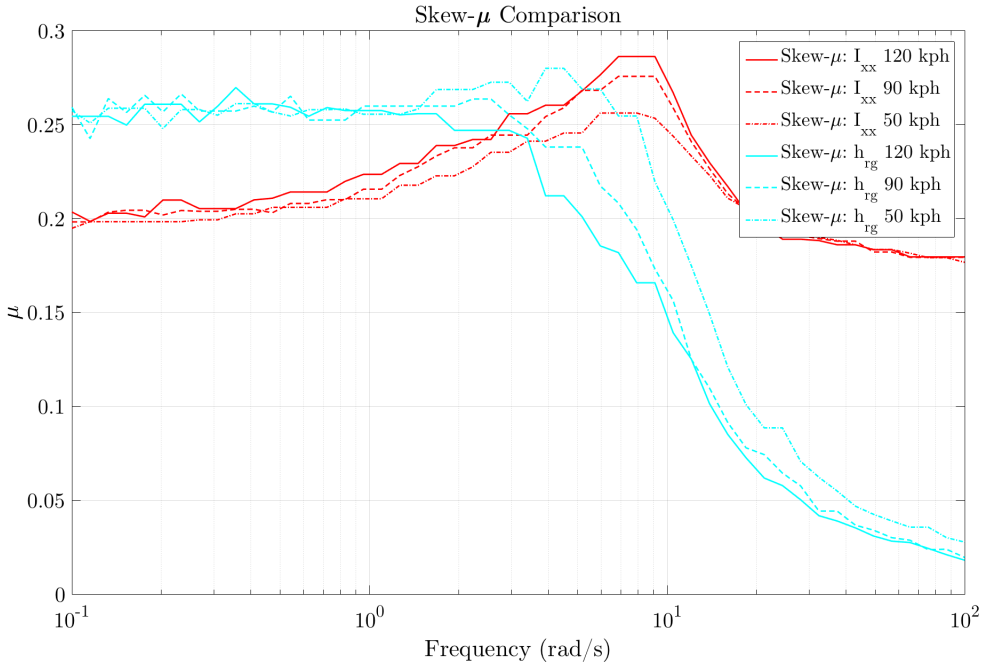

Figure 5.15: Skew μ of Roll Inertia and c.g. Height with 15% Initial Uncertainty on Each Parameter for Speeds of 50, 90 and 120 kph

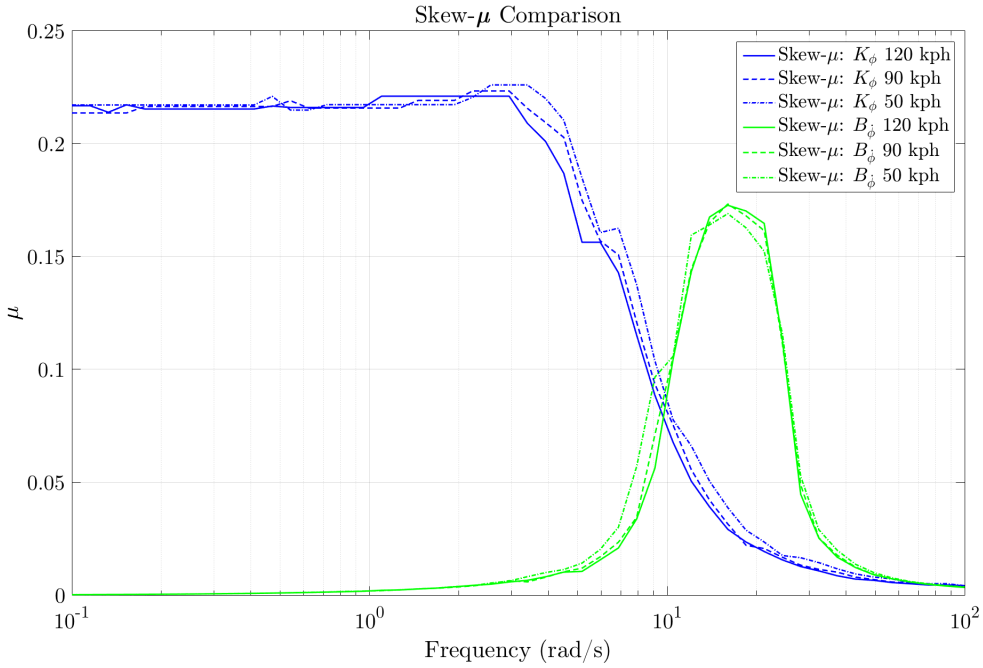

Figure 5.16: Skew μ of Roll Stiffness and Roll Damping with 15% Initial Uncertainty on Each Parameter for Speeds of 50, 90 and 120 kph

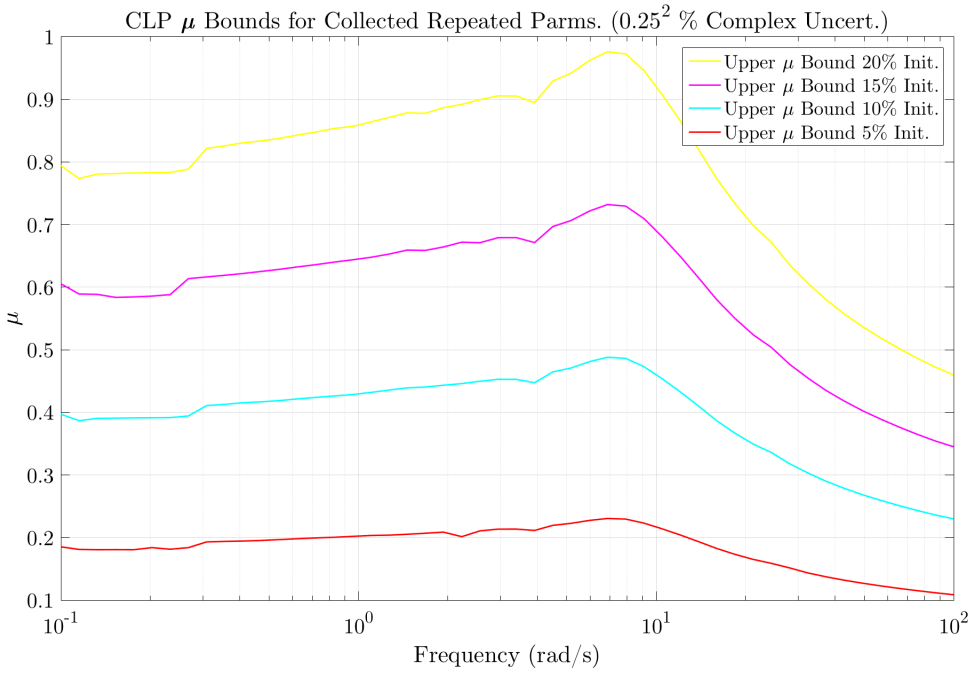

Figure 5.17: μ of System for Several Initial Uncertainty Values on Each Parameter for Speed of 120 kph

presented in this chapter only a single parameter is placed in the varying subset, Δ_v, but the varying subset may not be scalar due to repeated instances of the isolated parameter.

The processing time for the vehicle yaw-roll model with full parametric uncertainty is quite long, anywhere from 20 to 45 minute run times depending on the number of frequency points specified. Therefore, the closed loop system with different initial uncertainty is presented only at the 120 kph speed. First, a basic μ analysis is performed, meaning the entire set of parameters is fixed at the initial uncertainty. This baseline analysis is always recommended to check if the system is capable of additional variance before performing any skew μ analysis. The baseline μ values for cases of initial uncertainty set at 20%, 15%, 10% and 5% for all 10 of parameters is presented in Figure 5.17. In this plot of the upper bound μ value versus frequency observe that as the uncertainty rises on the initial condition the μ value gets closer to the unity value of one. Thus, the increase in uncertainty for the cases is correlated with μ values that indicate lesser additional system variance is available. Figure 5.18 contains the skew μ of the mass and the yaw inertia for cases of initial uncertainty at

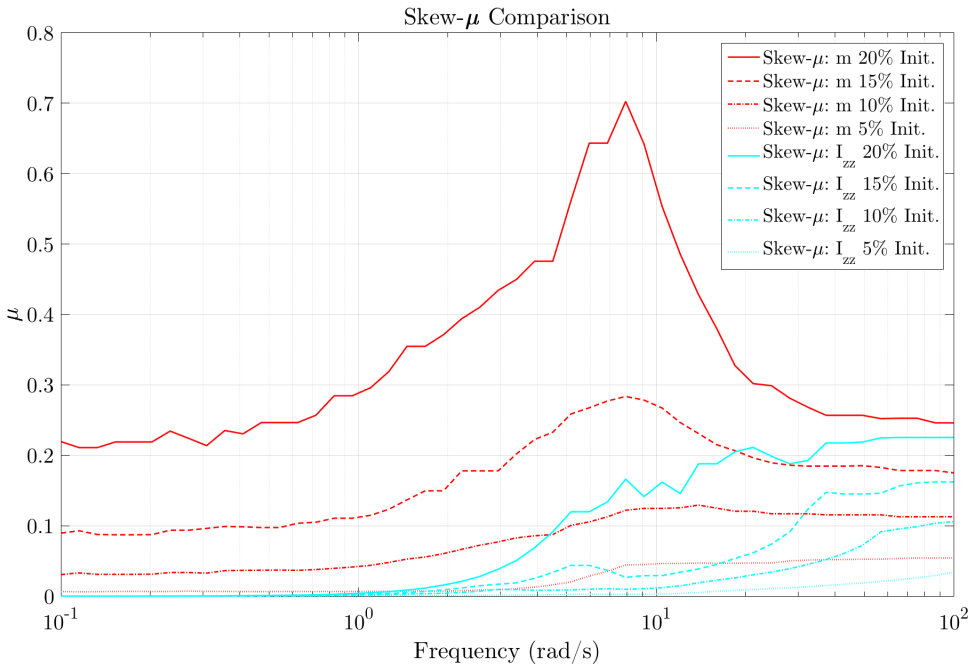

Figure 5.18: Skew μ of Mass and Yaw Inertia for Several Initial Uncertainty Values on Each Parameter for Speed of 120 kph

20%, 15%, 10% and 5% for all 10 of parameters. A similar trend to the μ of the system is observed in Figure 5.18 for the skew μ values of the parameter that is allowed to vary to the limit of μ equal to unity for the system. However, the amount of additional variation is not the same as evidenced by the dissimilar peak values for the mass and yaw. A look at the peak values for each isolated parameter case versus the initial uncertainty percentage gives an indication to the influence a particular parameter has on the total system. A lower skew μ value means the parameter scaling is relatively large and the particular parameter can take on on a larger variation before the stability and or the performance of the closed loop system is violated, i.e. μ greater than or equal to one. For example, the peak 0.7 skew μ for mass means the mass can be scaled 1/0.7 times, roughly 1.2 times, before the conditions are such that performance can no longer be guaranteed. Whereas, the peak of 0.23 means the inertia can be scaled 4.8 times. Therefore the uncertainty of mass has a larger influence then on the system performance. A better method though of understanding the influence from each parameter though is discussed next in Chapter 6.

5.4 Conclusions

The concept of μ and the skew μ was explored for real parametric uncertainty of the the coupled yaw-roll vehicle model. The skewed μ analysis showed the model parameters had remaining "space" to vary given an initial uncertainty for each parameter. If the initial uncertainty is increased for some or all of the parameters then there is less space remaining for further variation in the parameters. Assuming the model is an accurate representation of the system, a designer can use the technique to answer the question of how much uncertainty is allowable for a single isolated parameter in the closed loop and still maintain a specific performance criteria.

Chapter 6

μ Sensitivity and the Determination of Parameter Scaling Groups

6.1 Introduction

In this chapter a method to analyze the sensitivity is presented. It has been shown in [3] that the sensitivity of the open loop is not necessarily the same as the closed loop sensitivity due to the influence of the controller. Additionally, the closed loop sensitivity calculation based on the eigenvalues does not capture any information with respect to operating frequency spectrum. The μ based sensitivity approach, however, is a method that provides a sensitivity value at each frequency point for the parametrically perturbed system with reference to the nominal system. The μ sensitivity discloses which parameters are most influenced by the μ scaling. This is important to know for the skew μ analysis. With the μ sensitivities known the parameters can be intelligently grouped together into the fixed and varying subsets of the uncertain matrix, Δ.

6.2 Methodology Sensitivity

Section 2.3 discussed the details of the setup of the μ sensitivity calculation. In brief, the eigenvalue sensitivity calculation is the change of the "perturbed" system eigenvalue with respect to the nominal system eigenvalue divided by the amount of the parameter change. For the eigenvalue sensitivity calculation, each parameter was perturbed individually by 10% from the nominal value of the respective parameter.

For the μ sensitivity calculation the parameters were effectively perturbed by 1%. Specifically, the initial uncertainty was set to 10% for all parameters in the entire set of Δ. Then, the parameter of interest, placed in side the subset of Δ_v, was set to vary by 10%. Thus,

the net change in the parameter was 0.10 times 0.10 or 1 % for the resulting perturbation that the skew μ was calculated from.

With respect to the eigen sensitivity, the μ sensitivity calculation is similar except that it is the change in μ value from the "perturbed" system with respect to the μ of the nominal system that is divided by the change in parameter value at each frequency point. The division of the change in parameter ensures the parameters are dimensionless. The sensitivities can be compared relative to each other for a given method. However, both of the two methods are not meant to compare directly because the scale of the sensitivity from the eigenvalue method is different from that of the μ based sensitivity method. What is important is determining the most sensitive parameter with the eigenvalue calculations and comparing that set with the most sensitive group of parameters from the μ sensitivity calculations.

6.3 Application to Yaw-Roll Vehicle Model with Full Parametric Uncertainty

Here the sensitivities for the yaw-roll vehicle model are calculated and analyzed across the operating frequency and in terms of the the maximum sensitivity value from the frequency range. The yaw-roll model with full parametric uncertainty is used for the μ sensitivity analysis. Uniform initial uncertainty of 10 % is set with a single varying parameter of interest and placed in the Δ_v set for the skew μ calculation.

6.3.1 Aggregate Sensitivity

First, and most importantly, the peak sensitivity is examined and compared to the eigenvalue sensitivity which is itself an aggregate characteristic of the system with respect to the frequency. Figure 6.1 shows the eigen sensitivity, for the open and closed loop system in blue and green bars, respectively. Observe that the open loop eigenvalue sensitivity maximum values are slightly different than the maximums for the closed loop eigenvalue sensitivity, but there is very little difference in the most sensitive parameters. Both the open loop and closed loop analysis indicates that I_{xx}, K_ϕ and $B_{\dot{\phi}}$ are quite influential parameters

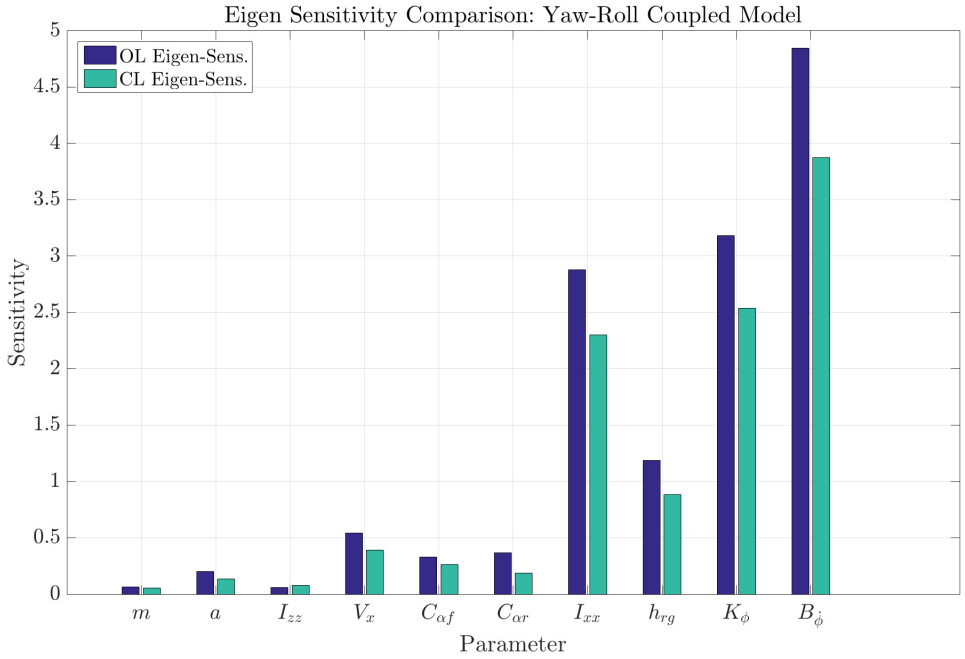

Figure 6.1: Eigen Sensitivity Yaw-Roll model 15% Initial Uncertainty at 120 kph

for the system. This should make sense given that the a PI controller is used, which adds a zero and a pole and then shifts the dominate poles of the system a bit via the proportional gain. Therefore the PI controller does not create a large change in the system eigenvalues. In general, however, the controller implemented may have a greater influence on the sensitivity depending on the specific controller and specific system. It would be expected though that a system with derivative or other poles added from the controller may have a sensitivity results that are not as similar as the the yaw-roll vehicle model and PI controller presented here. For this vehicle system, the eigenvalue sensitivity indicates only a slight attenuation of the sensitivity of the parameters in the presence of the controller. The most influential parameters, I_{xx}, K_ϕ and $B_{\dot{\phi}}$, in the open loop remain the most influential in the closed loop but have a more visibly reduced sensitivity.

Turning to the μ sensitivity analysis for the same parameter cases, which is presented in Figure 6.2, it is evident that the frequency based μ sensitivity reveals a different result for the closed loop eigen analysis. The reason for this difference is that the μ value calculated

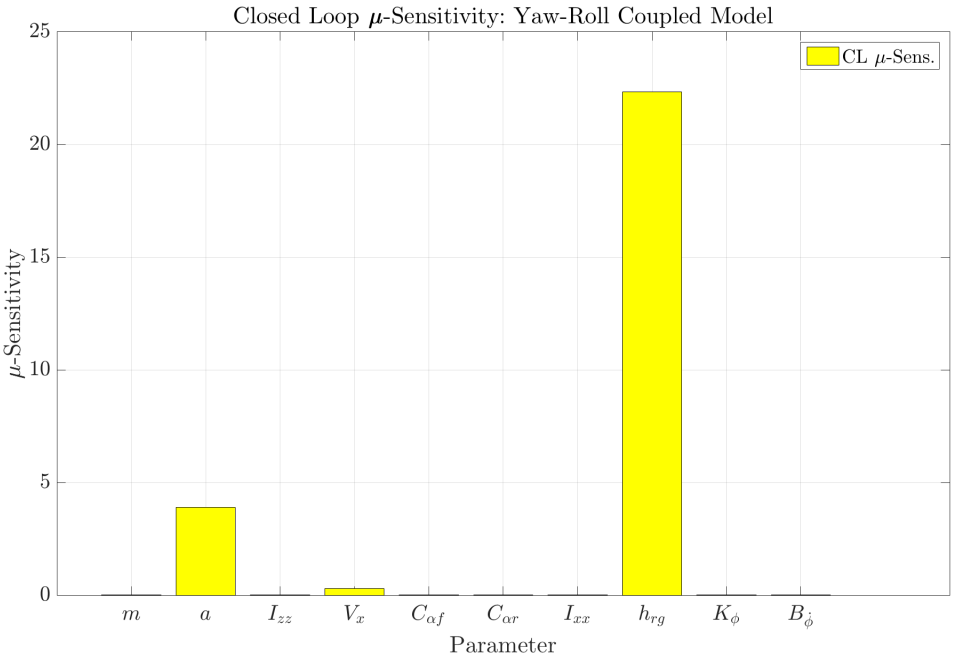

Figure 6.2: μ Sensitivity Yaw-Roll Model 10% Initial Uncertainty at 120 kph

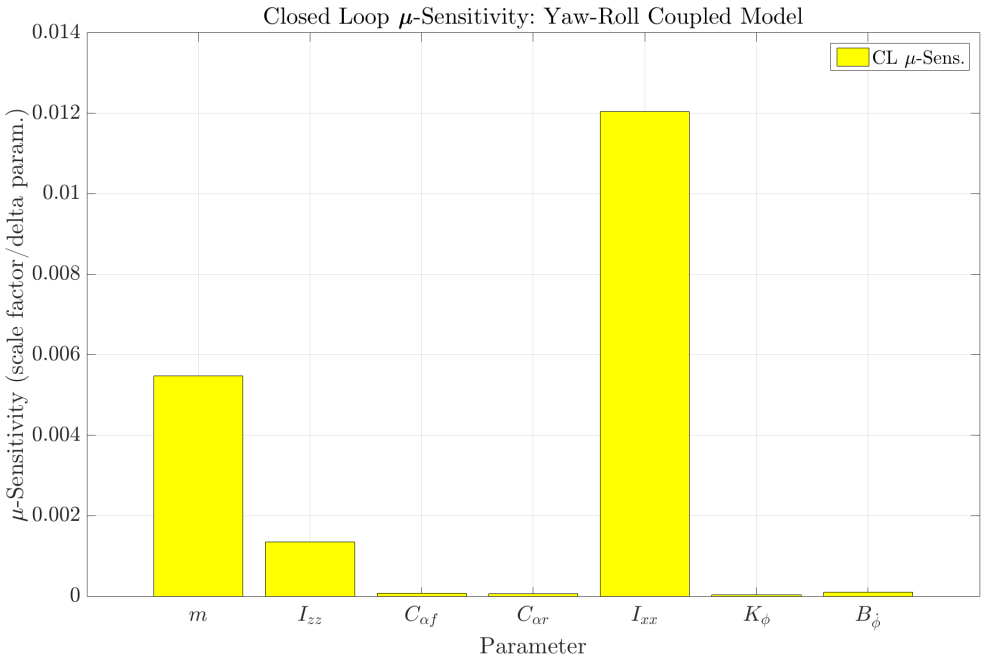

Figure 6.3: μ Sensitivity Select Parameters Yaw-Roll Model 10% Initial Uncertainty at 120 kph

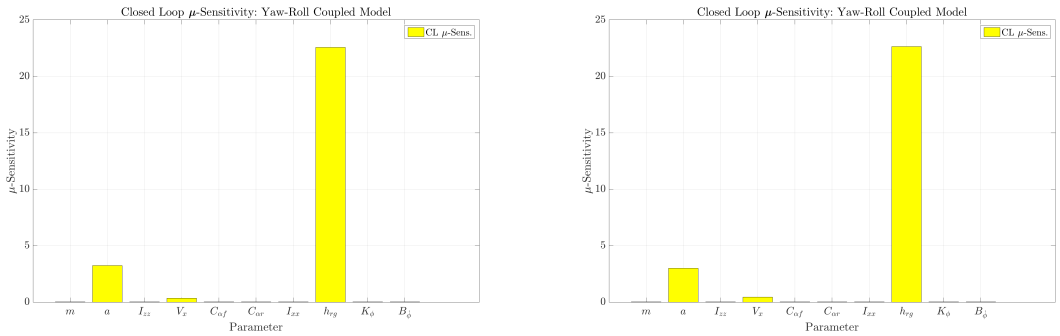

Figure 6.4: μ Sensitivity Yaw-Roll model 10% Initial Uncertainty (Left at 90 kph; right at 50 kph)

over the range of frequencies, incorporates initial uncertainty assigned to parameters and better accounts for the "directional" effects of the system eigenvalues, which is more relevant for MIMO systems.

Studying the μ sensitivity closer, the top influential terms in the closed loop are h_{rg}, a and V_x. The terms deemed most sensitive in the closed loop eigenvalue analysis, I_{xx}, K_ϕ and $B_{\dot{\phi}}$, are in fact of the least influence to the closed loop system per the μ sensitivity as shown in Figure 6.3 where the h_{rg}, $a$and V_x have been removed form the bar chart. Additionally, the closed loop μ sensitivity suggest that weight split parameter a has close to the least effect on performance and stability in the closed loop with the PI controller included. For completeness the maximum μ sensitivities for the 50 and 90 kph velocities are represented in Figures 6.4 and 6.5 respectively. The characteristics are largely the same for both the sensitivity at 90 and 120 kph.

6.3.2 Sensitivity Trends Across Frequency

While the maximum μ sensitivity is useful to characterize broadly the influence of parameters on the system, a look at the the μ sensitivity across the frequency spectrum can be useful as well. First, a look at the μ sensitivity for the mass, yaw inertia and roll inertia in Figure 6.6 shows that the maximum uncertainty value tends to occur at the frequency in which the max skew μ value occurs. Referring back to Figure 5.12 it can be seen that the

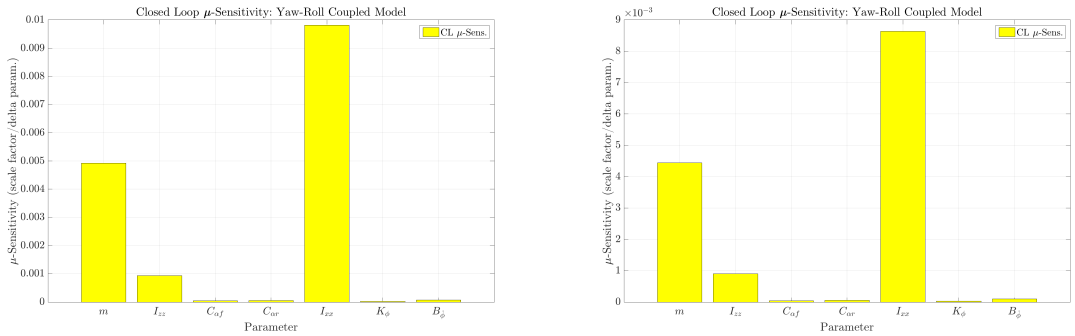

Figure 6.5: μ Sensitivity Select Parameters Yaw-Roll model 10% Initial Uncertainty (Left at 90 kph; right at 50 kph)

max skew μ value for the roll inertia is between 8 and 11 rad/s depending on the operating velocity, and in Figure 6.6 the μ sensitivity maximum occurs within the 8 to 11 rad/s as well. The mass μ sensitivity and skew μ have a similar locations of the peak as well. The yaw inertia sensitivity is without a true peak and seems to rise proportionally with the frequency. Recall from Figure 5.12 that the skew μ for the yaw inertia increased with velocity as well. Thus, there is a loose correlation between the frequency at which the maximum skew μ and the maximum sensitivity occurs. There are a few cases where the frequency locations of the maximum μ and maximum μ sensitivity value do not correlate exactly. Figure 6.7 contains the μ sensitivity for case of an isolated velocity parameter and an isolated weight split parameter. The μ sensitivity for $V_x$is not marked by any clear peak where as in the skew μ analysis a peak was observed in the 8 to 10 rad/s range in Figure 5.13. Physically this means that the maximum allowable scaled value is determined by the peak in the skew μ plot. This scaled value is by nature of the μ analysis, the maximum conservative scaling. However, the μ sensitivity indicates that changes of V_x have roughly the same impact across the range of frequencies; there is no frequency in which velocity affects the system to any greater or lesser degree. The sensitivity of a has a peak that is aligned near the same 4 rad/s location as the peak of the skew μ value from Figure 5.14 for the 50 and 90 kph velocities.

Figures 6.8-6.11 represent the mu- sensitivity for the remaining parameter cases: the pair h_{rg} and a(for reference), the pair $C_{\alpha r}$ and K_ϕ, the single $C_{\alpha f}$ parameter and finally the

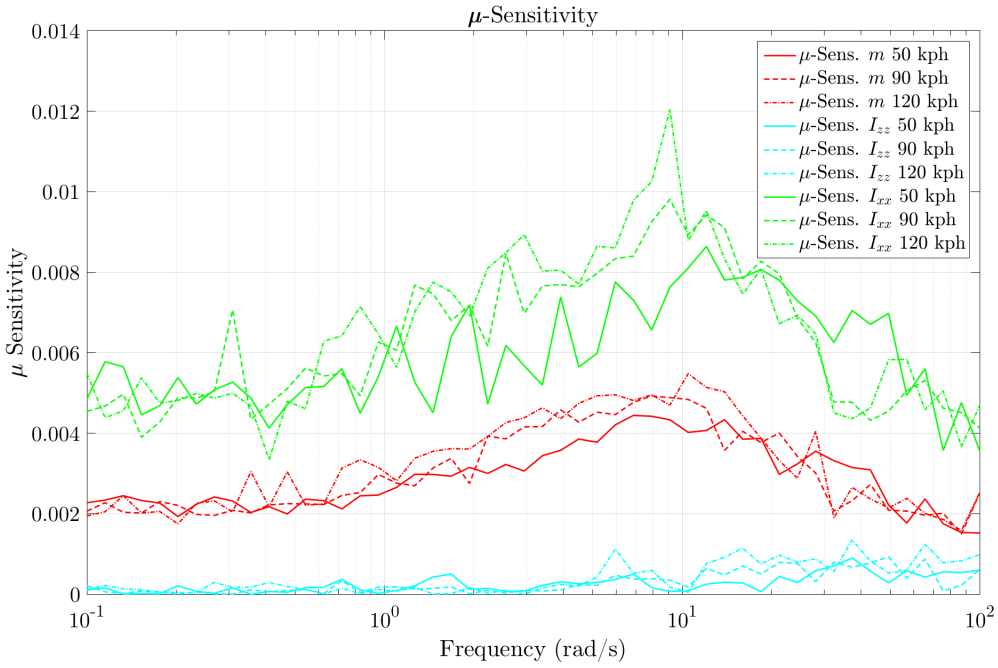

Figure 6.6: μ Sensitivity vs. Frequency of m , I_{zz} and I_{xx} for the Yaw-Roll model 15% Initial Uncertainty at 50, 90 and 120 kph

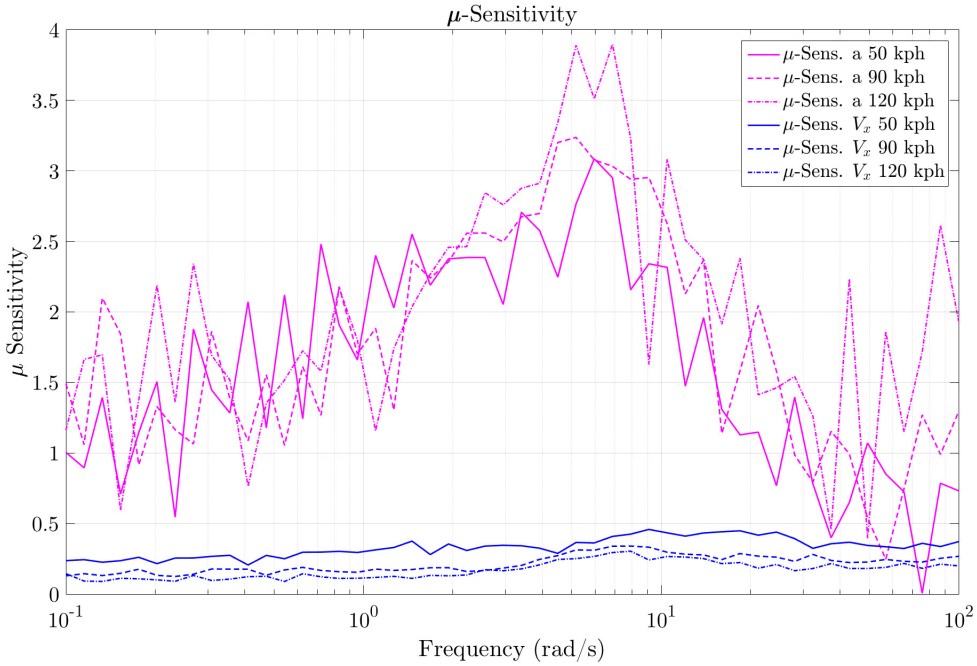

Figure 6.7: μ Sensitivity vs. Frequency of a and V_x for the Yaw-Roll model 15% Initial Uncertainty at 50, 90 and 120 kph

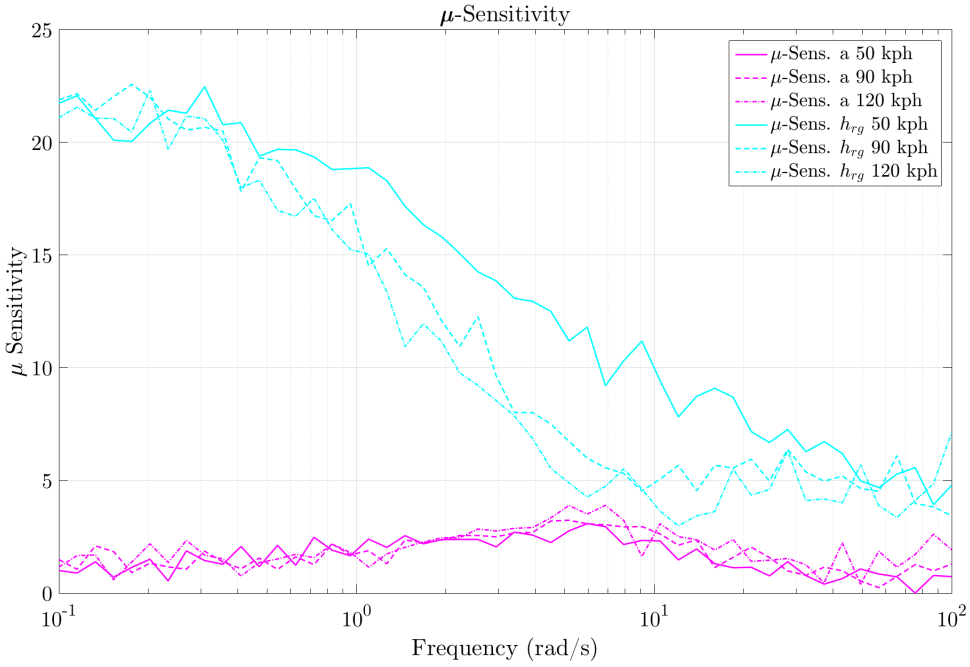

Figure 6.8: μ Sensitivity vs. Frequency of a and h_{rg} for the Yaw-Roll model 15% Initial Uncertainty at 50, 90 and 120 kph

single $B_{\dot{\phi}}$ parameter. The sensitivity for h_{rg} in Figure 6.8 rolls off much more gradually than the sudden "drop" observed in the skew μ for h_{rg} in Figure 5.15. In fact, here the"cutoff" frequency in low pass filtering terminology is much different: 2-4 rad/s for the skew μ cutoff vs. 0.3-0.4 rad/s cutoff frequency range for the μ sensitivity. A possible interpretation of this difference is that changes to the cg height have a greater effect on the μ value at low frequencies than at higher frequencies. Where as, the frequency which determines the maximum cg height that is allowable occurs under much more excitation in the high frequency band. So, a change to the cg has more "noticeable" effect on the μ value at lower frequencies, but the most change the system can handle occurs in the faster to mid range of the frequency response.

The μ sensitivity for $C_{\alpha r}$ and K_{ϕ} over the frequency range are also marked by a trend where the lower frequencies are where highest sensitivity occurs while simultaneously the lower frequency skew μ values in Figure 5.14 and 5.16 are very "flat" and almost match the maximum allowable frequency that occurs in the middle of the range. Oddly, the least

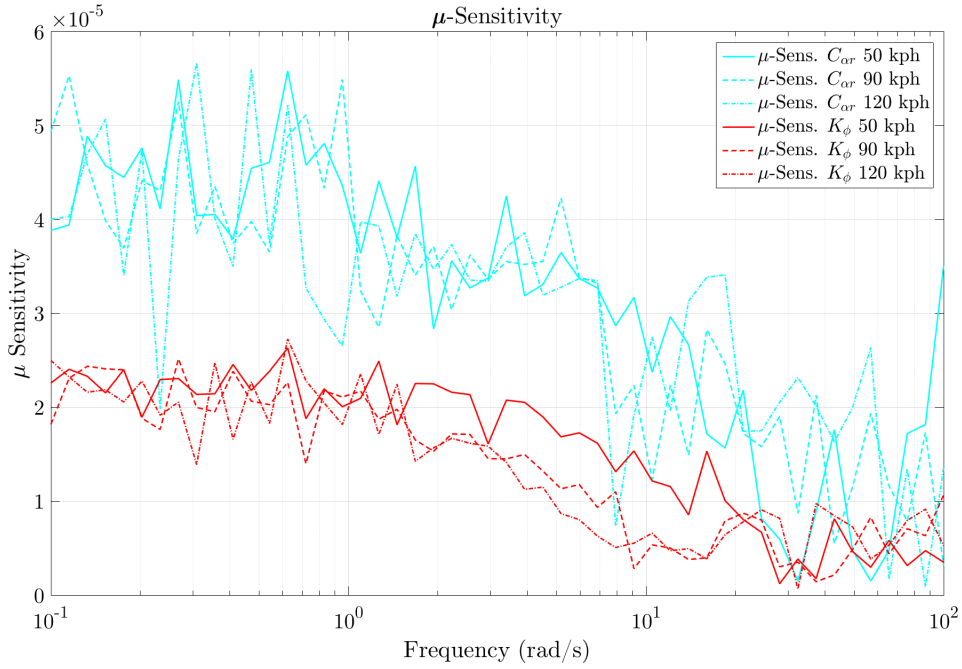

Figure 6.9: μ Sensitivity vs. Frequency of $C_{\alpha r}$ and K_ϕ for the Yaw-Roll model 15% Initial Uncertainty at 50, 90 and 120 kph

amount of correlation between peak sensitivity and peak skew μ is found in the $C_{\alpha f}$ and $B_{\dot{\phi}}$ parameters. The front cornering stiffness is marked by a skew value with a noticeable peak for the 90 and 120 kph speeds as well as a relatively flat trend in the low frequency range. The sensitivity is mainly flat across the range, with a slight peak detectable around the 8-9 rad/s frequencies. The sensitivity for the $B_{\dot{\phi}}$, however, displays no noticeable trend in sensitivity across the spectrum. This is much different than the skew μ analysis in Figures 6.6 - 5.15 where a very noticeable skew μ peak occurs. This simply means that the parameter $B_{\dot{\phi}}$ is both not very sensitive overall and is not marked by any frequencies in which a small change in $B_{\dot{\phi}}$ would significantly alter the closed loop response.

6.4 Conclusion

The sensitivity analysis is a useful tool to determine how small changes to the parameters affect the overall system performance and stability. The closed loop and open loop eigen sensitivity may not yield the same results due to the influence of the control in the closed

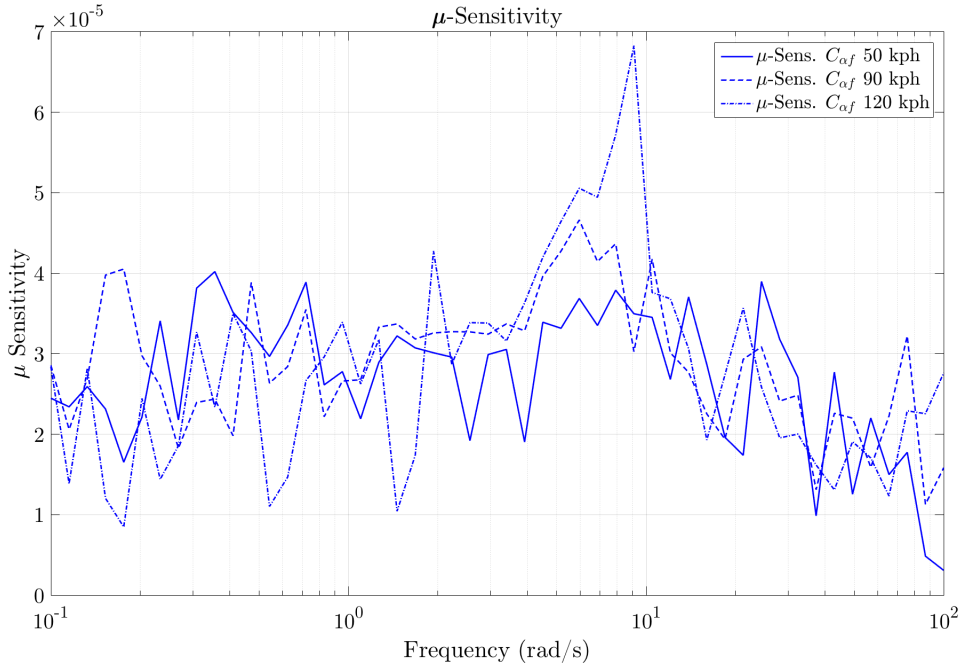

Figure 6.10: μ Sensitivity vs. Frequency of $C_{\alpha f}$ for the Yaw-Roll model 15% Initial Uncertainty at 50, 90 and 120 kph

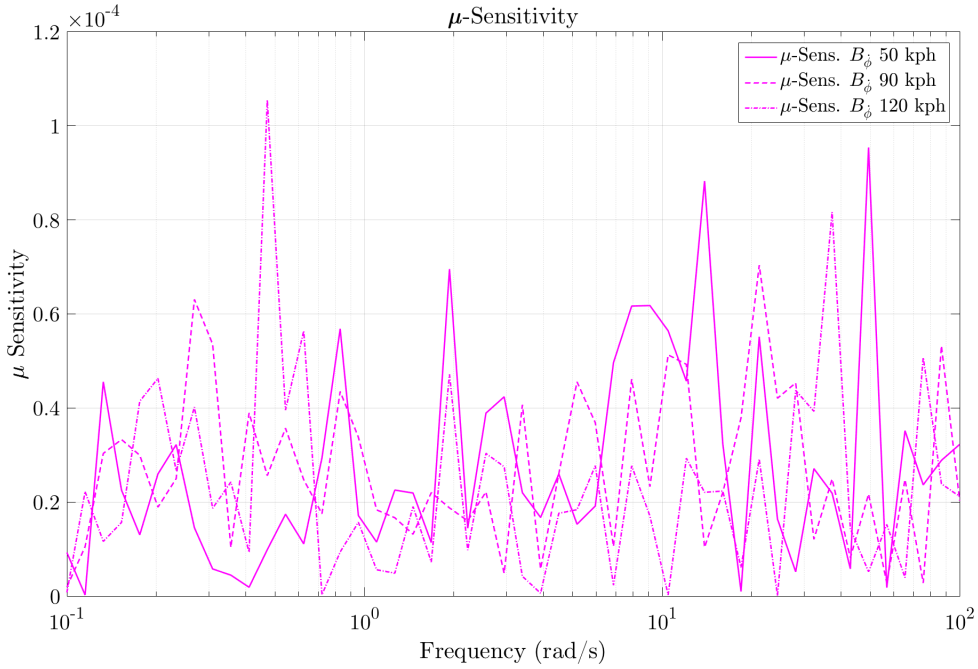

Figure 6.11: μ Sensitivity vs. Frequency of $B_{\dot{\phi}}$ for the Yaw-Roll model 15% Initial Uncertainty at 50, 90 and 120 kph

loop form. Though here for the yaw-roll model with the specified PI controller the open and closed loop eigen sensitivity were quite similar. The μ sensitivity, however, is a much better method of assessing the parameter sensitivity in the closed loop since the effect of parameter changes is considered across the frequency spectrum, which enables the determination of peak sensitivity. For the yaw-roll vehicle model a noticeable difference between the closed loop eigen sensitivity and the μ sensitivity was observed. For the the skew μ analysis in the next chapter the μ sensitivity is recommended for the purpose of grouping parameters together that have similar sensitivities, which can be interpreted as similar scaling effects.

The cg height parameter h_{rg} was found to be highly sensitive to the system with respect to system response and small changes in the parameter value. The next two most sensitive parameters are the weight split a and velocity V_x. But these sensitivities are almost a magnitude smaller in value from the sensitivity of the h_{rg} parameter. Specifically, the sensitivity value for h_{rg} of roughly 23 as compared to approximately 4 and 0.5 for the weight split a and velocity V_x sensitivities, respectively.

This sensitivity information is useful to the control or system designer to determine which parameters are most critical for estimation requirements and which parameters can either be allowed to vary quite significantly under operational conditions and/or which parameters nominal value measurements or estimates can be roughly acquired. With the understanding of these sensitivity relationships the yaw-roll vehicle model is reexamined in the next chapter with a set of initial uncertainties based off the μ sensitivity analysis.

Chapter 7

Skew μ and μ Sensitivity for Practical Initial Uncertainty Models

7.1 Introduction

In practice a designer would rarely be concerned with only how much just one parameter could vary as was explored in Chapter 5. Additionally, it is more realistic to assign initial uncertainty values that reflect the level of certainty in the measurements or estimated values of the parameter and/or the expected (or experimentally measured) variation of the parameters under the system operating conditions. In this chapter, measurement and operating condition assumptions with respect to the initial uncertainty are made and applied to the skew μ analysis. Also, given the results of the sensitivity analysis in Chapter 6, certain parameters will remain only in the "fixed" subset, Δ_f, of uncertainty block set, Δ_s, for the skew μ analysis.

7.2 Yaw-Roll Vehicle Model-Specific Assumptions on Parameter Uncertainties

In [5] a set of variances were used to synthesize a controller for a vehicle system with the $\mathcal{H}_\infty$ techniques. The variance used for some of the primary parameters of the vehicle system were 80% for each cornering stiffness, 15% for the mass, 15% for the yaw inertia. These parameter uncertainties were first presented in [31] under the California Partners for Transportation Technology organization.

The cornering stiffness, mass and inertia uncertainty values from [31] were applied to the Class D SUV along with percentages for the other parameters displayed in Table 7.1. With cornering stiffness set to 80% the μ for the system yielded a value above 1 meaning the performance conditions were already not being met and also that there is no further

space to vary other parameters via the skew μ technique. Thus, the cornering stiffnesses were dropped to an initial uncertainty of 55%.

Table 7.1: Class D SUV Initial Parameter Uncertainty

Parameter	Symbol	Value	Units	Initial Uncertainty (%)
Mass	m	1430	Kg	15%
Inertia x axis	I_{xx}	700.7	$\text{Kg} \cdot \text{m}^2$	15%
Velocity	V_x	50/90/120	$^{m}/_{\text{s}}$	5%
Inertia z axis	I_{zz}	2059.2	$\text{Kg} \cdot \text{m}^2$	15%
Front Split	a	1.050	m	10%
Cornering Stiffness Front Axle	$C_{\alpha f}$	1194.5	$^{N}/_{\text{deg}}$	55%
Cornering Stiffness Rear Axle	$C_{\alpha r}$	1194.5	$^{N}/_{\text{deg}}$	55%
CG Height	h_{rg}	0.650	m	15%
Roll Stiffness	k_ϕ	3772.5	$^{N \cdot m}/_{\text{deg}}$	10%
Roll Damping	$b_{\dot{\phi}}$	16825.9	$^{N \cdot s}/_{\text{m}}$	5%

Analysis for the skew μ was performed at 50, 90 and 120 kph. The μ uncertainty analysis from Chapter 6 indicated that the roll center height, h_{rg}, weight split, a, and longitudinal velocity, V_x, were the most sensitive parameters, with the roll center height being especially sensitive. To study the effect of remaining variation in the parameters it is best to create several uncertainty block, Δ, models or cases. These models are grouped by the magnitude of sensitivity. Table 7.2 contains the set of skew μ uncertainty block models, where again Δ_v subset is the group of parameters that is scaled during the search for the skew μ value.

The first look at the skew μ analysis for this case with intelligent assumptions placed on initial uncertainty comprises skew μ value for all nine varying block models at an operating speed of 90 kph. Here in Figure 7.1, the models containing cornering stiffnesses (light blue and yellow solid lines) have the highest skew μ value meaning the additional scaling applied to the terms in the varying subset, Δ_v , is the lowest. The fact that the cornering stiffnesses have so little additional variance available makes sense given that both have the highest initial uncertainty. Also, the model containing the cornering stiffnesses, roll stiffness and damping stiffness, model 5 (light blue line), is almost unaffected by the inclusion of the roll and damping parameters into the varying subset. This lack of influence can be attributed to

Table 7.2: Uncertainty Block Models for Scaling and Skew μ Analysis

Model	Δ_f	Δ_v
1	$\left\{\delta_m, \delta_{V_x}, \delta_{I_{zz}}, \delta_{C_{\alpha f}}, \delta_{C_{\alpha r}}, \delta_a, \delta_{I_{xx}}, \delta_{K_\phi}, \delta_{B_{\dot{\phi}}}\right\}$	$\left\{\delta_{h_{rg}}\right\}$
2	$\left\{\delta_m, \delta_{V_x}, \delta_{I_{zz}}, \delta_{C_{\alpha f}}, \delta_{C_{\alpha r}}, \delta_{I_{xx}}, \delta_{K_\phi}, \delta_{B_{\dot{\phi}}}\right\}$	$\left\{\delta_a, \delta_{h_{rg}}\right\}$
3	$\left\{\delta_m, \delta_{I_{zz}}, \delta_{C_{\alpha f}}, \delta_{C_{\alpha r}}, \delta_{I_{xx}}, \delta_{h_{rg}}, \delta_{K_\phi}, \delta_{B_{\dot{\phi}}}\right\}$	$\left\{\delta_a, \delta_{V_x}\right\}$
4	$\left\{\delta_{V_x}, \delta_{C_{\alpha f}}, \delta_{C_{\alpha r}}, \delta_a, \delta_{h_{rg}}, \delta_{K_\phi}, \delta_{B_{\dot{\phi}}}\right\}$	$\left\{\delta_m, \delta_{I_{zz}}, \delta_{I_{xx}}\right\}$
5	$\left\{\delta_m, \delta_{V_x}, \delta_{I_{zz}}, \delta_a, \delta_{h_{rg}}, \delta_{I_{xx}}\right\}$	$\left\{\delta_{C_{\alpha f}}, \delta_{C_{\alpha r}}, \delta_{K_\phi}, \delta_{B_{\dot{\phi}}}\right\}$
6	$\left\{\delta_m, \delta_{V_x}, \delta_{C_{\alpha f}}, \delta_{C_{\alpha r}}, \delta_{I_{zz}}, \delta_a, \delta_{h_{rg}}, \delta_{I_{xx}}\right\}$	$\left\{\delta_{K_\phi}, \delta_{B_{\dot{\phi}}}\right\}$
7	$\left\{\delta_m, \delta_{V_x}, \delta_{I_{zz}}, \delta_a, \delta_{h_{rg}}, \delta_{I_{xx}}, \delta_{K_\phi}, \delta_{B_{\dot{\phi}}}\right\}$	$\left\{\delta_{C_{\alpha f}}, \delta_{C_{\alpha r}}\right\}$
8	$\left\{\delta_{V_x}, \delta_{C_{\alpha f}}, \delta_{C_{\alpha r}}, \delta_{h_{rg}}, \delta_{K_\phi}, \delta_{B_{\dot{\phi}}}\right\}$	$\left\{\delta_a, \delta_m, \delta_{I_{zz}}, \delta_{I_{xx}}\right\}$
9	$\left\{\delta_{C_{\alpha f}}, \delta_{C_{\alpha r}}, \delta_a, \delta_{h_{rg}}, \delta_{K_\phi}, \delta_{B_{\dot{\phi}}}\right\}$	$\left\{\delta_a, \delta_m, \delta_{I_{zz}}, \delta_{I_{xx}}, \delta_{V_x}\right\}$

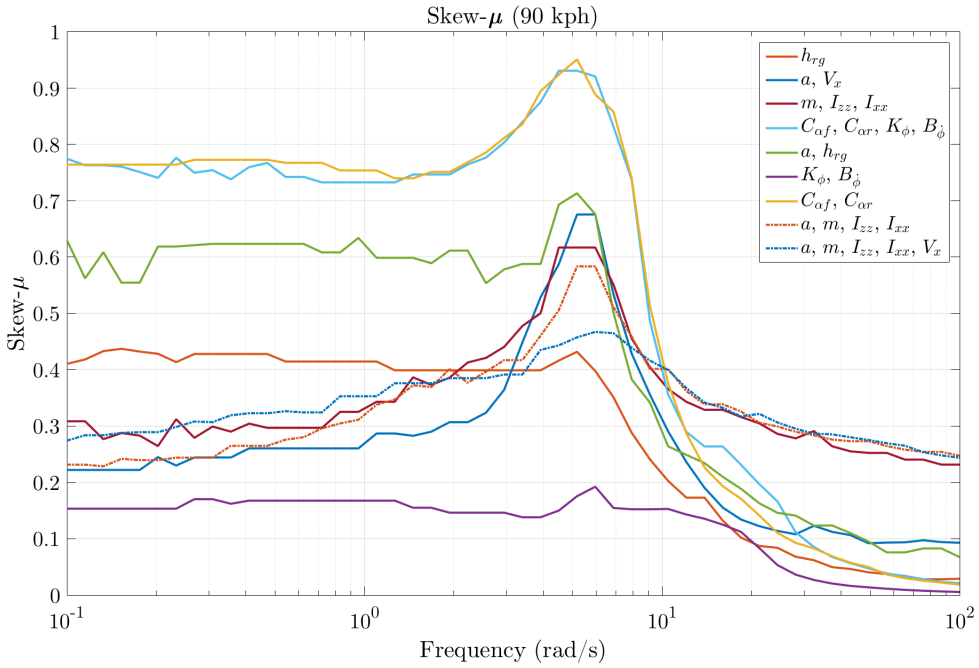

Figure 7.1: Skew μ for all Varying Subset Uncertainty Models at 90 kph for Yaw-Roll Vehicle Model with Assumptions on Initial Uncertainty

the initial uncertainty of 10 and 5 percent on the roll and damping parameters as well as the fact that these two parameters had the lowest μ sensitivity. In fact, model 6, represented by the purple line and which contains only K_ϕ and $B_{\dot{\phi}}$ in the varying subset, serves as an effective "lower bound" for the skew μ of all the models.

Looking at the other models in Figure 7.1, which all have initial uncertainties that are relatively close 5%-15%, the trend reflects the sensitivity analysis a bit more. Models 1-3 form a bit of a subgroup of the most sensitive parameters. The skew μ of model 2 containing the weight split and cg height parameter in the varying subset (represented by the green line) bounds the other varying subset models that don't contain cornering stiffness. This skew μ value of roughly 0.7 means a and h_{rg} could both be varied with scaling value of roughly 1.4 applied to both parameters and the system still remain within the performance specifications if the other parameters stay within the bounds of the initial uncertainties. Model 1 (represented by the light red line), which has the most sensitive parameter h_{rg} as the only parameter in the varying subset, the maximum skew μ is 0.43. The model containing the second most sensitive parameters in the varying subset, a and V_x, Model 3 (dark blue line), has a maximum skew μ of 0.68. The sensitivity analysis suggests that more sensitivity parameter might have a higher skew mu that is closer to a value of one (less additional scaling) than the less sensitive parameters. However, the skew μ analysis shows that while sensitivity can indicate a large scaling affect from a single parameter the combination of several parameters can have a greater impact on the additional uncertainty (or scaling) available. Thus several sets of uncertainty models are necessary to understand the affect of allowing multiple parameters to have additional variance in the varying subset Δ_v.

The remaining set of models are concerned with change in loading of the vehicle. Specifically, model 4 allows for additional variance in the mass and both inertias and models 8 and 9 add to the varying subset the weight split term and then both the weight split and velocity respectively. The assumption in these varying subset models is that the cg is not greatly

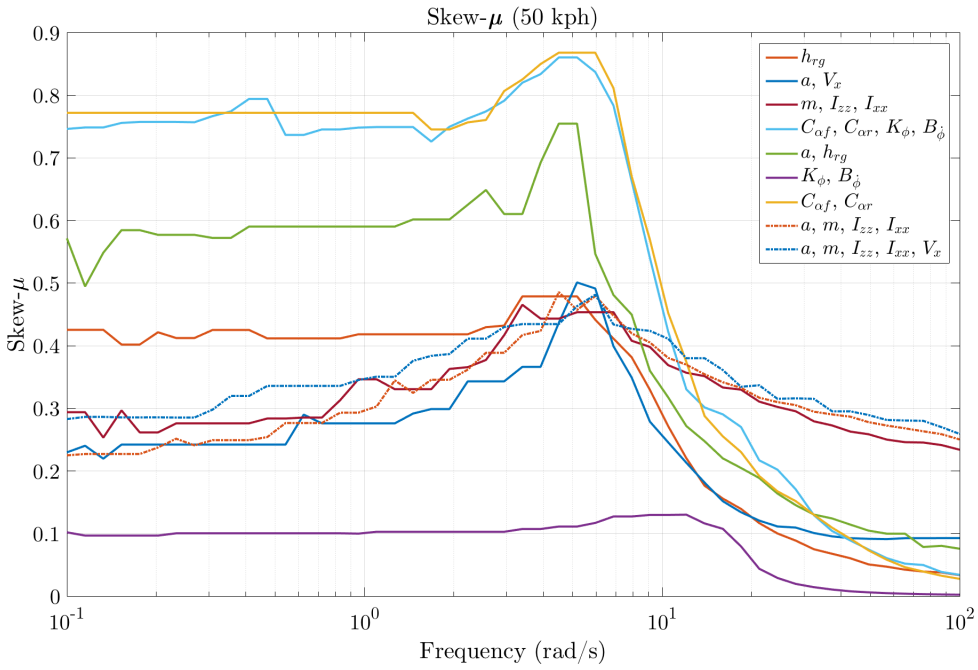

Figure 7.2: Skew μ for all Varying Subset Uncertainty Models at 50 kph for Yaw-Roll Vehicle Model with Assumptions on Initial Uncertainty

affected by the loading, i.e. mass added would not be placed at extreme elevations above the vehicle but within the dimensions of the vehicle. This may not be a safe assumption for all use cases as drivers do often attach roof racks for additional storage. Model 4 represented by the dark red line has a skew μ of 0.62 at 90 kph so there is a healthy amount of additional variance that is achievable when just m, I_{zz} and I_{xx} are allowed to vary. Oddly though the extra space for variance increases when the weight split and the combination of weight split and velocity are added to varying subset as evident in Figure 7.1 by the decreased maximum skew μ for model 8 (dashed light red line) and model 9 (dashed light blue line), respectively. This is quite unexpected as model 9 is essentially model 3 (dark blue) and model 4 (dark red) combined, both of which have skew μ values above 0.6. The search for μ and also skew μ is suboptimal so potentially this could be the reason. Additionally, the order of the terms on the diagonal in the subset may have a numerical influence on the solution.

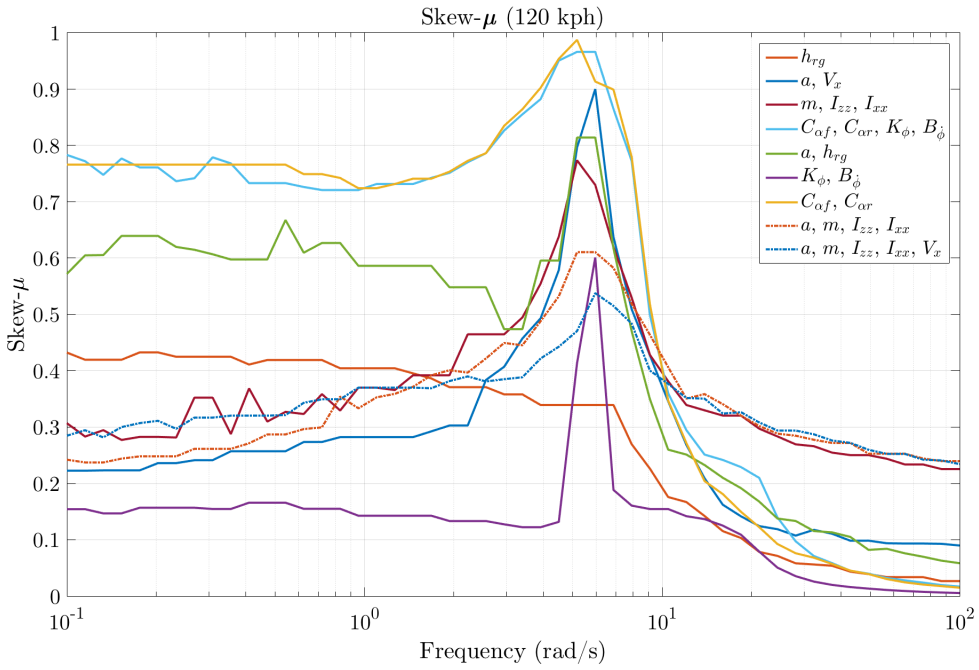

Figure 7.3: Skew μ for all Varying Subset Uncertainty Models at 120 kph for Yaw-Roll Vehicle Model with Assumptions on Initial Uncertainty

7.3 Experimental Comparison

It is important to verify the analyzed limits from the previous section of the actual closed loop system. Without the availability of a functional automated SUV, the CarSim simulation software was used in conjunction with Simulink. The Class D SUV with solid rear axle was again used only this time a loop was closed around the yaw rate output from the CarSim vehicle model. This control loop and supporting blocks is represented in Figure 7.4. The controller is the same PI controller from the presented in Chapter 5 with the gains $K_p = 2$ and $K_i = 0.125$. The CarSim model block took in steering wheel angle while the controller was designed with respect to the average steering angle of the front axle measured at the tire. Thus, several blocks were needed to convert the controller output steer angle into the steering wheel angle required from the CarSim block. The values and look-up tables for these steering conversions were sourced from the CarSim model data specific to the Class D

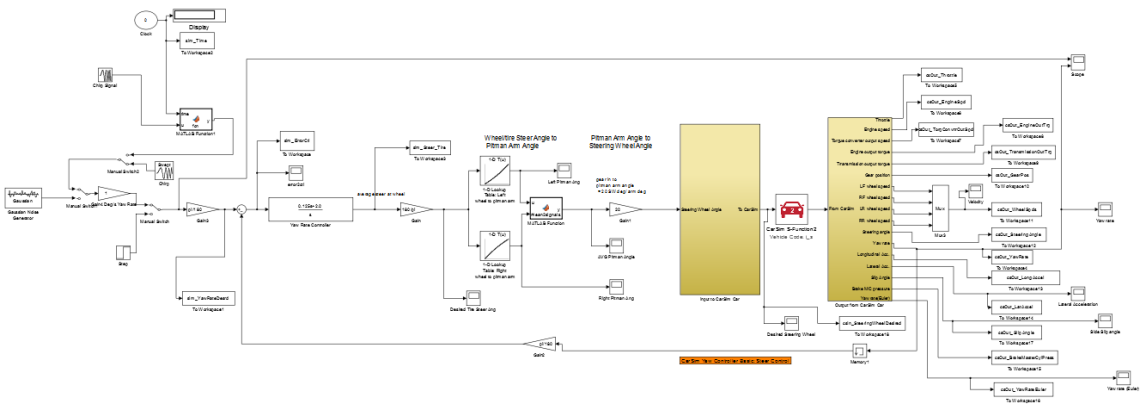

Figure 7.4: Simulink Experimental Closed Loop Yaw Rate Setup for Class D SUV

SUV that was used in the experimental simulation. The values for the Class D SUV can be found in Table A.1 of Appendix A.

The setup in Figure 7.4 also contains several input sources, but for the spectral analysis the Swept Chirp block as connected in the diagram was the source used for the desired yaw rate. A sample time of 1/100000 was used for the swept cosine chirp signal with an initial frequency of 0.0003 Hz and target frequency of 100 Hz (or 0.00188 rad/s and 628.32 rad/s respectively) over a duration of 40 seconds.

The steering conversion takes the steer angle at the tire and using the lookup tables converts the angle to a pitman arm angle for both the left and right steering, which is averaged and then scaled by the pitman arm to steering wheel angle ratio which is 20 deg of turning at the steering wheel per 1 deg of pitman arm rotation.

Several test cases were selected to examine the accuracy of the parameter perturbations, which are presented in Table 7.3. The two parameters with the highest μ sensitivity were chosen for the test cases. A value above and below the nominal value was chosen for both the weight split and cg height. Note, the cg height, while referenced to the road surface directly, affects the h_{rg} term in the coupled yaw-roll model.

The transient response is presented in Figure 7.5 to show a sample of the yaw rate outputs for each case of parameter alterations. The desired yaw rate signal is also included and is represented by the light blue line . Additionally, the nominal system is represented

Table 7.3: Experimental Cases of Select Parameter Extremes for the Class D SUV

Case	Alteration	h_{cg}	a
1	CG Low	50 mm	1050 mm
2	CG High	1250 mm	1050 mm
3	Nominal	650 mm	1050 mm
4	Weight Split Front	650 mm	10.5 mm
5	Weight Split Rear	650 mm	2600 mm

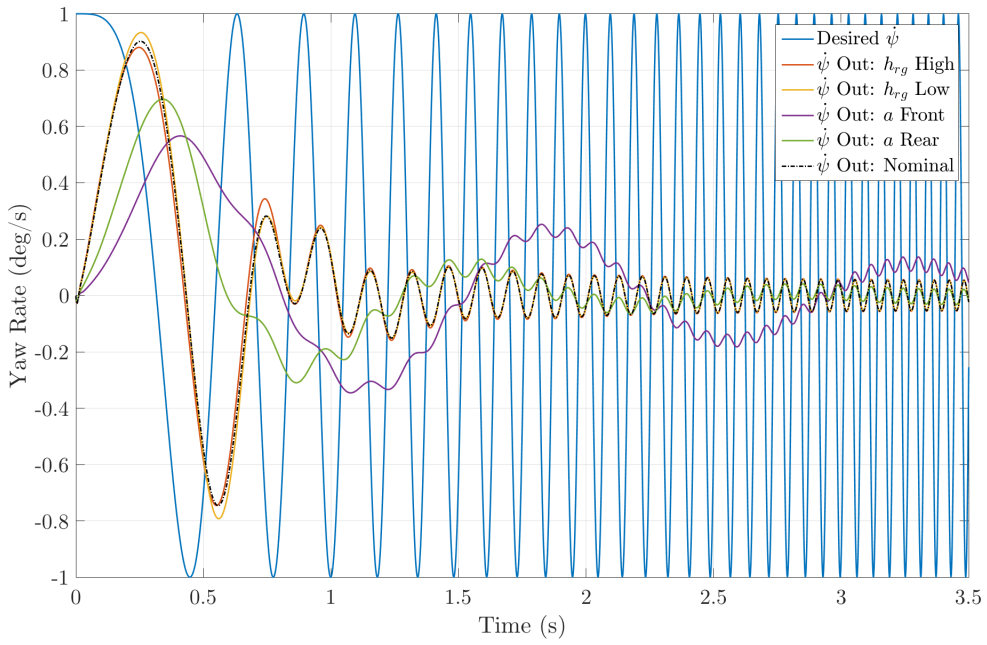

Figure 7.5: Transient Response Output for all Cases of Parameter Alterations for Class D SUV

by the dashed black line. All other system cases are represented per the legend. The desired yaw rate with peaks and troughs of 1 deg/s magnitude is not that great of a demand from the system but it is enough to characterize the frequency response across the range of frequencies using the fast Fourier transform (FFT), specifically the fft() function call in Matlab. Note, the CarSim model is set to a time step of 1e-05, a frequency of 100,000 Hz. So, there should be no aliasing effects at the higher frequencies of the spectral analysis given that the highest desired yaw rate input is 100 Hz. Also, the averaging of the spectral output was set to bands with a spacing of 2^4 .

The FFT spectral analysis yields an experimental Bode diagram shown in Figure 7.6 The figure represents the gain and phase of the Class D SUV at a speed of 90 kph for the high and low CG cases shown in red and yellow respectively as well as the nominal response which is shown in blue. Note that the nominal response peak gain matches closely with the response from the coupled yaw-roll model in Figure 5.3. There is a slight difference in the peak magnitude of 1.06 for the CarSim experimental system versus 1.03 for the yaw-roll coupled model. There is also a deviation in phase at higher frequencies. These differences are likely due to higher order dynamics that the yaw-roll coupled model does not account for. For example, the height of the cg does have an small effect on the closed loop system yaw dynamics. The changes to the weight split, however, have quite a bit of an effect on the yaw dynamics. The experimental Bode with weight split biased towards the front and rear is shown in Figure 7.7.

7.4 Conclusion

The Class D SUV vehicle model was used in analysis that sought to more realistically represent the initial uncertainty of the parameters of the vehicle system. The initial uncertainty values were derived from experimental analysis of variance observed under operation of the system as well as from assumptions made about the vehicle operating conditions. The

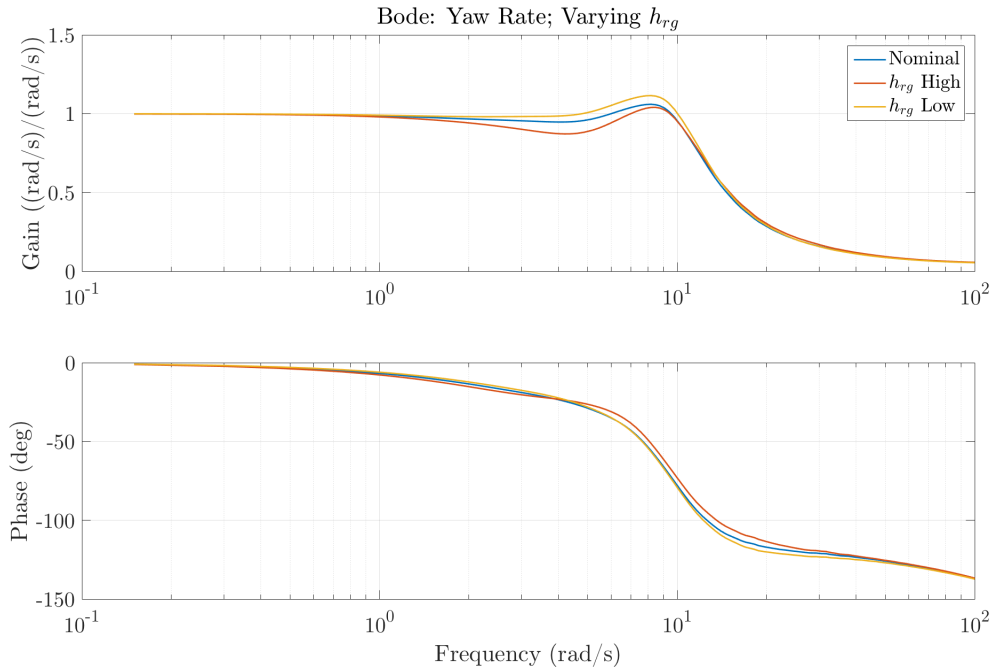

Figure 7.6: Bode for Alteration of the CG Height for Class D SUV

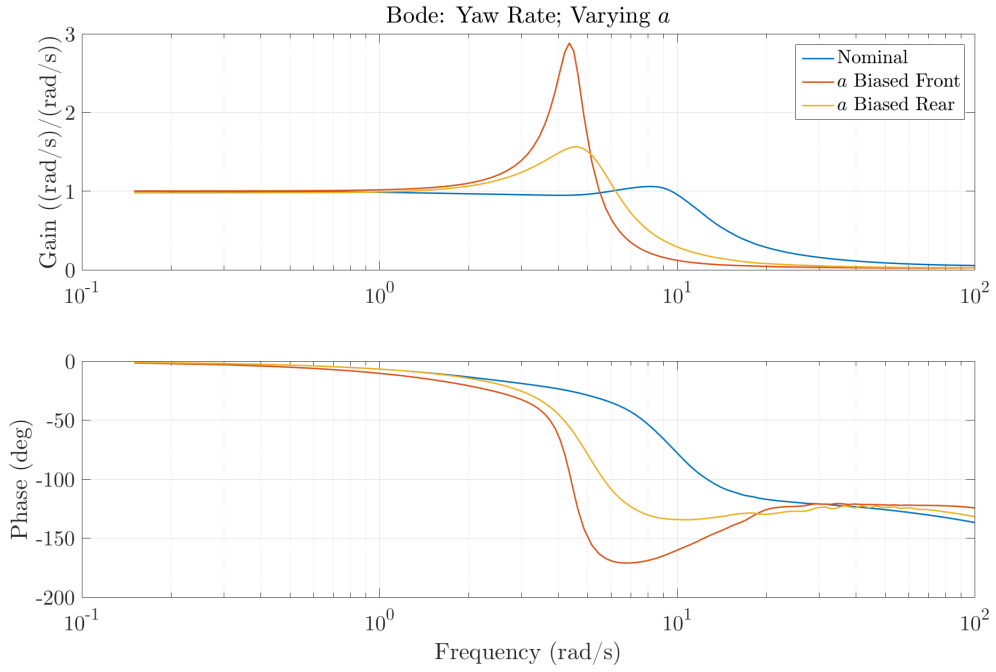

Figure 7.7: Bode for Alteration of the Weight Split for Class D SUV

μ for the system returned a value greater than one with the original set of initial uncertainties meaning, too much uncertainty was specified leaving no room for extra variance on any varying subset for any iteration of fixed-varying uncertainty cases.

The uncertainty of the cornering stiffness was then relaxed resulting in a base μ less than one, which allowed the development of several uncertainty models. These uncertainty models were created with reference to the μ sensitivity analysis results presented in Chapter 6. The resulting skew μ analysis primarily held with the understanding and expectation of how much more the parameters in the varying subset of each case could vary.

Finally, the Class D SUV vehicle from CarSim 9 and the previously designed controller were incorporated into a closed loop Simulink model. The CarSim block provided a link to the high fidelity dynamic vehicle model. This setup served as the experimental verification. Obviously, it is more feasible to alter the vehicle parameters in the CarSim environment than on a physical testbed to verify the uncertainty bounds determined via the skew μ analysis of the yaw-roll model. Additionally, the required road space for the swept chirp commanded input was easily handled in simulation

The spectral analysis from the experimental tests revealed a nominal closed loop response that was very close to the nominal closed loop response of the coupled yaw-roll model. The magnitude response for variations of the cg height and the weight split were explored. Spectral analysis was done using variations on just the parameter of interest. A better method of analysis would be to consider one of the specific initial uncertainty cases. Then for the fixed subset adjust the parameters therein to the limits of the respective initial uncertainties. For the varying subset parameters the skew μ analysis would be used to set the limits. A comparison of the experimental spectral analysis could then be made to the closed response of coupled-yaw roll model with all parameters also at the uncertainty limits. This is an area of future research to better verify the allowable parametric uncertainty bounds determined via the skew μ method.

Chapter 8

Conclusions & Future work

8.1 Conclusions

A methodical approach based on parametric uncertainty for determining how accurate a system model must be in order to meet the specifications of the controller be was presented. First, some of the robust control concepts were reviewed and then the modern control theory of loop shaping was presented. This led into the infinite norm concept and then to the structured singular value or μ value. The μ analysis and the structured of uncertainty was discussed as being primarily used to account for various types of uncertainty for the synthesis of a controller. The μ analysis, however, was also shown to be useful in analyzing the allowable uncertainty of a closed loop system for a previously designed controller.

The primary concern of this dissertation was the real parametric μ and skew μ analysis with repeated parameter instances. Prior work in the area of determining the allowable uncertainty considered system formulations where the parameters where lumped together such that the uncertainty matrix did not include any repeated terms. This dissertation leveraged the linear fractional transformation LFT to formulate a system model that incorporated uncertainty on the parameters in methodical manner. This base block LFT method allows for uncertain parameters that occur in multiple instances to incorporated into an uncertain system model with ease. The base-block LFT method presented also maintained certain types of parameter coupling.

Summarizing, the approach is as follows:

- Acquire the system equations and represent the system as a standard block diagram.

- In the block diagram convert all uncertain parameters to an LFT base block 2-by-2 matrix and non-varying parameters as gain blocks.
- Referencing the converted block diagram combine gain blocks and base LFT uncertainty blocks into larger subsystem LFT blocks.
- Combine subsystem LFT blocks into an open loop LFT system of $\Delta - M$.
- Close the loop according to the previously designed controller K to form the LFT system $\Delta - M - K$.
- Perform both the eigen sensitivity and μ sensitivity analysis to determine which parameters are most influential on the system and to better group parameters in the varying subset for the skew μ analysis
- Use the sensitivity analysis to generate uncertainty cases where parameters with similar sensitivity are placed in the varying subset together.
- Select initial uncertainty based off the operational variance of the parameters or based off the accuracy of measurements.
  - Note parameters which can be measured well or do not vary under operation can stay in the fixed subset. i.e. cases with these types of parameters in the varying subset are not needed.
- Check that the μ value for the closed loop system is less than one.
  - Adjust initial uncertainty if possible or reconsider system and controller feasibility.
- Perform skew μ analysis on the uncertainty cases.
  - Note: To find the upper limit of variance for a single parameter skip the sensitivity analysis and place only a single parameter in the varying subset for the skew μ

analysis and set initial uncertainty for all parameters equal. Construct uncertainty cases like this for each uncertain parameter.

This method for real parametric uncertainty was explored for the coupled yaw-roll vehicle model. It was shown that the parametric eigenvalue analysis may not reveal accurate information about the closed loop system for the coupled yaw-roll vehicle model. The μ sensitivity analysis showed that the cg height and weight split parameters were the most sensitive parameters for the coupled vehicle model. This means that small variations in these parameters has a large effect on the system output and overall performance as specified by the controller design. The system was also understandably sensitive to velocity.

In general, the skewed μ analysis showed the model parameters had remaining "space" to vary given an initial uncertainty for each parameter. If the initial uncertainty is increased for some or all of the parameters then there is less space remaining for further variation in the parameters. The μ sensitivity analysis can be a helpful tool to determine which vehicle parameters should be grouped together in the varying subset for skew μ analysis. The combination of μ sensitivity and skew μ was shown to be useful to determine which parameters need to be known precisely and which parameters can be allowed to vary under operation conditions or measured with less accuracy. The real parametric technique provides a method to determine the allowable uncertainty relative to the system model, the designed controller and the specific initial uncertainties of all the uncertain parameters. This bound on the uncertainty allowed, however, does rely on the assumption that the system model is an accurate representation of the system response.

8.2 Future Work

Future work should first encompass a study of the yaw-roll vehicle model with a loop closed around the roll and roll rate states to determine allowable uncertainty for the same ten uncertain parameters used in vehicle model for this dissertation. It is likely that the

most sensitive parameters of a system closed around roll or roll rate would be different from the most mu-sensitive parameters of closed loop yaw rate system.

An analysis of the uncertainty for a closed loop system that controls multiple outputs would be useful to the vehicle dynamics community. Most electronic vehicle stability controllers on production vehicles are being designed to manage the vehicle roll and roll rates in addition to the yaw rate. Skew μ results of the allowable parameter uncertainty on the coupled vehicle model with controllers on both the yaw axis and roll axis are again likely to be different than the results for the system with yaw rate controller only. The LFT approach presented in this dissertation can also handle MIMO systems.

Additionally in this dissertation, it was shown that at higher speeds and dynamics the coupled yaw-roll model matches the output of the more accurate CarSim model which was used as the experimental test case. Including some measure of confidence in model fit may be of use so that a quantitative confidence in the allowable uncertainty could be established. On similar note, the incorporation of a better tire model into the coupled vehicle model would better to capture tire saturation. The f-tire model which uses physical parameters to model the slip-force relationship is highly recommended.

Bibliography

[1] Sigurd Skogestad and Ian Postlethwaite. *Multivariable feedback control: analysis and design*, volume 2. Wiley New York, 2007.

[2] Kent H Rasmussen and Sten Bay Jørgensen. Parametric uncertainty modeling for robust control: a link to identification. *Computers & chemical engineering*, 23(8):987–1003, 1999.

[3] Andrés Marcos, Declan Bates, and Ian Postlethwaite. Control oriented uncertainty modelling using μ sensitivities and skewed μ analysis tools. In *Decision and Control, 2005 and 2005 European Control Conference. CDC-ECC'05. 44th IEEE Conference on*, pages 6436–6441. IEEE, 2005.

[4] G Rödönyi and P Gáspár. Iterative design of structured uncertainty models and robust controllers based on closed-loop data. *Control Theory & Applications, IET*, 4(12):2823–2836, 2010.

[5] Yingmin Jia. Robust control with decoupling performance for steering and traction of 4ws vehicles under velocity-varying motion. *Control Systems Technology, IEEE Transactions on*, 8(3):554–569, 2000.

[6] S Brennan and A Alleyne. H-infinity vehicle control using nondimensional perturbation measures. In *American Control Conference, 2002. Proceedings of the 2002*, volume 3, pages 2534–2539. IEEE, 2002.

[7] Manoj Karkee and Brian L Steward. Local and global sensitivity analysis of a tractor and single axle grain cart dynamic system model. *biosystems engineering*, 106(4):352–366, 2010.

[8] Manoj Karkee and Brian L Steward. Study of the open and closed loop characteristics of a tractor and a single axle towed implement system. *Journal of Terramechanics*, 47(6):379–393, 2010.

[9] Paul Lambrechts, Jan Terlouw, Samir Bennani, and Maarten Steinbuch. Parametric uncertainty modeling using lfts. In *American Control Conference, 1993*, pages 267–272. IEEE, 1993.

[10] Da-Wei Gu, Petko Petkov, and Mihail M Konstantinov. *Robust control design with MATLAB®*. Springer Science & Business Media, 2014.

[11] Gene F Franklin, J David Powell, Abbas Emami-Naeini, and J David Powell. *Feedback control of dynamic systems*, volume 3. Addison-Wesley Reading, MA, 1994.

[12] Katsuhiko Ogata. *System dynamics*, volume 3. Prentice Hall New Jersey, 1998.

[13] Rod Holland, Peter Young, and Chuanjiang Zhu. Development of a skew μ upper bound. *International Journal of Robust and Nonlinear Control*, 15(18):905–921, 2005.

[14] Alexander Lanzon and Michael Cantoni. On the formulation and solution of robust performance problems. *Automatica*, 39(10):1707–1720, 2003.

[15] Andrew Packard and John Doyle. The complex structured singular value. *Automatica*, 29(1):71–109, 1993.

[16] Huibert Kwakernaak. Robust control and h∞-optimization—tutorial paper. *Automatica*, 29(2):255–273, 1993.

[17] Kemin Zhou, John Comstock Doyle, Keith Glover, et al. *Robust and optimal control*, volume 40. Prentice hall New Jersey, 1996.

[18] Kemin Zhou and John Comstock Doyle. *Essentials of robust control*, volume 104. Prentice hall Upper Saddle River, NJ, 1998.

[19] Guilherme V Raffo, Manuel G Ortega, and Francisco R Rubio. An integral predictive/nonlinear h∞ control structure for a quadrotor helicopter. *Automatica*, 46(1):29–39, 2010.

[20] Gary J Balas, John C Doyle, Keith Glover, Andy Packard, and Roy Smith. μ-analysis and synthesis toolbox: For use with MATLAB. 2001.

[21] J. Ryu and J.C. Gerdes. Estimation of vehicle roll and road bank angle. In *Proc. Amer. Control Conf*, pages 2110–2115, 2004.

[22] Christopher R Carlson and J Christian Gerdes. Optimal rollover prevention with steer by wire and differential braking. In *Proceedings of IMECE*, volume 3, pages 16–21, 2003.

[23] Lowell S Brown and David M Bevly. Roll and bank estimation using gps/ins and suspension deflections. *Electronics*, 4(1):118–149, 2015.

[24] Lowell S Brown, Jeremy J Dawkins, Ryan S Hill, and David M Bevly. Road bank estimation on uneven terrain for unmanned ground vehicles. In *ASME 2010 Dynamic Systems and Control Conference*, pages 849–855. American Society of Mechanical Engineers, 2010.

[25] ISO 3888-2:2011. Passenger cars – test track for a severe lane-change manoeuvre – part 2: Obstacle avoidance.

[26] Lukáš Březina and Tomáš Březina. H-infinity controller design for a dc motor model with uncertain parameters. *Engineering Mechanics*, 18(5-6):271–279, 2011.

[27] Lowell S Brown and David M Bevly. Allowable parametric uncertainty in the closed loop for the yaw-roll vehicle model: A skew-μ based approach. In *American Control Conference (ACC), 2017*, pages 4309–4315. IEEE, 2017.

[28] B Ross Barmish, PP Khargonekar, ZC Shi, and R Tempo. Robustness margin need not be a continuous function of the problem data. *Systems & Control Letters*, 15(2):91–98, 1990.

[29] Michael KH Fan, André L Tits, and John C Doyle. Robustness in the presence of mixed parametric uncertainty and unmodeled dynamics. *Automatic Control, IEEE Transactions on*, 36(1):25–38, 1991.

[30] L El Ghaoui and SP Boyd. Stability robustness of linear systems to real parametric perturbations. In *Decision and Control, 1990., Proceedings of the 29th IEEE Conference on*, pages 1247–1248. IEEE, 1990.

[31] Huei Peng and Masayoshi Tomizuka. Lateral control of front-wheel-steering rubber-tire vehicles. *California Partners for Advanced Transit and Highways (PATH)*, 1990.

Appendices

Appendix A

Vehicle Properties

A.1 CarSim's Small SUV

Table A.1: Class D SUV Vehicle Parameters

Parameter	Symbol	Value	Units
Mass	m	1430	Kg
Inertia x axis	I_{xx}	700.7	$\text{Kg} \cdot \text{m}^2$
Inertia y axis	I_{yy}	2059.2	$\text{Kg} \cdot \text{m}^2$
Inertia z axis	I_{zz}	2059.2	$\text{Kg} \cdot \text{m}^2$
Track Width	t_w	1.565	m
Wheel Base	w_b or L	2.660	m
Front Split	a	1.050	m
Rear Split	b	1.610	m
Cornering Stiffness Front Axle	$C_{\alpha f}$	1194.5	N/deg
Cornering Stiffness Rear Axle	$C_{\alpha r}$	1194.5	N/deg
CG Height	h_{rg}	0.6350	m
Axle Height	h_{axle}	0.340	m
Roll Center Height	h_{rc}	0.020	m
Roll Stiffness	k_ϕ	3772.5	$N \cdot m/\text{deg}$
Roll Damping	$b_{\dot{\phi}}$	16825.9	$N \cdot s/\text{m}$

Table A.2: Class D SUV Suspension Parameters

Parameter	Symbol	Value	Units
Spring Mount Separation Front	$s_{1,s}$	1.565	m
Damper Mount Separation Front	$s_{1,d}$	1.565	m
Spring Stiffness Front	k_1	130,000	N/m
Damper Coefficient Front	b_1	9178.0	$N \cdot s/\text{m}$
Auxiliary Roll Stiffness Front (Anti-Sway Bar)	$k_{\phi,1,aux}$	32601.3	$N \cdot m/\text{deg}$
Spring Mount Separation Rear	$s_{2,s}$	1.103	m
Damper Mount Separation Rear	$s_{2,d}$	1.103	m
Spring Stiffness Rear	k_2	40,000	N/m
Damper Coefficient Rear	b_2	9178.0	$N \cdot s/\text{m}$
Auxiliary Roll Stiffness Rear (Anti-Sway Bar)	$k_{\phi,1,aux}$	0.0	$N \cdot m/\text{deg}$

Table A.3: Small SUV Roll Stiffness and Damping

Parameter	Symbol	Value	Units
Auxiliary Roll Stiffness Front (Anti-Sway Bar)	$k_{\phi,aux}$	32601.3	$^{N\cdot m}/_{\deg}$
Roll Stiffness	k_{ϕ}	12,384,349	$^{N\cdot m}/_{\deg}$
Roll Damping	$b_{\dot{\phi}}$	16825.9	$^{N\cdot s}/_{\mathrm{m}}$

$$k_{\phi,aux} = \frac{(k_{\phi,1,aux} + k_{\phi,2,aux})}{2} \tag{A.1}$$

$$k_{\phi} = \frac{\left(k_1 s_{1,s}^2 + k_2 s_{2,s}^2\right)}{2} + k_{\phi,aux} \tag{A.2}$$

$$b_{\dot{\phi}} = \frac{\left(b_1 s_{1,d}^2 + b_2 s_{2,d}^2\right)}{2} + k_{\phi,aux} \tag{A.3}$$

A.2 MATLAB

A.2.1 Construction of LFT for Vehicle yaw Model with Uncertain Cornering Stiffness

```
% model_smSUV_yaw_CaFR_LFTblocks.m
% Lowell Brown
% H-inf applied to simple statepace vehicle model at constant
   speed.


% dbstop if error
% clear
% clc
% close all
```

```
% Upper LFTs
% [z_Xx]  =          [w_Xx]
% [  y ]    [mXx] *  [ u  ]
% [mXx_invrt] == upper LFT
% y == output of LFT mXx_invrt
% zXx == applied perturbation state of mXx_invrt
% u == input state to mXx
% w_Xx == input perturbation multiplier [-1 1] into to
   mXx_invrt

% mUsys1
systemnames = 'mCaf gainVx'; % Lower LFTs
sysoutname = 'mUsys1';
inputvar = '[w_Caf; control]';
input_to_mCaf = '[control; w_Caf]';
input_to_gainVx = '[mCaf(1)]';
outputvar = '[mCaf(2); gainVx(1)]'; %[z_Caf; Caf*Vx]; %UpperLFT
    out
cleanupsysic = 'yes';
sysic;
minfo(mUsys1)

% mUsys2 systemnames = 'mUsys1 gaina'; %UpperLFT and LowerLFT
sysoutname = 'mUsys2';
inputvar = '[w_Caf; control]';
input_to_mUsys1 = '[w_Caf; control]';
input_to_gaina = '[mUsys1(2)]';
```

```
outputvar = '[mUsys1(1); gaina(1)]'; %[z_Caf;  Caf*Vx*a]; %
   UpperLFT
cleanupsysic = 'yes';
sysic;
minfo(mUsys2)

% mFwdPathVxM
systemnames = 'gainInvVx gainInvMass intgrtr'; %UpperLFT,
   scalarGain, 1out-1inSystem
sysoutname = 'mFwdPathVxM';
inputvar = '[error1]';
input_to_gainInvMass = '[error1]';
input_to_gainInvVx = '[gainInvMass(1)]';
input_to_intgrtr = '[gainInvVx(1)]';
outputvar = '[intgrtr(1)]'; %[1/(m*Vx)*1/s]; [x_1]; %UpperLFT
cleanupsysic = 'yes';
sysic;
minfo(mFwdPathVxM)

% mFwdPathVxIzz
systemnames = 'gainInvVx gainInvInertia intgrtr'; %UpperLFT,
   scalarGain, 1out-1inSystem
sysoutname = 'mFwdPathVxIzz';
inputvar = '[error2]';
input_to_gainInvInertia = '[error2]';
input_to_gainInvVx = '[gainInvInertia(1)]';
input_to_intgrtr = '[gainInvVx(1)]';
```

```
outputvar = '[intgrtr(1)]'; %[z_Vx; 1/(Izz*Vx)*1/s]; [z_Vx; x_2
   ]; %UpperLFT
cleanupsysic = 'yes';
sysic; minfo(mFwdPathVxIzz)
```

A.2.2 Construction of LFT Subsystems for Yaw-Roll Model with Uncertainty on All Parameters

```
% model_smSUV_yaw_CaFR_LFTblocks.m
% Lowell Brown
% H-inf applied to simple statepace vehicle model at constant
   speed.


% dbstop if error
% clear
% clc
% close all



% Upper LFTs
% [z_Xx]  =          [w_Xx]
% [  y ]    [mXx] *  [ u  ]
% [mXx_invrt] == upper LFT
% y == output of LFT mXx_invrt
% zXx == applied perturbation state of mXx_invrt
% u == input state to mXx
% w_Xx == input perturbation multiplier [-1 1] into to
   mXx_invrt


% mUsys1
systemnames = 'mCaf gainVx'; % Lower LFTs
sysoutname = 'mUsys1';
inputvar = '[w_Caf; control]';
```

```
input_to_mCaf = '[control; w_Caf]';
input_to_gainVx = '[mCaf(1)]';
outputvar = '[mCaf(2); gainVx(1)]'; %[z_Caf; Caf*Vx]; %UpperLFT
    out
cleanupsysic = 'yes';
sysic;
minfo(mUsys1)

% mUsys2 systemnames = 'mUsys1 gaina'; %UpperLFT and LowerLFT
sysoutname = 'mUsys2';
inputvar = '[w_Caf; control]';
input_to_mUsys1 = '[w_Caf; control]';
input_to_gaina = '[mUsys1(2)]';
outputvar = '[mUsys1(1); gaina(1)]'; %[z_Caf;  Caf*Vx*a]; %
   UpperLFT
cleanupsysic = 'yes';
sysic;
minfo(mUsys2)

% mFwdPathVxM
systemnames = 'gainInvVx gainInvMass intgrtr'; %UpperLFT,
   scalarGain, 1out-1inSystem
sysoutname = 'mFwdPathVxM';
inputvar = '[error1]';
input_to_gainInvMass = '[error1]';
input_to_gainInvVx = '[gainInvMass(1)]';
input_to_intgrtr = '[gainInvVx(1)]';
```

```
outputvar = '[intgrtr(1)]'; %[1/(m*Vx)*1/s]; [x_1]; %UpperLFT
cleanupsysic = 'yes';
sysic;
minfo(mFwdPathVxM)

% mFwdPathVxIzz
systemnames = 'gainInvVx gainInvInertia intgrtr'; %UpperLFT,
   scalarGain, 1out-1inSystem
sysoutname = 'mFwdPathVxIzz';
inputvar = '[error2]';
input_to_gainInvInertia = '[error2]';
input_to_gainInvVx = '[gainInvInertia(1)]';
input_to_intgrtr = '[gainInvVx(1)]';
outputvar = '[intgrtr(1)]'; %[z_Vx; 1/(Izz*Vx)*1/s]; [z_Vx; x_2
   ]; %UpperLFT
cleanupsysic = 'yes';
sysic; minfo(mFwdPathVxIzz)
```

A.2.3 Construction from Yaw-Roll Model with Full Parametric Uncertainty from the LFT Subsystems

```
%IMPORTANT: inputvar, outputvar and delta block (order of
   perturbations)
%are all correlated must have order correct

% G_vYawRoll_FullLFT
systemnames = ['mUsysVy mUsysPsi mUsysPhi '...
               'mFwdPathVy mFwdPathPsi mFwdPathPhi '...
               'mIeqCo mVxIeqC1 mBphid4Vy mKphi4Vy '...
               'mC2 mC1 '...
               'mBphid4Phi mKphi4Phi mC1hrg4Phi mCohrg4Phi'];
sysoutname = 'G_vYawRoll_FullLFT';
inputvar = ['[w_Ixx1; w_m1; w_Vx1; '... %Fwd Paths
             'w_Izz1; w_Vx2; '...
             'w_Ixx2; w_Vx3; ' ...
             'w_Caf1; w_Car1; w_Ixx3; w_m2; w_hrg1; w_hrg2; '
                ... % subcomponents
            'w_Ixx4; w_m3; w_Vx4; w_Vx5; w_Caf2; w_Car2; w_a1;
              w_a2; w_Ixx5; w_m4; w_hrg3; w_hrg4;'...
            'w_Bphid1; w_hrg5; w_Vx6; w_m5;'...
            'w_hrg6; w_Vx7; w_m6; w_Kphi1; w_m7; w_hrg7;'...
            'w_Caf3; w_Car3; w_a3; w_a4; w_a5; w_a6;' ...
            'w_Caf4; w_Car4; w_a7; w_a8;' ...
            'w_Bphid2; w_Vx8;' ...
            'w_Vx9; w_Kphi2; w_m8; w_hrg8;' ...
            'w_hrg9; w_Caf5; w_Car5; w_a9; w_a10;' ...
```

```
            'w_hrg10; w_Caf6; w_Car6; ' ...
            'w_Caf7; w_Vx10; w_Ixx6; w_m9; w_hrg11; w_hrg12; '
               ... % system input pre mults
            'w_Caf8; w_Vx11; w_a11; '...
            'w_Caf9; w_Vx12; w_hrg13; ' ...
            'u_steer]']; %actual input to system
input_to_mFwdPathVy = '[w_Ixx1; w_m1; w_Vx1; mUsysVy(7)-mIeqCo
   (7)-mVxIeqC1(13)-mBphid4Vy(5)+mKphi4Vy(7)]'; %out: x1;
   mFwdPathVy(4)
input_to_mFwdPathPsi = '[w_Izz1; w_Vx2; mUsysPsi(4)-mC2(7)-mC1
   (5)]'; %out: x2; mFwdPathPsi(3)
input_to_mFwdPathPhi = '[w_Ixx2; w_Vx3; mUsysPhi(4)-mBphid4Phi
   (3)+mKphi4Phi(5)-mC1hrg4Phi(6)-mCohrg4Phi(4)]'; %out: x3 &
   x4; mFwdPathPhi(3) & mFwdPathPhi(4)
input_to_mIeqCo = '[w_Caf1; w_Car1; w_Ixx3; w_m2; w_hrg1;
   w_hrg2; mFwdPathVy(4)]'; %sigIn = x1
input_to_mVxIeqC1 = '[w_Ixx4; w_m3; w_Vx4; w_Vx5; w_Caf2;
   w_Car2; w_a1; w_a2; w_Ixx5; w_m4; w_hrg3; w_hrg4;
   mFwdPathPsi(3)]'; %sigIn = x2
input_to_mBphid4Vy = '[w_Bphid1; w_hrg5; w_Vx6; w_m5;
   mFwdPathPhi(3)]'; %sigIn = x3
input_to_mKphi4Vy = '[w_hrg6; w_Vx7; w_m6; w_Kphi1; w_m7;
   w_hrg7; mFwdPathPhi(4)]'; %sigIn = x4
input_to_mC2 = '[w_Caf3; w_Car3; w_a3; w_a4; w_a5; w_a6;
   mFwdPathPsi(3)]'; %sigIn = x2
input_to_mC1 = '[w_Caf4; w_Car4; w_a7; w_a8; mFwdPathVy(4)]'; %
   sigIn = x1
```

```
input_to_mBphid4Phi = '[w_Bphid2; w_Vx8; mFwdPathPhi(3)]'; %
   sigIn = x3
input_to_mKphi4Phi = '[w_Vx9; w_Kphi2; w_m8; w_hrg8;
   mFwdPathPhi(4)]'; %sigIn = x4
input_to_mC1hrg4Phi = '[w_hrg9; w_Caf5; w_Car5; w_a9; w_a10;
   mFwdPathPsi(3)]'; %sigIn = x2
input_to_mCohrg4Phi = '[w_hrg10; w_Caf6; w_Car6; mFwdPathVy(4)]
   '; %sigIn = x2
input_to_mUsysVy = '[w_Caf7; w_Vx10; w_Ixx6; w_m9; w_hrg11;
   w_hrg12; u_steer]';
input_to_mUsysPsi = '[w_Caf8; w_Vx11; w_a11; u_steer]';
input_to_mUsysPhi = '[w_Caf9; w_Vx12; w_hrg13; u_steer]';
%Note: output variables are represented explictly to visually
   match with %inputs. only the repeated outputs are
   represented as ranges i.e. z_a is mVxC1(5:6)
outputvar = ['[ mFwdPathVy(1); mFwdPathVy(2); mFwdPathVy(3);'
   ...
               'mFwdPathPsi(1); mFwdPathPsi(2);'...
               'mFwdPathPhi(1); mFwdPathPhi(2);'...
               'mIeqCo(1); mIeqCo(2); mIeqCo(3); mIeqCo(4);
                  mIeqCo(5:6);'...
                           'mVxIeqC1(1);  mVxIeqC1(2); mVxIeqC1
                              (3:4); mVxIeqC1(5);  mVxIeqC1(6);
                               mVxIeqC1(7:8); mVxIeqC1(9);
                              mVxIeqC1(10); mVxIeqC1(11:12);'
                              ...
```

```
                'mBphid4Vy(1); mBphid4Vy(2); mBphid4Vy(3);
                   mBphid4Vy(4);' ...
                'mKphi4Vy(1); mKphi4Vy(2); mKphi4Vy(3); mKphi4Vy
                   (4); mKphi4Vy(5); mKphi4Vy(6);' ...
'mC2(1); mC2(2); mC2(3:6);' ...
                 'mC1(1); mC1(2); mC1(3:4);' ...
                'mBphid4Phi(1); mBphid4Phi(2);' ...
                'mKphi4Phi(1); mKphi4Phi(2); mKphi4Phi(3);
                   mKphi4Phi(4);' ...
                'mC1hrg4Phi(1); mC1hrg4Phi(2); mC1hrg4Phi(3);
                   mC1hrg4Phi(4:5);' ...
                'mCohrg4Phi(1); mCohrg4Phi(2); mCohrg4Phi(3);'
                   ...
                'mUsysVy(1); mUsysVy(2); mUsysVy(3); mUsysVy(4);
                    mUsysVy(5:6);'...
                'mUsysPsi(1); mUsysPsi(2); mUsysPsi(3);'...
                'mUsysPhi(1); mUsysPhi(2); mUsysPhi(3);'...
                'mFwdPathPsi(3)]']; % output of plant: x2,
                   yawRate (psi_dot)
cleanupsysic = 'yes';
sysic; minfo(G_vYawRoll_FullLFT)
seesys(G_vYawRoll_FullLFT)
```